

Investigation into the Mechanics and Feasibility of Continuous Counter-Current Extraction

A thesis submitted for the degree of Doctor of Philosophy

By

Remco Nicolaas Antonius Maria van den Heuvel

Department of Biological Sciences, Brunel University

November 2007

Foreword

“The timing of Remco’s research on “Continuous Counter-current Extraction” has proved to be very insightful as his research, and the concurrent research programme grant from Pfizer which helped fund it, led to a much deeper understanding of continuous processing, which is now a key priority for the pharmaceutical industry.

The team’s research on continuous processing, of which Remco’s research was an important part, became the platform from which our successful intermittent counter-current extraction grew and became an integral part of our success in gaining subsequent funding such as the TSB programme grant for “Scalable Technology for the Extraction of Pharmaceuticals (STEP)” in which continuous processing remains a key priority.

Continuous processing, along with automation and rapid method development, are now seen as the key development areas to establish the Institute’s liquid flow processes as platform technology for the pharmaceutical industry.”

Professor Ian Sutherland

Director of the Advanced Bioprocessing Centre at Brunel University

Abstract

Continuous counter current extraction (CCCE) or dual flow counter current chromatography (DFCCC) is a promising technique where components can be separated continuously by two liquid phases that flow in opposite directions through a continuous length of coiled tubing. Specially designed end connectors and a coil planet centrifuge allow each respective phase to be pumped into each end of the tubing and the other phase to elute at each opposite end. In this thesis the feasibility and the mechanics of CCCE are investigated using stroboscopic photography on an experimental rig and a specially built pilot-scale CCCE centrifuge.

The mechanics of the hydrodynamics in the coil was investigated systematically by comparing the measured volumes with photographic images of the process. This investigation revealed that the phases are not distributed evenly throughout the coil, which was previously assumed, but that there is a transition area where the phases switch from mainly upper phase at the head end of the tubing to mainly lower phase at the tail end. This means that the sample encounter three different phase distribution zones in the coil. At the head the upper phase is the dominant phase with a small volume of lower phase running through. At the tail the reverse situation is found and lower phase is dominant. The third zone is a short segment of the coil where there is a transition between the dominant phase conditions that exist at each end. The position of the transition zone and the volume of the other two zones are profoundly affected by the relative flow rates of the two phases. This work indicates that the volume distribution in the coil is affected most by the upper phase flow rate.

The pilot-scale CCCE centrifuge was used to successfully separate industrially supplied samples. Crude reaction liquor was processed in both batch and continuous modes achieving the separation of the multi-component mixture into two groups. Changing the flow rate combinations changed the location of elution of some of the components in the mixture. Separation efficiency was maintained even when sample loading was increased. The separations were shown to be predictable with the dual flow theoretical model.

Table of Contents

CHAPTER 1	INTRODUCTION AND LITERATURE REVIEW ...	15
1.1	OUTLINE	15
1.2	HISTORY OF CHROMATOGRAPHY	15
1.3	COUNTER-CURRENT CHROMATOGRAPHY THEORY.....	16
1.3.1	Counter-current Distribution (CCD)	16
1.3.2	Counter-current Chromatography (CCC).....	19
1.3.2.1	“Archimedean screw effect” and the “Head and Tail”.	23
1.3.2.2	Retention of the stationary phase	26
1.3.2.3	Chromatographic separations.....	30
1.3.3	Phase systems used in Counter-current separations	35
1.4	LITERATURE REVIEW	37
1.4.1	Different types of CCC centrifuges	37
1.4.2	Solvent phase systems	39
1.4.2.1	Head and Tail study	39
1.4.2.2	Solvent selection.....	40
1.4.2.3	Modes of operation	48
1.4.2.4	The liquid nature of the Stationary Phase	49
1.4.3	CCC and CCD models	52
1.4.4	Dual flow CCC.....	61
1.4.5	Other “Continuous” techniques	65
1.5	OBJECTIVES OF THIS THESIS	66
CHAPTER 2	METHODS AND MATERIALS.....	67
2.1	OUTLINE	67
2.2	PREPARATION OF PHASE SYSTEMS	67
2.3	PHOTOGRAPHIC RIG SET-UP AND METHODS	68
2.3.1	Experimental CCCE Centrifuge	68
2.3.2	Experimental Rig Set-up	69
2.3.3	Method used on the Photographic rig.....	71
2.3.4	Photograph Analysis Method	72
2.4	APPLICATIONS STUDY AT PFIZER	76
2.4.1	Phase System Selection	77
2.4.2	Process size CCCE Coil	80
2.4.3	Experimental set-up at Pfizer.....	81
2.4.4	Four protocols for the CCCE separations.....	82

2.4.5	HPLC analysis of the sample mixtures and the fractions	83
2.4.6	Mass balance procedure.....	84
CHAPTER 3 THEORY AND MODELS OF CCCE		86
3.1	OUTLINE	86
3.2	PHASE DISTRIBUTION IN THE COIL.....	86
3.2.1	Calculations to determine the transition area	86
3.3	ORIGINAL CCD MODEL	88
3.3.1	Theory	88
3.3.1.1	Single Withdrawal	93
3.3.2	Model in Excel.....	95
3.4	CONTINUOUS DUAL FLOW CCD MODEL	99
3.4.1	Theory	99
3.4.2	Model in Excel.....	102
3.5	DISCUSSION AND CONCLUSION	108
3.5.1	Discussion.....	108
3.5.2	Conclusion	109
CHAPTER 4 EXPERIMENTS ON THE PHOTOGRAPHIC RIG111		
4.1	OUTLINE	111
4.2	VISUALISATION STUDIES.....	111
4.2.1	Aim	111
4.2.2	Experiments Performed	111
4.2.3	Results	112
4.2.3.1	Visualisation.....	112
4.2.3.2	Phase ratio.....	113
4.2.4	Discussion.....	114
4.2.5	Conclusion of initial visualisation studies	116
4.3	NORMAL AND REVERSE PHASE MODE	116
4.3.1	Aim	116
4.3.2	Experiments Performed	117
4.3.3	Results and Analysis.....	117
4.3.4	Discussion and Conclusion.....	120
4.4	RETENTION STUDY ON THE PHOTOGRAPHIC RIG	120
4.4.1	Aim	121
4.4.2	Experiments Performed	121
4.4.3	Results and Analysis.....	122
4.4.3.1	The effect of the starting condition on the phase distribution	123

4.4.3.2	Statistical analysis of the data.....	125
4.4.3.3	Ideal operating conditions analysis	127
4.4.3.4	Analysis of the number of loops filled with upper phase	132
4.4.4	Discussion of Results.....	137
4.5	CONCLUSIONS.....	138
CHAPTER 5	APPLICATIONS STUDY AT PFIZER LTD	140
5.1	OUTLINE	140
5.2	AIM	140
5.3	SAMPLE MIXTURE SCREENING	140
5.3.1	Screening Experiments.....	140
5.3.2	Screening Results.....	141
5.3.2.1	Project Pfizer-A.....	141
5.3.2.2	Project Pfizer-B.....	141
5.3.2.3	Project Pfizer-C.....	142
5.3.2.4	Project Pfizer-D.....	146
5.3.3	Screening Results Discussion & Conclusions	148
5.4	SAMPLE MIXTURE SEPARATIONS	148
5.4.1	Project Pfizer-C “Batch” separations:	148
5.4.2	Project Pfizer-C “Continuous” separations (loading study)	153
5.4.3	Project Pfizer-D “Continuous” separation	157
5.5	SEPARATION RESULTS VERSUS THE DFCCD MODEL	161
5.6	DISCUSSION AND CONCLUSIONS.....	164
5.6.1	Discussion.....	164
5.6.2	Conclusion	166
CHAPTER 6	DISCUSSIONS AND CONCLUSIONS	167
6.1	DISCUSSIONS	167
6.1.1	Model	167
6.1.2	Visualisation study	167
6.1.3	Application study.....	168
6.1.3.1	Phase system selection	168
6.1.3.2	The CCCE Separation	169
6.1.3.3	CCCE predictions	169
6.2	CONCLUSIONS.....	170
6.2.1	Advantages	170
6.2.2	Disadvantages	171
6.2.3	Summary.....	172
6.3	FUTURE WORK.....	172

6.4	CONCLUDING REMARKS.....	173
APPENDIX I	LOCUS OF COIL CALCULATIONS.....	174
APPENDIX II	DERIVATION OF THE POLAR LIMAÇON EQUATION	175
APPENDIX III	ACCELERATION CALCULATIONS.....	177
APPENDIX IV	TERNARY AND TETRAHEDRON CALCULATIONS	181
APPENDIX V	APPLICATION STUDY PROTOCOLS	184
APPENDIX VI	PUBLICATION OF VISUALISATION RESULTS	190
APPENDIX VII	DATA FROM RETENTION STUDY 4.3.....	194
APPENDIX VIII	EXPERIMENTAL DESIGN CALCULATIONS	196
APPENDIX IX	APPLICATION STUDY: “BATCH” CHROMATOGRAMS	199
APPENDIX X	APPLICATION STUDY: “CONTINUOUS” CHROMATOGRAMS	203
APPENDIX XI	APPLICATION STUDY: “CONTINUOUS” PFIZER- D SEPARATION.....	206
APPENDIX XII	REFERENCES	208

Acknowledgements

First I would like to give a big thank you to my supervisor, Professor Ian Sutherland, for giving me the opportunity to study at the Brunel Institute for Bioengineering at Brunel University, and for his continuing invaluable support, encouragement and guidance.

I would also like to thank the other people at the Brunel Institute for Bioengineering for their support and advice. In particular, Mr David Hawes for the design and building of both the experimental (visualisation) Dual Flow CCC coil and the process scale Dual Flow CCC coils and Dr Ian Garrard for reading through my thesis several times and providing me with an outlet on his sailing boat.

I would also like to thank the EPSRC for their financial support of my Doctoral Training Post which provided me the resources to support myself and, more importantly, for the building and setting up the equipment and experimental rigs.

Thanks are also extended to Pfizer Ltd, Sandwich, Kent for supporting my PhD both financially and with their expertise. In particular I would like to thank Robert Crook, Ben Mathews and Stephane Dubant for supporting this research work and for allowing me to work in their labs for two months to gain invaluable research results and an industrial perspective on the project.

I would like to thank Brunel University for the support I received over the three years. In particular I would like to say thank you for the Travel Award I received to present my work at CCC 2006 in Washington DC.

Finally, I would like to thank my wife Eleanor for putting up with me and understanding me and supporting me throughout the three years of this research project.

Nomenclature

β -value	ratio of r over R
A	Intercept with the y-axis on the Du-plot [%]
B	Gradient of the Du-plot [(min/ml) ^{1/2}]
B_L	Gradient of the Du-plot where lower phase is mobile [(min/ml) ^{1/2}]
B_U	Gradient of the Du-plot where upper phase is mobile [(min/ml) ^{1/2}]
C_{Aq}	Concentration of the solute in the aqueous phase [mg/ml]
C_L	Concentration of the solute in the lower phase [mg/ml]
C_M	Concentration of the solute in the mobile phase [mg/ml]
C_{Org}	Concentration of the solute in the organic phase [mg/ml]
C_S	Concentration of the solute in the stationary phase [mg/ml]
C_U	Concentration of the solute in the upper phase [mg/ml]
$D_{L/M}$	Distribution coefficient (C_L / C_U)
$D_{S/M}$	Distribution coefficient (C_S / C_M)
MF	Mass fraction of the component [-]
MF_L	Mass fraction of the component in the lower phase [-]
MF_U	Mass fraction of the component in the upper phase [-]
m_L	Mass of the component in the lower phase in the tube [mg]
m_M	Mass of the component in the mobile phase in the tube [mg]
m_S	Mass of the component in the stationary phase in the tube [mg]
m_U	Mass of the component in the upper phase in the tube [mg]
p	Plate, Funnel or Tube number
Q_L	Flow rate of the lower phase [ml/min]

Q_M	Flow rate of the mobile phase [ml/min]
Q_S	Flow rate of the stationary phase [ml/min]
Q_U	Flow rate of the upper phase [ml/min]
r	distance from the planetary axis to a point on the coil [m]
R	distance from the centre of the centre axis to the planetary axis [m]
V_C	Coil or test tube volume [ml]
V_D	Volume of displaced stationary phase [ml]
V_{EXT}	Extra coil volume [ml]
V_L	Volume of the lower phase in the coil or tube [ml]
V_M	Volume of the mobile phase in the coil or tube [ml]
V_R	Solute Retention volume [ml]
V_S	Volume of the stationary phase in the coil or tube [ml]
V_U	Volume of the upper phase in the coil or tube [ml]
$X_{S/M}$	Volume ratio (V_S / V_M)

Abbreviations

ATPS	Aqueous Two Phase System
CCC	Counter-Current Chromatography
CCCD	Continuous Counter-Current Distribution
CCCE	Continuous Counter-Current Extraction
CCD	Counter-Current Distribution
CDCD	Counter Double Current Distribution
DCM	Dichloromethane
DFCCC	Dual Flow Counter-Current Chromatography
DFCCD	Dual Flow Counter-Current Distribution
DMCCC	Dual Mode Counter-Current Chromatography
DMF	Dimethylformamide
EECCC	Elution-Extrusion Counter-Current Chromatography
EtOAc	Ethyl acetate
FID	Flame Ionisation Detector
GC	Gas Chromatography
H ₂ O	Water
HPLC	High Performance Liquid Chromatography
HSCCC	High Speed Counter-Current Chromatography
LHR	Liquid Handling Robot
MeCN	Acetonitrile
MEK	Methyl ethyl ketone
MeOH	Methanol
PEG	Polyethylene Glycol
SMB	Simulated Moving Bed
TBME	tert-butyl methyl ether
TCD	Thermal Conductivity Detector
TFA	Trifluoroacetic acid
TLC	Thin Layer Chromatography
TMB	True Moving Bed

Chapter 1 Introduction and Literature Review

1.1 Outline

Following a brief section on the history of Counter-current Chromatography (CCC), the theory of CCC in a J-type centrifuge is described. The theory of Counter-current Distribution (CCD) will be used for the description of CCC theory. An overview of the available literature on CCC will follow highlighting some of the areas where research is needed. From the literature review, the scope of this thesis will be defined.

1.2 History of Chromatography

The Russian botanist Mikhail Tswett invented the first chromatography technique during his investigation on plant pigments in around 1900 [Tswett 1903]. A few years later he first described the technique using the name Chromatography [Tswett 1906A, B]. In Greek the term 'Chroma-to-graphy' means "to write in colour". A number of publications have suggested that the name 'Tswett' means colour in Russian, and speculate that Tswett named the technique after himself, literally 'Tswett's writing' [Abraham 2004]. 'Colour writing' is exactly what Mikhail Tswett did when he used paper to separate plant pigments and the different colours where shown. Abraham [2004], however, points out that the term "Chromatography" was first described and used by George Field in 1835 [Field 1835] when he described a device to view colours the "Chromascope". Field was researching colours and pigments in paint and the name "Chromatography" most likely inspired and intrigued Tswett.

Throughout the 20th century the technology advanced rapidly. Scientists found ways of improving the technique constantly and chromatography became a widely used separation technique. In 1941 Martin and Synge published a new form of chromatography employing two liquid phases [Martin and Synge 1941]. This type of chromatography is based on the difference in solubility of the component between the mobile and the stationary phase and is the basis for Counter-current Distribution and Counter-current

Chromatography. Martin and Synge published a number of papers describing this new form of chromatography with a theory that would later form the basis of the current CCC theory. In 1952 Martin and Synge received the Nobel Prize for their invention of partition chromatography.

1.3 Counter-current Chromatography Theory

The theory of CCC will be described using CCD and the differential partitioning of a component in two immiscible fluids.

1.3.1 Counter-current Distribution (CCD)

CCD, like CCC, is based on the differential partitioning of components in two immiscible liquids. These liquids are called the phases, the light liquid is the upper phase and the heavy liquid the lower phase. Components that are to be separated using these liquids distribute differently between the two phases and usually show a greater affinity for one of these phases. This affinity based on the distribution law which was first developed and described by Nernst [1891]. The concentration of a component in the organic phase over the concentration of a component in the aqueous phase is called the "Distribution coefficient ($D_{O/A}$)" and is defined as

$$D_{O/A} = \frac{C_{Org}}{C_{Aq}} \qquad \text{Equation 1-1}$$

where C_{Org} and C_{Aq} are respectively the concentrations of the solute in the organic phase and aqueous phase.

If the affinity of the component is the same for both phases the distribution coefficient will be 1. When the component has a higher affinity for the organic phase the distribution coefficient will be >1 and when the component has a higher affinity for the aqueous phase the distribution coefficient will be <1 .

In most situations, the organic phase is the upper phase and the aqueous phase is the lower phase. Then the distribution ratio is defined as

$$D_{U/L} = \frac{C_U}{C_L} \qquad \text{Equation 1-2}$$

where $D_{U/L}$ is the distribution coefficient, C_U and C_L are respectively the concentration of the solute in the upper phase and lower phase. As the distribution ratio can be defined in many ways, the notation of the D-value should indicate how it is defined, i.e. $D_{X/Y}$ means that the D-value is defined as the concentration of the component in phase X over the concentration in phase Y.

In CCD both phases are put into each tube of a train of test tubes. The components which need to be separated are introduced into the first test tube. Then all the test tubes go through a mixing and settling step. When the liquids are settled and fully separated, the upper or lower phase (mobile phase) is moved to the next tube. This process is shown in Figure 1-1, where the upper phase is mobile and the train is made up of three test tubes. There are two components which are partly separated in two mixing and settling steps. The blue component has a $D_{U/L}$ of 0.5 and the red component has a $D_{U/L}$ of 2.

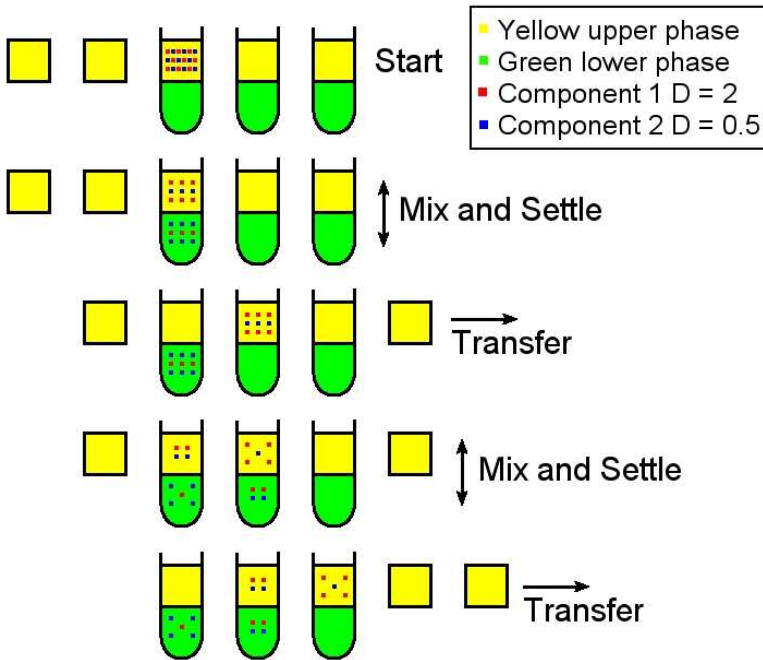


Figure 1-1: CCD process with three test tubes, two mixing and two settling steps. The yellow upper phase is the mobile phase and the green lower phase is stationary. [Sutherland et al. 2003]

In CCD the lower phase can also be the mobile phase. This would give the same resolution and inversed separation compared to the condition when the upper phase is mobile. Depending on further processing of the eluent from the CCD process and the properties of the desired component, the mobile phase can be either the upper or lower phase. To be able to compare separations the Distribution coefficient can be redefined as the ratio of the concentration of the component in the stationary phase (C_S) to the concentration of the component in the mobile phase (C_M). This new Distribution coefficient ($D_{S/M}$) incorporates the choice of mobile and stationary phase and is

$$D_{S/M} = \frac{C_S}{C_M} \qquad \text{Equation 1-3}$$

Note, that when the stationary phase is the upper phase, $D_{S/M} = D_{U/L}$ and when the mobile phase is the upper phase $D_{S/M} = 1/D_{U/L} = D_{L/U}$.

1.3.2 Counter-current Chromatography (CCC)

In the early 1960's Yoichiro Ito developed the first coil planet centrifuge [Ito *et al.* 1966]. In this centrifuge a closed coil was rotated slowly around its own axis while being in a g-force field due to another rotation. Initially the two immiscible liquids were placed on either end of the coil. Due to the forces on the liquid produced by the rotation these two liquids flowed in opposite directions through the coil and this was the first real Counter-current Chromatography (CCC). This centrifuge was developed into a belt driven centrifuge, which was later referred to as the I-type centrifuge due to the flying lead configuration (Figure 1-2). This coil planet centrifuge consists of a coil of tubing which is spun around its own axis while rotating around a solar axis. One of the two liquids from the phase system is retained inside the coil while the other is pumped through the coil. Ito's pioneering work continued and produced several coil configurations. The two most famous are the I-type and the J-type centrifuge (Figure 1-2). The J-type centrifuge was developed in the 1980's and with this CCC started to become popular. In later years the J-type CCC centrifuge was renamed to High Speed CCC (HSCCC). Pulleys are used to drive the I-type centrifuge and gears are used to drive the J-type centrifuge. For the thesis the latter centrifuge is used and is therefore also described in detail in this theory. The planetary gear configuration of the J-type centrifuge is shown in Figure 1-3.

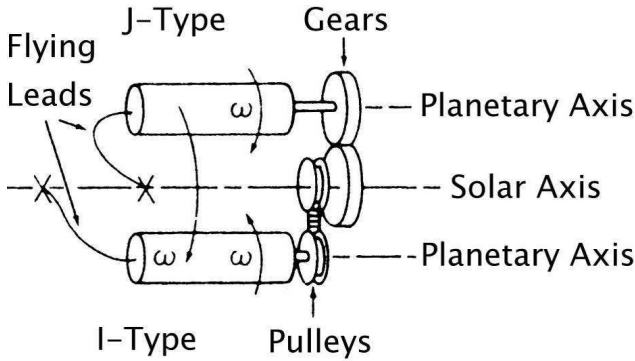


Figure 1-2: I-type and J-type centrifuge with the flying leads shown [Ito 1981]

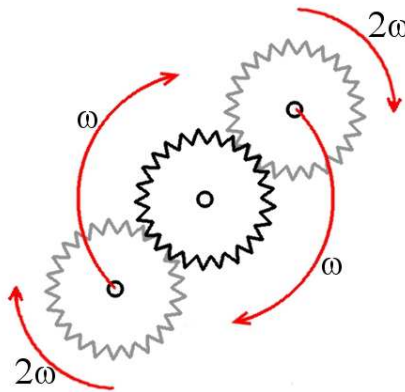


Figure 1-3: Planetary gear system of the J-type centrifuge with the centre gear stationary

The coil, which consists of a length of tubing wound around a drum, is attached to the planetary gear. The solar gear is held stationary while the coil is forced to move around through a rotor attached to an electrical motor. Due to the gear configuration, the coil will spin around its own axis twice while rotating once around the solar axis.

This is shown in Figure 1-4 for the J-type gear system where the coil (blue) is shown twice in the same position (relative to its own axis) for one solar rotation.

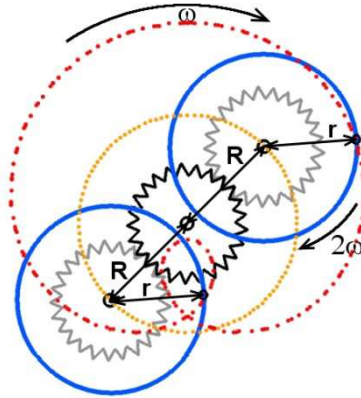


Figure 1-4: J-type gear system with the locus of one point (red) on the coil (blue) and the dimensions to determine the β -value.

For the J-type centrifuge shown in Figure 1-3 these two rotations are in the same direction. Depending on the radii of these two rotations one point on the coil will follow a certain path (locus). The ratio of the radius of the coil (r) over the distance between the coil axis and the solar axis (R) gives the β -value as follows.

$$\beta = \frac{r}{R} \quad \text{Equation 1-4}$$

When the β -value is varied, the locus of one point on the coil describes a different shape. This shape can be mathematically expressed by the following two equations [Ito and Bowman 1978]:

$$x(\theta) = R \cdot (\cos \theta + \beta \cdot \cos(2\theta)) \quad \text{Equation 1-5}$$

$$y(\theta) = R \cdot (\sin \theta + \beta \cdot \sin(2\theta)) \quad \text{Equation 1-6}$$

where θ is the angle around the centre axis ranging from 0 to 2π , $x(\theta)$ and $y(\theta)$ are respectively the x-axis and y-axis coordinates at the angle θ .

Figure 1-5 shows how the locus of one point on the coil varies as a function of the β -value.

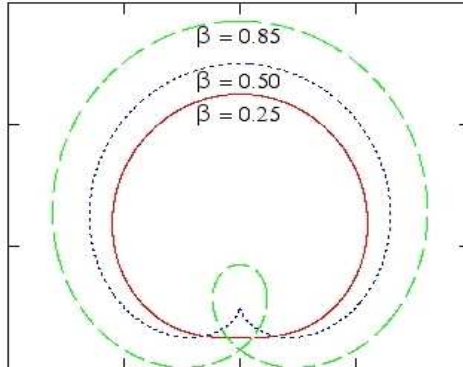


Figure 1-5: Three Loci of one point on the coil at three different β -values. (0.85, green dashed line; 0.50, blue dotted line; 0.25 red solid line). MathCAD 13 was used to calculate the locus of one point on the coil at the various β -values. The calculations are show in Appendix I

The shape of the locus of one point on the coil is called a Limaçon (which comes from the Latin *limax* meaning “snail”). Except at a β -value of 0.5 where the radius of the coil is the same as the radius of one gear the shape is called a Cardioid [Rutter 2000]. The x and y coordinates (Equation 1-5 and Equation 1-6) are derived by Ito and Bowman [1978] and the derivation from the original polar expression for the Limaçon is shown in Appendix II.

Single layer helical coils have one β -value and multi-layer helical coils and spiral coils have a range of β -values.

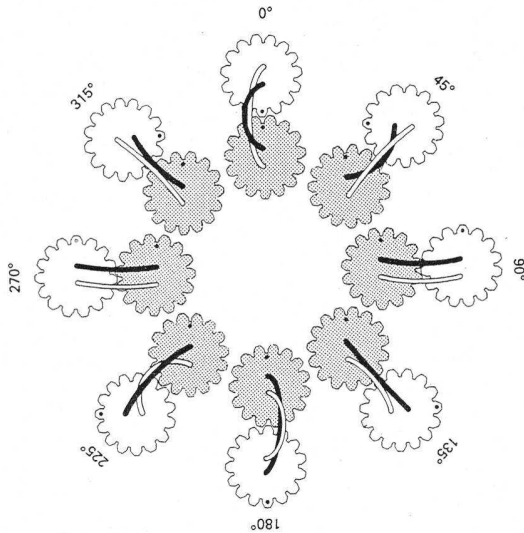


Figure 1-6: Successive gear positions during one revolution showing a twist-free mechanism. The grey gear is stationary while the white gear rotates around it. The white and black lines are the two flying leads that do not twist. [Ito 1986]

The tubes that connect the ends of the coil to the outside of the centrifuge are called the “flying leads”. These flying leads are shown Figure 1-2 and Figure 1-6. In the former figure the path the leads describe looks like a “J”, hence the name “J-type” centrifuge. Due to the fact that the solar and the planetary gears in a J-type centrifuge have the same size the leads do not twist when the coil is rotated.

1.3.2.1 “Archimedean screw effect” and the “Head and Tail”

Fluids in a rotating coil will be displaced from one end of the coil (the tail) to the other end of the coil (the head). This is called the “Archimedean screw effect”, which is shown in Figure 1-7.



Figure 1-7: Archimedean screw used to pump up water¹.

The “Archimedean screw effect” is one of the forces working on the fluids inside the coil and is also called the “Hydrodynamic force”. The other force working on the phases inside the coil is the centrifugal force, which is also referred to as the “Hydrostatic force”. The acceleration (or unit force) working on the fluids inside the coil as a result of the motion will be described by the second derivative of Equation 1-5 and Equation 1-6. This process is shown in Appendix III and the results are

$$A_r = -\cos(2\theta) \cdot AccnX(\theta) - \sin(2\theta) \cdot AccnY(\theta) \quad \text{Equation 1-7}$$

$$A_t = -\sin(2\theta) \cdot AccnX(\theta) + \cos(2\theta) \cdot AccnY(\theta) \quad \text{Equation 1-8}$$

where A_r and A_t are respectively the accelerations in the radial and tangential direction. This unit force is shown in Figure 1-8. The

¹ The American Heritage® Dictionary of the English Language, Fourth Edition. Copyright © 2000 by Houghton Mifflin Company. Published by the Houghton Mifflin Company. Precision Graphics. <http://www.bartleby.com/61/imagepages/A4arcsM1.html>

force vectors shown in this figure all pass through the point F_0 which is not the centre of the coil.

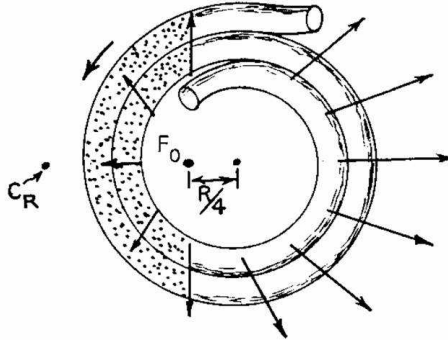


Figure 1-8: Spiral coil spinning with planetary gear motion showing the schematic relationship between the mixing zone with the force field pattern. C_R is the centre of rotation and F_0 is the force origin [Conway 1990].

The coils are wound and spun so that the Archimedean and centrifugal forces work in the same direction and the tail of the coil is at the periphery and the head is at the centre. When this is done, the forces on the liquid due to the rotation will be used to their full potential as they will work into the same direction. Two immiscible fluids in a rotating coil will distribute according to their density. The upper phase will go to the head of the coil and the lower phase will go to the tail [Sutherland et al 2000]. Either the upper or the lower phase can be used as the mobile phase while the other is the stationary phase. When the polar aqueous phase (generally the lower phase) is stationary and the non-polar organic phase (generally upper phase) is mobile the running mode is called Normal Phase Mode. The running mode is called Reverse Phase Mode when the non-polar phase is stationary and the polar is mobile. When chlorinated solvents are used (which are heavier than water) they will be the non-polar lower phase and the aqueous phase will be the polar upper phase. For a non-aqueous phase system (e.g.

heptane-methanol) the mobile phase for the Normal and Reverse phase mode will be determined by the polarity of the phases. The most polar phase will be mobile for the Reverse phase mode. The modes of operation and the hydrodynamic equilibrium are shown in Figure 1-9.

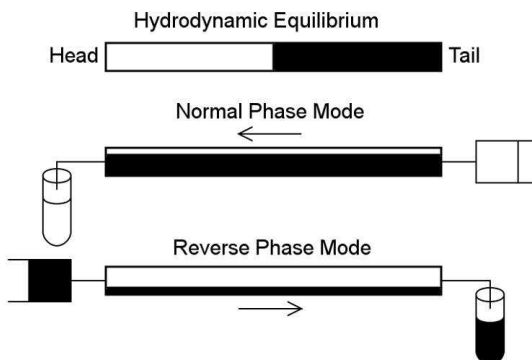


Figure 1-9: Schematic representation of the Hydrodynamic equilibrium inside a spinning coil and the two situations where either the lower (black) or the upper (white) phase are the mobile phase [Ito 1985].

1.3.2.2 Retention of the stationary phase

In CCC, as in CCD, one of the two immiscible phases is the mobile phase. This phase transports the sample into the system and the separated components out of the system. The other phase is the stationary phase which stays in the coil and interacts with the components. Due to the forces working on the fluids in a CCC centrifuge, the stationary phase tends to travel in a certain direction. The mobile phase, which could be either the upper or the lower phase, is pumped through the coil in the direction it wants to go due to the forces. These forces move the stationary phase in the opposite direction of the mobile phase towards the mobile phase inlet. When the mobile phase flow is started the two phases in the coil will equilibrate and during this some of the stationary phase, with which the coil was filled initially, is displaced out of the coil to make room for the mobile phase. The amount of stationary phase retained inside the coil is dependent on a number of the process variables

which are mainly the mobile phase flow rate, the rotational speed and the phase system. At a higher mobile phase flow rate more stationary phase will be replaced by the mobile phase. The amount of stationary phase retained inside the coil will influence the chromatographic separation and is therefore an important parameter. The ratio of stationary phase retained in the coil to the total coil volume is called the stationary phase retention (S_f) and is defined as:

$$S_f = \frac{V_S}{V_C} \cdot 100\% \quad \text{Equation 1-9}$$

where V_S is the volume of stationary phase [ml], V_C is the coil volume [ml] ($V_C = V_S + V_M$), and V_M is the mobile phase volume [ml].

There is a linear relationship between the stationary phase retention and the square root of the mobile phase flow rate [Du et al. 1999]. This is only valid for low mobile phase flow rates. This linear relationship is shown in Figure 1-10 and expressed in the equation

$$S_f = A - B \cdot \sqrt{Q_M} \quad \text{Equation 1-10}$$

where Q_m is the volumetric flow rate of the mobile phase [ml/min], A is the intercept with the y-axis at a flow rate of 0[ml/min], and B is the gradient of the relationship [(ml/min)²].

At a flow rate of 0 ml/min the stationary phase retention can be assumed to be 100%, therefore the term A in the equation can be replaced by 100%. The gradient of the linear relationship is negative, as when the mobile flow rate increases the stationary phase retention decreases. This relationship is shown in a Du plot, shown in Figure 1-10.

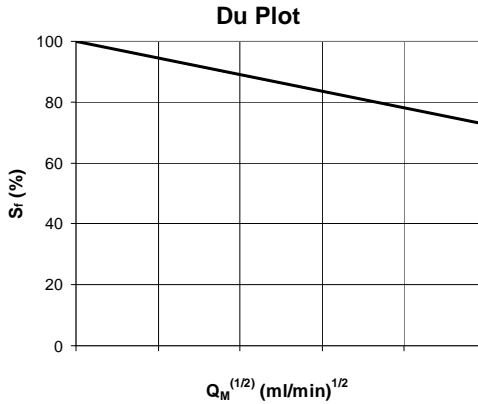


Figure 1-10: Du-plot showing the linear relationship between Stationary phase retention and the square root of the mobile phase flow rate.

Substituting Equation 1-9 into Equation 1-10 and rearranging with respect to V_S gives Equation 1-11.

$$V_S = V_C - \frac{V_C \cdot B}{100} \cdot \sqrt{Q_M} \quad \text{Equation 1-11}$$

Equation 1-11 is only valid if the extra coil volume is taken into account [Wood 2002]. The extra coil volume (V_{EXT}) is the volume from the injection port to the detector minus the actual coil volume. The volume of stationary phase displaced (V_D) is the amount of mobile phase in the extra coil volume V_{EXT} and in the coil V_M . This gives the following expression for the amount of mobile phase inside the coil.

$$V_M = V_D - V_{EXT} \quad \text{Equation 1-12}$$

This equation substituted into the definition for the coil volume gives the following expression for V_C .

$$V_C = V_S + V_D - V_{EXT} \quad \text{Equation 1-13}$$

Substituting the stationary phase volume in Equation 1-13 with Equation 1-11 and rearranging for V_D gives Equation 1-14.

$$V_D = \frac{V_C \cdot B}{100} \cdot \sqrt{Q_M} + V_{EXT} \quad \text{Equation 1-14}$$

The relationship between the volume of eluted stationary phase, V_D , and the square root of the mobile phase flow rate is shown in Figure 1-11 [Wood *et al.* 2003]. The intercept of the linear line with the y-axis is the extra coil volume.

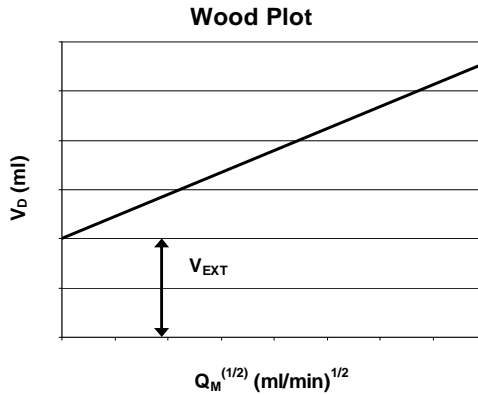


Figure 1-11: Wood plot shows the eluted stationary phase plotted against the square root of the mobile phase flow rate.

Wood [2002] showed that the ratio of the slopes of the Du-plots for Normal and Reverse phase mode are related to the ratio of the viscosities of the mobile phases for these modes according to Equation 1-15.

$$\frac{B_{LP}}{B_{UP}} = \sqrt{\frac{\mu_{LP}}{\mu_{UP}}} \quad \text{Equation 1-15}$$

In this equation B_{LP} and the μ_{LP} are respectively the slope of the Du-plot and the viscosity of the mobile phase when the lower phase is mobile (mostly in Reverse phase mode), whereas B_{UP} and μ_{UP} represent the slope and the viscosity respectively when the upper phase is mobile (mostly in Normal phase mode).

1.3.2.3 Chromatographic separations

The mobile phase moves through the coil, as described in sections 1.3.2.1 and 1.3.2.2. This mobile phase is used to transport sample mixtures into the coil and to transport fully or partly separated components out of the coil. Components travelling through the coil within the mobile phase, also referred to as “bands”, are retained differentially due to the partitioning of these components between the two liquid phases. The concentration of component eluting with the mobile phase is detected and a graph of the concentration versus time is generated to show a chromatogram (Figure 1-12). If separation of the components has occurred, this will be visible on the chromatogram as the shape of peaks. The peaks representing the components will approximately follow the normal distribution and are narrow for the first eluting component and gradually become wider for the later eluting components. This is called band broadening and is due to the fact that part of the component in the stationary phase does not move whereas the component in question in the mobile phase does [Berthod 2006]. Components that are retained longer in the coil therefore have broader peaks (or bands). Further, because the latter part of the component eluting from the column is retained longer than the first part, peak tailing will occur. A chromatogram can be plotted against the running time or the eluted volume or in coil volumes.

The volume eluted from the coil where the component elutes is called the solute retention volume (V_R). This solute retention volume is theoretically calculated using the following equation.

$$V_R = V_M + D_{S/M} \cdot V_S$$

Equation 1-16

For real systems the extra coil volume (V_{EXT}) will also need to be taken into account. An ideal CCC chromatogram for a 100 ml coil showing the separation of three components is shown in Figure 1-12. The stationary phase retention is 90%, i.e. the mobile and stationary phase volumes are 10 ml and 90 ml respectively. Component 1 ($D_{S/M,1}=0.5$) has a solute retention volume (V_{R1}) of 55 ml (10 ml mobile phase plus 0.5 times 90 ml stationary phase). The second component ($D_{S/M,2}=1$) has a solute retention volume (V_{R2}) equal to the coil volume. Note that regardless of the stationary phase retention, a component with a D-value of one will always have a solute retention volume equal to the coil volume. Component 3 ($D_{S/M,3}=2$) has a solute retention volume (V_{R3}) of 190 ml (10 ml mobile phase and 2 times 90 ml stationary phase).

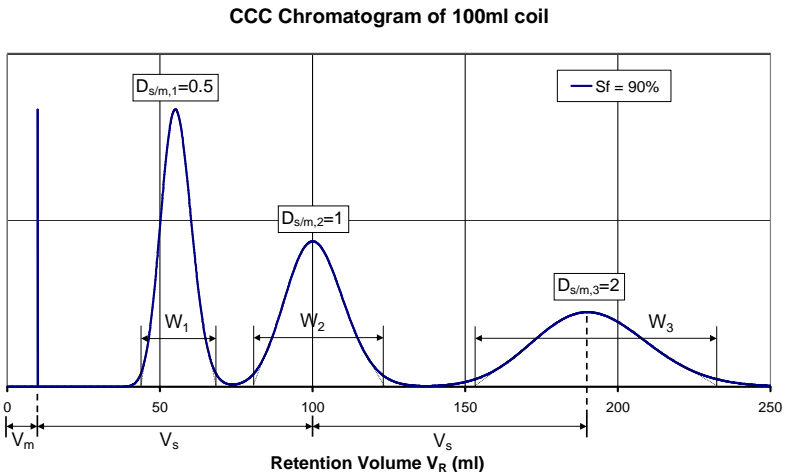


Figure 1-12: Ideal CCC chromatogram of a separation of three components ($D_{S/M,1}=0.5$, $D_{S/M,2}=1$ and $D_{S/M,3}=2$) and stationary phase retention of 90%

To calculate how well the components in the mixture have separated the solute retention volume and the peak width (W) are used. Each normal distributed peak can be divided into six standard deviations as is shown in Figure 1-13.

Normal Distribution

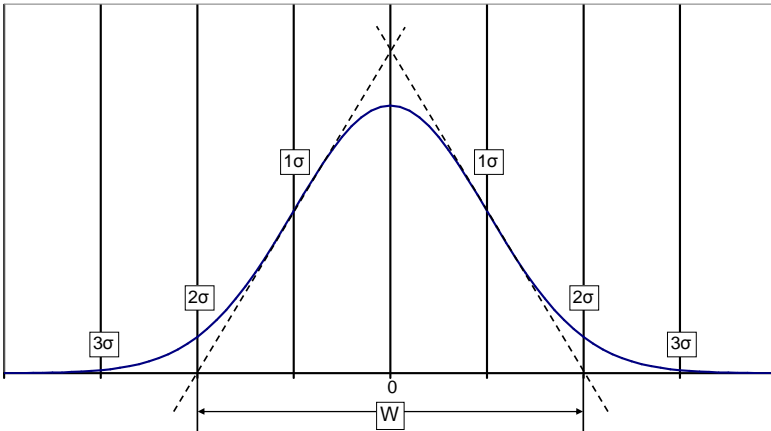


Figure 1-13: Normal distribution peak divided into standard deviations.

The standard deviations are labelled from the perpendicular bisector and the peak width is measured by drawing tangents through the points of inflexion on each side of the peak. The peak width is the distance between the point of intersection between the tangents and the baseline of the trace and is defined by four standard deviations. Both the width and the solute retention volume of the peaks are important to measure how the sample has been resolved. When there are four standard deviations between the two perpendicular bisectors of the peaks, the resolution (R_s) equals 1. With this definition, the equation for the resolution which was proposed by Phillips [1958] and discussed by Giddings [1965] is given by

$$R_s = \frac{V_{R2} - V_{R1}}{\frac{1}{2}W_1 + \frac{1}{2}W_2} = \frac{2(V_{R2} - V_{R1})}{W_1 + W_2} \quad \text{Equation 1-17}$$

where R_s is the resolution between the two peaks [-], V_{R1} is the solute retention volume of peak 1 [ml], V_{R2} is the solute retention volume of peak 2 [ml], W_1 is the width of peak 1 [ml] and, W_2 is the width of peak 2 [ml].

At three standard deviations from the perpendicular bisector, the line of the peak is approximately at the same level as the baseline. Therefore, if there are six standard deviations between the two perpendicular bisectors of the peaks, the sample is completely separated and the $R_S = 1.5$. This is called a baseline separation and this gives 100% pure components.

The resolution of components separated depends on the stationary phase retention as can be seen from Equation 1-16. Figure 1-14 presents two chromatograms depicting separations of three components ($D_{S/M,1} = 0.5$; $D_{S/M,2} = 1$; $D_{S/M,3} = 2$) in the same coil at two different stationary phase retention volumes, i.e. 40% for the top trace and 90% for the bottom trace.

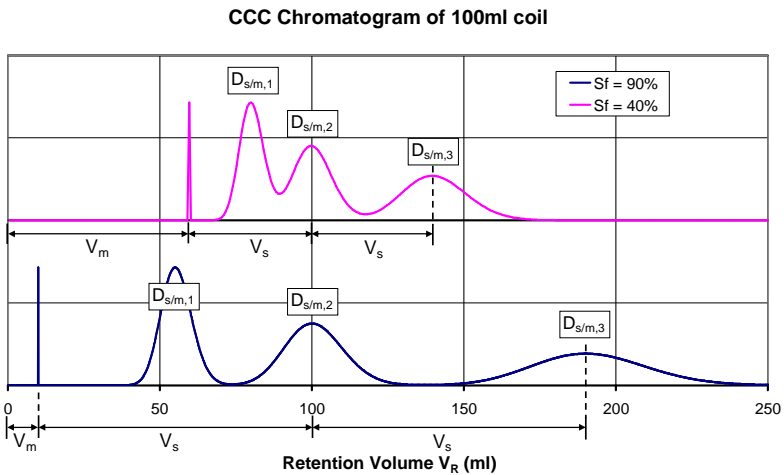


Figure 1-14: Ideal CCC chromatogram showing two traces of the same separation of three components ($D_{S/M,1} = 0.5$, $D_{S/M,2} = 1$ and $D_{S/M,3} = 2$) with different stationary phase retention. The top trace is from a separation with stationary phase retention of 40% and the bottom trace is from a separation with stationary phase retention of 90%.

As is evident from inspection of Figure 1-14 and Equation 1-16, the component with a D-value equal to 1 always elutes in a volume equal to that of the coil.

The solute retention volume changes linearly with the stationary phase volume (Figure 1-15) and with the distribution ratio (Figure 1-16). When the stationary phase volume in the coil decreases the components with D -values <1 will elute later (V_R increases) whereas those with D -value >1 will elute earlier (V_R decreases).

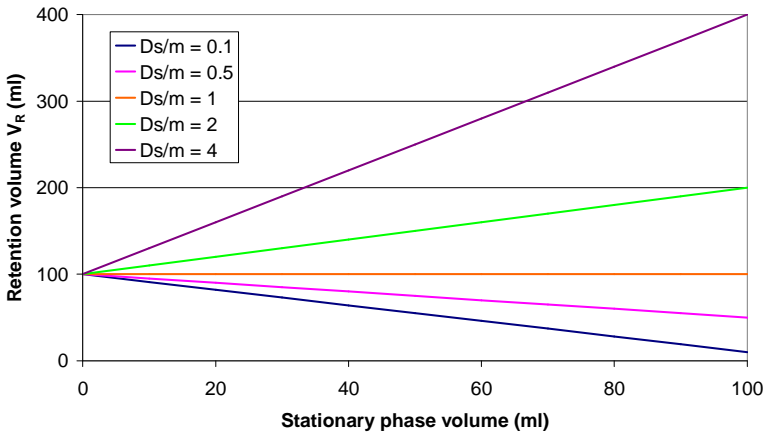


Figure 1-15: Solute retention volume versus the stationary phase volume in a 100 ml CCC coil. [Berthod 2002]

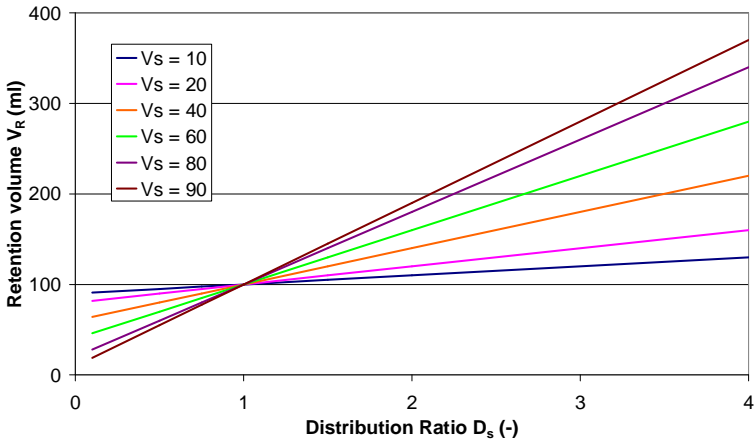


Figure 1-16: Solute retention volume versus the Distribution ratio in a 100 ml CCC coil.

1.3.3 Phase systems used in Counter-current separations

Phase systems are one of the most important parts of the counter-current chromatographic separations. The phase system determines the distribution ratio of the components that need to be separated as is seen for counter-current distribution. For different phase systems the components will show a different affinity for the phases. This means that a phase system should be chosen carefully.

Phase systems are made up of two or more components. These components consist mainly of fluids, however sometimes solids are dissolved into liquids to create a specific phase system. These phase systems range from polar to non-polar. Polar components are attracted to polar phases, and non-polar compounds to non-polar phases. An example of phase systems ranging from polar to non-polar (lipohyphic) is shown in Table 1-1.

Table 1-1: Biphasic liquid systems useful in CCC, sorted by increasing polarity [Renault et al. 2002]

Polarity	No.	Solvents system	Composition
Lipophilic	1	Hexane – ACN	1:1
Lipophilic	2	Hexane – ACN – CHCl ₃	5:5:1
Lipophilic	3	Hexane – EtOH – H ₂ O	6:5:1
Semi-polar	4	Hexane – EtOAc – ACN – MeOH	5:2:5:4
Semi-polar	5	Hexane – EtOAc – MeOH – H ₂ O	1:1:1:1
Semi-polar	6	CHCl ₃ – MeOH – H ₂ O	13:7:2
Semi-polar	7	CHCl ₃ – MeOH – H ₂ O	1:1:1
Semi-polar	8	CHCl ₃ – MeOH – H ₂ O	7:13:8
Polar	9	Toluene – ACN – H ₂ O – EtOH	3:4:3:2
Polar	10	CHCl ₃ – MeOH – H ₂ O (AcOH 0.2 M)	1:1:1
Polar	11	EtOAc – EtOH – H ₂ O	2:1:2
Polar	12	1-BuOH - AcOH – H ₂ O	4:1:5
Polar	13	1-BuOH – EtOAc – H ₂ O	4:1:4

ACN = Acetonitrile, AcOH = acetic acid, EtOH = ethanol, EtOAc = ethyl acetate, MeOH = methanol, 1-BuOH = 1-butanol. Heptane, as a less toxic solvent, can replace hexane with minimum change.

1.4 Literature review

In the early 1960s, Ito's pioneering work in Japan resulted in the first coil planet centrifuge [Ito et al. 1966], which was later known as the I-type centrifuge. It observed how two immiscible liquids on opposite sides of the coil at the start of the experiment would displace in a counter-current fashion when the coil was rotated in the centrifuge. The name Counter-current Chromatography is taken from these first experiments with the coil planet centrifuges and their findings. The early papers describe the performance of this centrifuge. Further research of Ito and co-workers in the USA resulted in centrifuges with different coil orientations. The design, use and performance of one of these configurations, which was later named the J-type centrifuge, was investigated in detail between 1977 and 1980 [Ito and Bowman 1977A, B, 1978; Ito 1980A and B]. The J-type centrifuge can achieve higher stationary phase retention at the same mobile phase flow rate than the I-type centrifuge. This means that the J-type centrifuge can have the same stationary phase retention as the I-type centrifuge when used at a higher mobile phase flow rate which means that a separation can be performed in a shorter time.

1.4.1 Different types of CCC centrifuges

The difference between the J-type and I-type centrifuge is in the driving mechanism and therefore the rotation of the coil as shown in Figure 1-2 [Ito 1981]. For both types the coil axis is parallel to the solar axis. The coil of the I-type centrifuge is driven by pulleys and a belt which makes the rotation in the opposite direction from the rotation around the solar axis. This means that the same point faces the solar axis at all times and the path described by one point on the coil is a circle. In a J-type centrifuge the coil is driven by gears which make the rotation of the coil around its own axis as around the solar axis. The locus of a point on the coil is, as mentioned before, a cardioid.

According to Sutherland [1987] the main benefits of the J-type centrifuge over the I-type centrifuge are:

1. Increased stationary phase retention (up to 90%);
2. Higher mobile phase flow rates with reduced loss of stationary phase retention;
3. Greater stability, allowing the use of lower interfacial tension solvent systems; and
4. Higher capacity, the sequence of mixing and settling is independent of tubing size and hence can be scaled up.

The main benefits described are due to the enhanced “wave mixing” in the J-Type centrifuge compared to the “cascade mixing” in the I-Type centrifuge. Due to the “cascade mixing” the I-Type centrifuge can only achieve maximum stationary phase retention of 50%. These different types of mixing are shown in Figure 1-17 and Figure 1-18 and are due to the different planetary rotor motion of the coil.

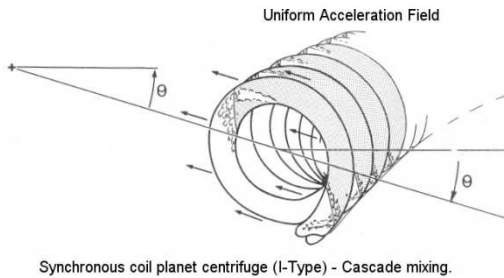


Figure 1-17: Mixing inside I-Type coil planet centrifuge [Sutherland et al. 1987].

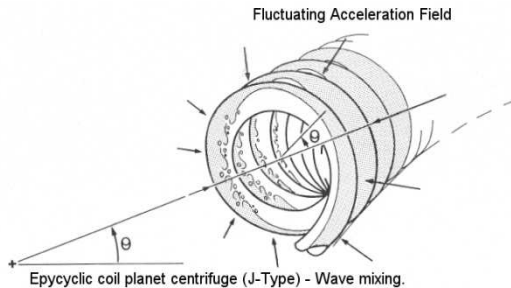


Figure 1-18: Mixing inside J-Type coil planet centrifuge [Sutherland et al. 1987].

After the invention of the J-Type centrifuge in the 1980's with all the described benefits CCC became a popular technique which can be concluded from the strong rise in the number of CCC journal papers being published (Figure 1-19).

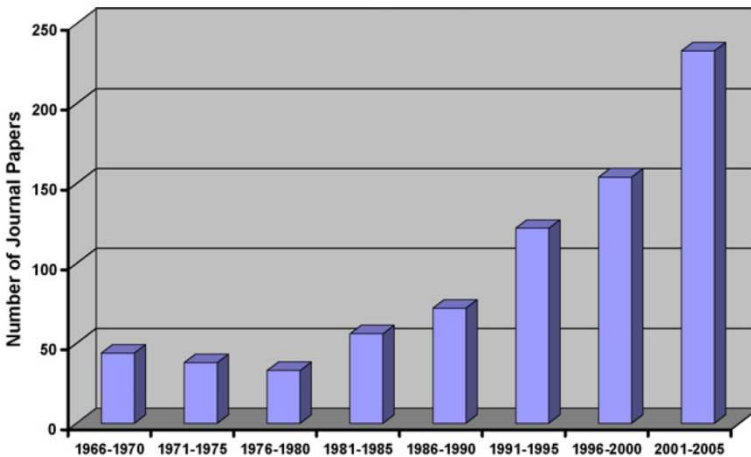


Figure 1-19: Journal publications on Counter-current Chromatography since its invention [Sutherland 2007].

1.4.2 Solvent phase systems

1.4.2.1 Head and Tail study

According to Ito's studies on the hydrodynamic behaviour of solvent systems in High-Speed Counter-current Chromatography the phase systems can be categorized according to their hydrophobicity [Ito 1984]. The upper phase of hydrophobic systems goes to the head of the coil and the bottom phase to the tail. For hydrophilic systems, the lower phase goes to the head and the upper phase goes to the tail. The intermediate phase systems behaviour depends on the centrifugal conditions. Seven years ago Sutherland and co-workers questioned Ito's observations after studying the research conducted by three Dutch placement students under the supervision of

Sutherland and co-workers [2000]. From this study it was concluded that the phase systems should be characterised by physical properties such as density, viscosity and interfacial tension rather than hydrophobicity. It was found that the light phase goes to the head and the heavy phase to the tail for the different phase systems across the hydrophobicity range. They also noted that it was important to have the Archimedean forces and the hydrostatic forces aligned (with the head at the centre). A limitation of the study was the use of β -values > 0.55 and a tube bore of 3.2 mm [Sutherland et al. 2000].

1.4.2.2 Solvent selection

When designing a CCC separation system the selection of the two phase solvent system is the initial and most important stage [Ito 2005]. This also proves to be the most important step in the separation design. Criteria to look at when selecting a solvent system are the polarity of the sample, the sample's solubility, its pH, ability to form complexes and other chemical and physical parameters of the component that could indicate a suitable solvent two phase system. According to [Ito 2005], the first step to take is to study the literature to determine a similar separation and take the described phase system as a starting point. Failing to find a starting point a trial and error method should be undertaken aiming to obtain the distribution coefficients of the components in the sample spread around the value of $D = 1$.

A trial and error method should start with the search of a solvent that dissolves the sample mixture best. Once this solvent is identified a phase system with this solvent should be found. The identified solvent should partition between the phases of the two phase solvent system. Phase systems can consist of two solvents or components, but can also be composed of multiple components. Three component solvent systems can be represented using ternary diagrams. A ternary diagram such as the one shown in Figure 1-20 (for the Butanol, Ethyl Acetate and water phase system) shows a lot of information about the phase systems made from these components.

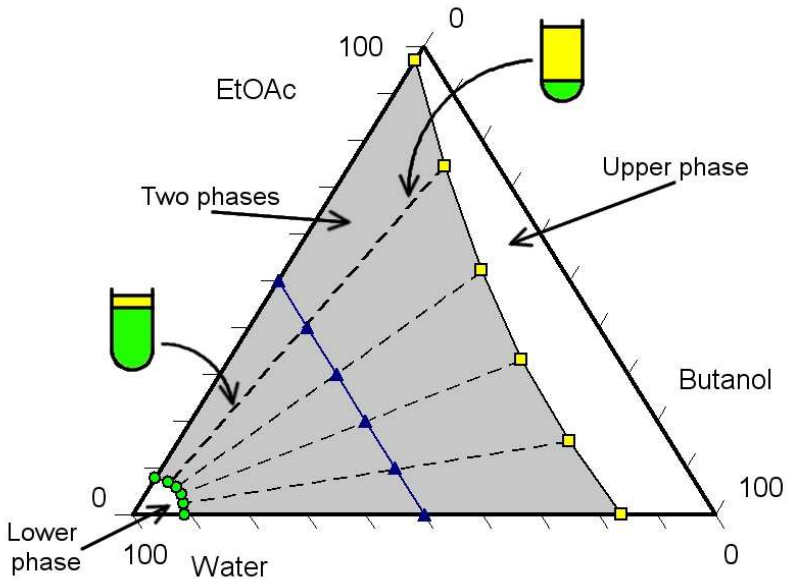


Figure 1-20: Ternary diagram of a Butanol, Ethyl Acetate (EtOAc) and Water phase system. Data taken from [Garrard 2005A].

The ternary diagram shows three regions, two white areas in which the mixtures made from the components have one phase, and a shaded area in which the mixtures made from the components have two immiscible phases. The lines between these regions represent the composition of these two immiscible phases. A ternary diagram is made by making a series of phase systems, for example the six points (triangles) on the blue line. Each layer of the two phases that occur are analysed for their compositions. This results in the two other lines with their six points, the line with the yellow squares represents the upper phase and the line with the green circles represent the lower phase. A tie line connects the upper and the lower phase of one phase system. This means that any phase system made on this tie line will give the same upper and lower phase compositions, the only thing that changes with the location on the line is the phase ratio. As indicated in Figure 1-20 a phase

system made on a tie line near the upper phase line will have more upper than lower phase and a phase system made on the tie line near the lower phase line will have more lower than upper phase. When more of a particular phase is required the ternary diagram could be used to determine the quantity of ingredients to obtain this phase ratio.

Four or more component solvent systems can also be analysed in a similar way. The phase system made from Heptane, Ethyl Acetate, Methanol and Water is a common four-component phase system. Such a system can be analysed by making a tetrahedron, which given that it is a three dimensional image is more difficult to analyse than the two dimensional ternary diagram.

Garrard [2005A] reviewed a large number of papers describing a large number of different two phase systems and ways of selecting an appropriate one. He noted that over 50 different solvent systems were described and that the most favoured solvents were Butanol, Chloroform, Ethyl Acetate (EtOAc), Hexane and Methanol (MeOH). With these components a large number of two phase systems can be made and Garrard [2005A, B] proposed a table with four of the before mentioned solvents making 28 different two phase systems (Table 1-2). It is worth noting that this table was adapted from two phase system ranges described earlier by Camacho-Frias and Foucault [1996] and Oka [1991], but differs in that the Heptane was substituted for the less environmentally "friendly" Hexane. When using natural products it was found that when some or all of the EtOAc in Table 1-2 was substituted with acetonitrile (MeCN) better solubility was obtained.

Table 1-2: Selection table for determining a CCC solvent system. The volumes are in ml to make a 4 ml phase system. [Garrard 2005A and Garrard 2005B]

No	Heptane	EtOAc	MeOH	Butanol	Water
1	0	0	0	2	2
2	0	0.4	0	1.6	2
3	0	0.8	0	1.2	2
4	0	1.2	0	0.8	2
5	0	1.6	0	0.4	2
6	0	2	0	0	2
7	0.1	1.9	0.1	0	1.9
8	0.2	1.8	0.2	0	1.8
9	0.29	1.71	0.29	0	1.71
10	0.33	1.67	0.33	0	1.67
11	0.4	1.6	0.4	0	1.6
12	0.5	1.5	0.5	0	1.5
13	0.57	1.43	0.57	0	1.43
14	0.67	1.33	0.67	0	1.33
15	0.8	1.2	0.8	0	1.2
16	0.91	1.09	0.91	0	1.09
17	1	1	1	0	1
18	1.09	0.91	1.09	0	0.91
19	1.2	0.8	1.2	0	0.8
20	1.33	0.67	1.33	0	0.67
21	1.43	0.57	1.43	0	0.57
22	1.5	0.5	1.5	0	0.5
23	1.6	0.4	1.6	0	0.4
24	1.67	0.33	1.67	0	0.33
25	1.71	0.29	1.71	0	0.29
26	1.8	0.2	1.8	0	0.2
27	1.9	0.1	1.9	0	0.1
28	2	0	2	0	0

Garrard [2005A] described three approaches in which the table can be used. The phase systems made in each approach have the components of interest added. After mixing and allowing each

system to settle both the upper and lower layer of the phase system is analysed. The analysis is commonly done by an analytical chromatographic method like HPLC or GC. In some cases spectrophotometry, thin layer chromatography (TLC) or biological assays are required. The test basically determines the concentration of the component of interest in each phase to calculate the D-value.

The first approach is to make a phase system in the middle of the table. Often phase system number 17 (highlighted in the darker grey shade) is used as a starting point because the makeup is especially straightforward. The compound of interest is partitioned in this phase system, each layer is analysed and the D-value is determined. A new phase system is subsequently chosen from the table depending on the result obtained. This iterative process is repeated until a suitable system is found. A second approach employing this table is to make every 6th system listed, i.e. phase systems 1, 6, 12, 17, 22 and 28 (highlighted in light grey). Again these particular systems are easy to make. After screening with the compound of interest it should be possible to identify which area of the table needs to be focused on. The final and favoured approach described by Garrard [2005A, B] is to make all the systems in the table using an automated method such as a liquid handling robot (LHR) and test them all automatically. A simple study of the results from this approach will allow quick selection of an appropriate system for CCC separation. While the advantages of this approach are clear (reduced time, effort and skill) necessary prerequisites are the availability of appropriate equipment and validated mixing protocols.

Garrard [2005A] analysed both layers of the two phase systems using a GC with both the flame ionisation detector (FID) and thermal conductivity detector (TCD). The results from these experiments gave knowledge about how to make both layers up separately. This could be very useful when significantly more is required of one phase compared to the other [Garrard 2005A]. With these results a ternary diagram can be drawn for phase systems 1 to 6 as is shown in Figure 1-20. Whereas phase systems 6 to 28 resume representation as tetrahedron's (Figure 1-21) which only show surfaces because Heptane and Methanol components and Ethyl Acetate and Water components of each system have the same volumes.

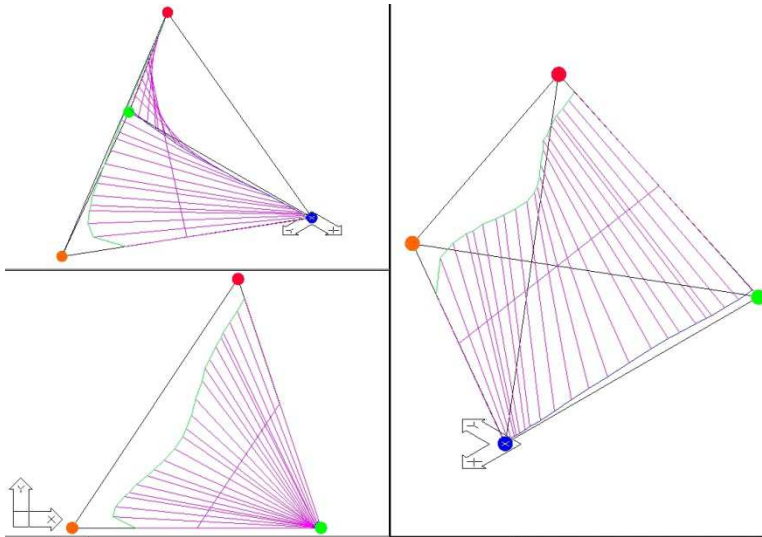


Figure 1-21: Tetrahedron of the analysis done by Garrard on the heptane, EtOAc, MeOH and water phase system. Heptane is orange, EtOAc is green, MeOH is blue and water is red. The upper phase is the blue line (near the blue and green dots) and the lower phase is the green line (on the side of the orange and red dots). Drawn in AutoCAD 2000 by the Author. See Appendix IV for the conversion equations.

Table 1-3: Physical properties of the phase systems made from Heptane, Ethyl Acetate, Methanol and Water respectively [Sutherland et al. 2001].

	Comp	ρ_{LP} kg/m ³	ρ_{UP} kg/m ³	$\rho_l - \rho_u$ kg/m ³	μ_{LP} mNs/m ²	μ_{UP} mNs/m ²	T_i mNm
4A	1.4:0.1: 0.5:1.0	947	679	268	1.36	0.36	17.9
4B	1.4:0.6: 1.0:1.0	938	708	230	1.35	0.35	6.2
4C	1.4:4.5: 1.0:1.0	931	833	98	1.35	0.42	1.0

A series of phase systems across the hydrophobicity range were developed around 2000 and described by Sutherland and co-workers [2000, 2001]. These phase systems are also made up of heptane, EtOAc, MeOH and water, are well characterised and have been used in many different projects and applications at the Brunel Institute for Bioengineering (BIB). Table 1-3 shows the composition and other characteristics of this phase system series.

Table 1-4: Basic screen compositions [Dubant 2007]. The last column indicates whether the upper phase (UP) is either organic (org) or aqueous (aq).

	Heptane	EtOAc	DCM	MeOH	H ₂ O	UP
EtOAc						
A	25.0%	25.0%	0.0%	37.5%	12.5%	Org
B	37.5%	12.5%	0.0%	37.5%	12.5%	Org
C	12.5%	37.5%	0.0%	25.0%	25.0%	Org
D	25.0%	25.0%	0.0%	25.0%	25.0%	Org
E	25.0%	25.0%	0.0%	25.0%	25.0%	Org
F	37.5%	12.5%	0.0%	25.0%	25.0%	Org
G	12.5%	37.5%	0.0%	12.5%	37.5%	Org
H	25.0%	25.0%	0.0%	12.5%	37.5%	Org
I	37.5%	12.5%	0.0%	12.5%	37.5%	Org
DCM						
A	25.0%	0.0%	25.0%	37.5%	12.5%	Aq
B	37.5%	0.0%	12.5%	37.5%	12.5%	Org
C	12.5%	0.0%	37.5%	25.0%	25.0%	Aq
D	25.0%	0.0%	25.0%	25.0%	25.0%	Aq
E	25.0%	0.0%	25.0%	25.0%	25.0%	Aq
F	37.5%	0.0%	12.5%	25.0%	25.0%	Org
G	12.5%	0.0%	37.5%	12.5%	37.5%	Aq
H	25.0%	0.0%	25.0%	12.5%	37.5%	Aq
I	37.5%	0.0%	12.5%	12.5%	37.5%	Org

A statistical approach using a table of five components making a total of 18 phase systems was developed at Pfizer Ltd. by Dubant [2007]. These 18 phase systems are shown in Table 1-4. The top half of the table (from EtOAc-A to EtOAc-I) differs from the bottom half in that EtOAc is used instead of Dichloromethane (DCM). These phase systems were all made either using a liquid handling robot

(LHR) or manually and the D-values of the components were determined. The ideal phase system was identified by entering the results from either the EtOAc or the DCM series into a statistical package (Statgraphics) [Dubant 2007]. This programme then analyses the results from the designed experiment and predicts the phase system that would give $D=1$. Dubant has also identified an extended list of solvents that can be used (Table 1-5) when those shown in Table 1-4 fail (insufficient selectivity, poor solubility) to produce an appropriate phase system.

Table 1-5: Solvents used in the extended screen divided into the solvents which go into the aqueous and organic phase [Dubant 2007].

Aqueous phase components	Organic phase components
Water (H ₂ O)	Heptane
MeOH (Methanol)	Toluene
MeCN (Acetonitrile)	EtOAc (Ethyl acetate)
Acetone	DCM (Dichloromethane)
DMF (Dimethylformamide)	TBME (tert-butyl methyl ether)
	Butanol
	MEK (Methyl ethyl ketone)

The phase systems in the extended screen consist of four components of equal volume: two components from the aqueous side of Table 1-5 (water and another component) and two components from the organic side of the table (Heptane or Toluene and another component). In this way every possible combination is made, which gives a total of 40 different phase systems.

1.4.2.3 Modes of operation

As is discussed in Section 1.3.2 and shown in Figure 1-9, either the non-polar (mostly upper and organic) phase or the polar (mostly lower and aqueous) phase can be used as the mobile phase, while the other phase is stationary. To reiterate, these modes of operation

are called “Normal Phase Mode” when the organic phase is mobile and “Reverse Phase Mode” when the aqueous phase is mobile. Recently a number of new modes have been described and investigated. In these, both phases are pumped into the coil either simultaneously or alternately [Berthod and Hassoun 2006]. When both phases are pumped in simultaneously in opposite directions through the coil, it is called “Dual Flow CCC” (DFCCC) or “Continuous Counter-Current Extraction” (CCCE). This technique has been investigated in the present PhD thesis. Other modes are “Co-current CCC” where both phases are flowed simultaneously in the same direction (originally suggested by Sutherland et al. [1984]), “Simulated Counter-Current Extraction” (SCCE) where normal and reverse phase flow modes are alternated and Elution-Extrusion CCC (EECCC) where after the elution of some components the remaining coil contents are extruded. These modes are summarised in Table 1-6 and some are discussed in the following section.

Table 1-6: Summary of the different modes of operation of the CCC centrifuge.

Dual Flow CCC (DFCCC) or Continuous Counter-current Extraction (CCCE)	Both phases flow through the coil simultaneously into the direction they want to go.
Co-current CCC	Both phases flow through the coil simultaneously into the same direction.
Dual Mode CCC (DMCCC) or Simulated Counter-current Extraction (SCCE)	Alternating between Normal and Reverse phase mode, switching between phase and its direction.
Elution-Extrusion CCC (EECCC)	Normal or Reverse phase CCC where after the elution of some components the coil contents is extruded.

1.4.2.4 The liquid nature of the Stationary Phase

From 1998 Berthod and co-workers started describing ways of operating a CCC centrifuge which cannot be done with a conventional chromatographic method employs solid stationary phase supports. The liquid nature of the stationary phase in CCC

was used to prevent band broadening which happens in any chromatographic method. Three main ways of doing this were identified by Berthod and his co-workers [2003].

The first one is Dual Mode CCC (DMCCC) which, like SCCE, is a discontinuous mode of operation. At first the separation is performed as conventional CCC (shown in Figure 1-22 A to D) and then at a certain point the roles of the two liquids are reversed. The mobile phase becomes stationary and the stationary phase become mobile which is pumped in from the opposite end (as shown in Figure 1-22 E). To switch over the mobile phase pump will need to be stopped, not the rotation, and the pump with the new mobile phase needs to be started. The main advantage of the method is the quickness of the separation. [Berthod et al. 2003]

Another way of using the liquid nature of the stationary phase is Elution-Extrusion CCC (EECCC). For this mode of operation the separation is performed as for conventional CCC (Figure 1-22 A to D) and then at a certain point the flow of the mobile phase and the rotation are stopped and stationary phase is pumped into the coil to extrude the coil contents (Figure 1-22 F). The advantages of this technique is that the separation is faster, the peaks are sharper compared to classical elution methods and the coil is ready for the next experiment given that fresh stationary phase has been used to extrude the coil contents [Berthod et al. 2003].

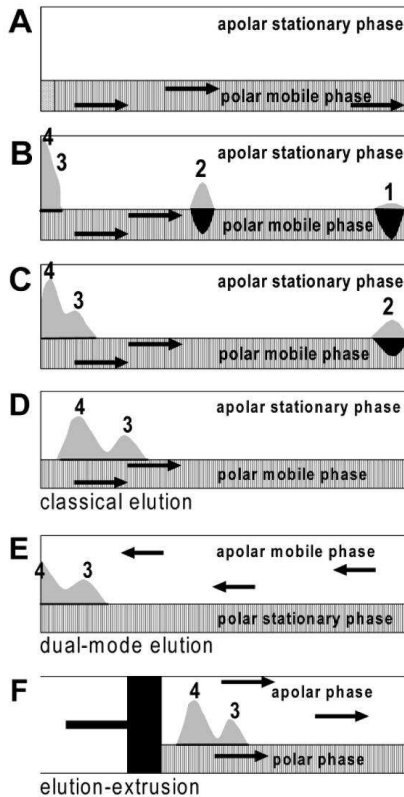


Figure 1-22: A to D shows the motion of a four component mixture in classical CCC. (A) is the start; (B) shows 1 and 2 well separated from 3 and 4; (C) shows that 1 has eluted and 2 is about to elute; (D) shows that 2 has eluted and 3 and 4 start to become separated; (E) shows the dual-mode elution where the apolar phase now is the mobile phase and (F) illustrates Elution-extrusion where at a certain point in the separation both phases are extruded out of the coil. [Berthod et al. 2003]

A third option developed by Berthod and Hassoun [2006] is a chromatographic method in which both the mobile and the stationary phase move in the same direction. The slowly moving stationary phase ensures that no component will be retained in the coil. Even

the most retained compound will partition to the stationary phase and will eventually elute with this phase. This mode of running a CCC centrifuge is called Co-current CCC [Berthod and Hassoun 2006]. The main advantages of this mode of operation would be a faster separation compared to conventional elution modes, less solvent and phase system use and less band broadening.

1.4.3 CCC and CCD models

This section describes some of the existing CCC and CCD models. To do this some of the chromatographic theory concerning calculated and predicted peak shapes is reviewed. In 1941 Martin and Synge described the first theory of column chromatography considering it to be analogous in operation to that of distillation and extraction fractionation columns [Martin and Synge 1941]. The mass fraction (MF) of the component can be worked out at any time and at any place in the column. Although is designed for two liquid phases, the theory uses distillation column principles. Each theoretical mixing and settling zone is represented by a plate (p) (numbered from $p = 1$ to $p = p$) and the height of this plate (h) is called the "height-equivalent-to-a-theoretical-plate" (H.E.T.P.) which was first described by Peters [1922]. These theoretical plates are equivalent to the test tubes in CCD and this theory was later referred to as Martin and Synge Distribution (MSD). The following equation describes the quantity of the component in each plate.

$$\left(\left(1 - \frac{\partial v}{V} \right) + \left(\frac{\partial v}{V} \right) \right)^n = 1 \quad \text{Equation 1-18}$$

where ∂v is the part of mobile phase passed through; n is the number of ∂v that have passed through; v is the volume of solvent used to develop the chromatogram; V is the volume in the plate calculated as $(V = h(A_L + \alpha A_S))$; A_L is the area of cross section of mobile phase; A_S is the area or cross section of non-mobile phase; and α is the distribution coefficient (concentration of the component in the non-mobile phase over the concentration of the component in the mobile phase).

The fraction of component in each plate is a term of the binominal expansion of this equation in which the left hand side describes the quantity staying in the plate and the right hand side describes the quantity moving to the next plate. This equation can be solved using the binominal theorem to give

$$MF_{r+1} = \frac{n!}{p!(n-p)!} \cdot \left(1 - \frac{\partial v}{V}\right)^{(n-p)} \cdot \left(\frac{\partial v}{V}\right)^p \quad \text{Equation 1-19}$$

which can calculate the quantity of the component at any plate at any step without having to calculate the previous steps or plates. Using Stirling's approximation on factorials Martin and Synge [1941] simplified the equation to

$$MF_{r+1} = \frac{1}{\sqrt{2 \cdot \pi \cdot p}} \cdot \left(\frac{v}{p \cdot V}\right)^p \cdot e^{p \cdot \frac{v}{V}} \quad \text{Equation 1-20}$$

Equation 1-20 is only valid when n and p are large numbers (p > 10).

Later Williamson and Craig [1947] proposed a theory on CCD which described how theoretical curves could be calculated. This theory is based on the distribution of the component between the two liquid phases and in common with Martin and Synge also uses binominal expansion of the obtained equation. In basic form it is a simplified version of the Martin and Synge column chromatograph theory given that a greater number of assumptions are made for the CCD process. The extra assumptions that Williamson and Craig made are that the volumes of the upper and lower phase in the tube (p), previously called the plate, are equal and that all the upper (mobile) phase is moved from one tube to the next. With these assumptions both Equation 1-19 and Equation 1-20 can be rearranged to give the following expressions.

$$\left(\left(\frac{1}{D+1}\right) + \left(\frac{D}{D+1}\right)\right)^n = 1 \quad \text{Equation 1-21}$$

$$MF_{n,p} = \frac{n!}{p!(n-p)!} \cdot \left(\frac{1}{D+1}\right)^n \cdot \left(\frac{D}{1}\right)^p \quad \text{Equation 1-22}$$

Williamson and Craig [1947] also proposed the use of the normal distribution function for the prediction of the amount of component inside each tube in a CCD process. Abraham de Moivre [1756] defines the normal distribution as:

$$f(x) = \frac{1}{\sigma \cdot \sqrt{2\pi}} \cdot e^{-\frac{(x-\mu)^2}{2\sigma^2}} \quad \text{Equation 1-23}$$

where x is the location (tube number) of the fraction calculated; σ is the standard deviation; and μ is the location (tube number) of the maximum fraction.

From Williamson and Craig [1947] the fraction of the component in the tubes is calculated using the normal distribution equation is:

$$MF_x = \frac{1}{\sqrt{2\pi \cdot \frac{D}{(D+1)^2} \cdot n}} \cdot e^{\frac{-x^2}{2 \cdot \frac{D}{(D+1)^2} \cdot n}} \quad \text{Equation 1-24}$$

where n is the number of transfers, and x is the number of tubes between the one in question and the tube with the maxima ($p - \mu$). The calculation of the tube with the maxima is described by Craig [1944] and using this x-value can be calculated using the following equation.

$$x = p - \frac{D}{D+1} \cdot n \quad \text{Equation 1-25}$$

In Equation 1-24 the standard deviation, which is needed to describe the normal distribution, is described as:

$$\sigma = \sqrt{\frac{D}{(D+1)^2} \cdot n} \quad \text{Equation 1-26}$$

The equation from the binominal theorem and its approximation using the normal distribution are compared using Microsoft Excel. With number of steps (n) equal to the total number of tubes and

D=0.5 the graph shown in Figure 1-23 was produced. Note that the approximation using the normal distribution and binominal theorem equations give the same result.

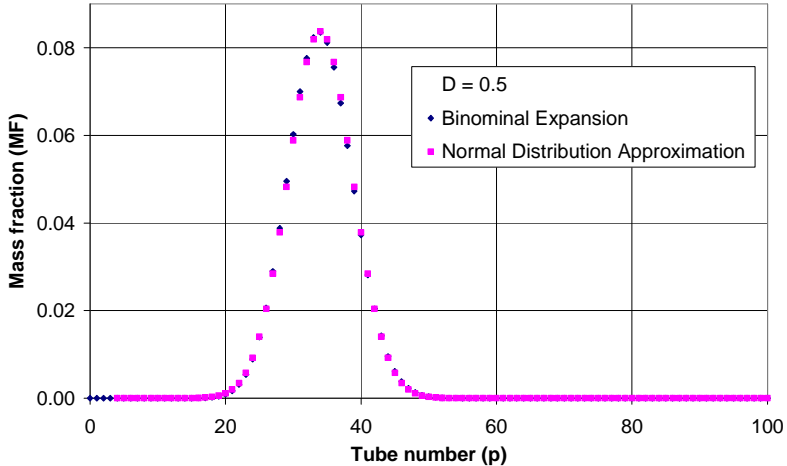


Figure 1-23: Comparison of the binomial expansion Equation 1-22 and the normal distribution approximation Equation 1-24. The latter uses Equation 1-25. This comparison uses 100 tubes and is also made in by Williamson and Craig [1947].

Nichols [1950] took Craig [1944] and Williamson and Craig [1947] equations and determined a new set to work out the number of transfers required to give an experimentally detectable difference. In his work Nichols shows that the distance between the maximum and the intercept of the peak should be 1.22 times the standard deviation for the difference to be experimentally detectable. This results in Equation 1-27 where the number 2.44 is the number of standard deviations between the peak maximums.

$$n = \left[\frac{2.44 \cdot \sqrt{D_a} \cdot (1 + D_b)}{D_b - D_a} \right]^2 \quad \text{Equation 1-27}$$

Figure 1-24 shows the separation of two components (a and b) with the number of transfers (n) suggested by Equation 1-27, i.e. 24.

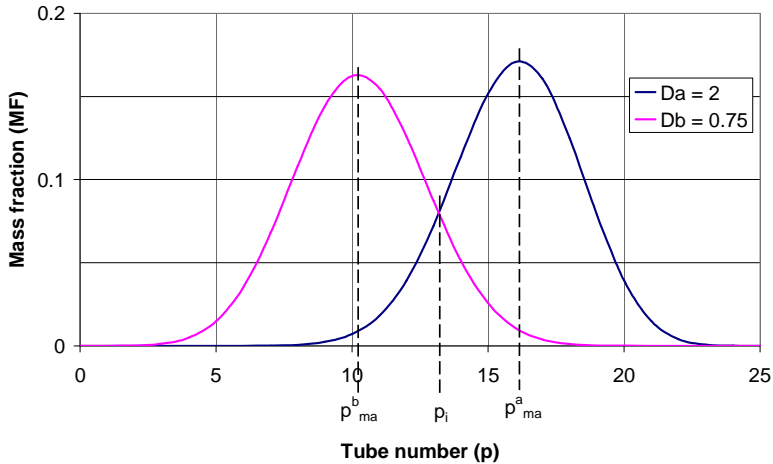


Figure 1-24: Theoretical separation of two components using 24 transfers to reach experimentally detectable difference. The Resolution, R_s , between the two peaks is 0.61.

The resolution of the two peaks is calculated from Equation 1-28.

$$R_s = \frac{2(V_{R2} - V_{R1})}{W_1 + W_2} = \frac{2 \cdot (2.44 \cdot \sigma)}{8 \cdot \sigma} = 0.61 \quad \text{Equation 1-28}$$

The peaks in Figure 1-24 are not fully resolved. This is because the criteria Nichols [1950] employed were that the difference should be experimentally detectable, not fully resolved. As was mentioned earlier, the criteria for baseline separation are that there should be 6 standard deviations between the peak maximums. When this is taken into account Equation 1-27 is modified to:

$$n = \left[\frac{6 \cdot \sqrt{D_a} \cdot (1 + D_b)}{D_b - D_a} \right]^2 \quad \text{Equation 1-29}$$

Using Equation 1-29 it is possible to work out the number of transfers required to achieve baseline separation or alternatively if the resolution is known from graphical determination, the number of transfers done can be worked out. Figure 1-25 shows that at least 142 transfers are required to achieve baseline separation.

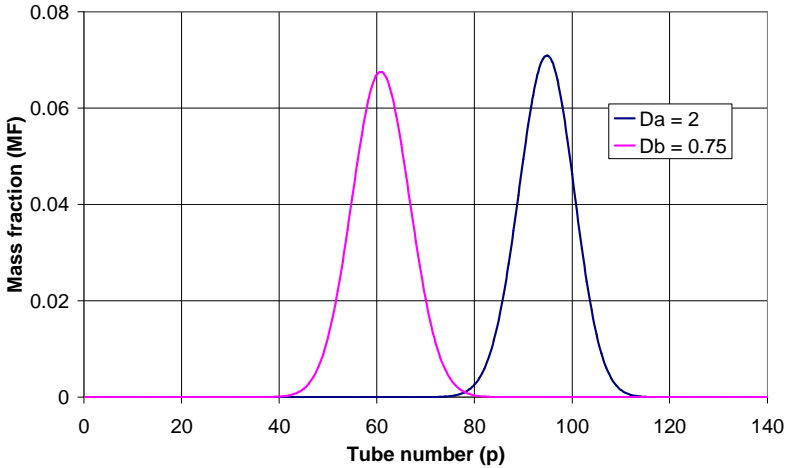


Figure 1-25: Theoretical separation of two components using 142 transfers reaching baseline separation. The resolution between the peaks (R_s) is 1.5.

Mandava and Ruth [1988] asserted that the Williamson and Craig binominal expansion could be applied for situations where the volumes of the phases in the tubes are not equal. To apply the binominal expansion the D-value in the equation should be multiplied by the ratio of the volumes of the phases in the tube. This ratio (X) is defined as the volume of the upper phase in the tube over the volume of the lower phase. The binominal expansion then becomes as follows.

$$\left(\left(\frac{1}{X \cdot D + 1} \right) + \left(\frac{X \cdot D}{X \cdot D + 1} \right) \right)^n = 1 \quad \text{Equation 1-30}$$

The theory and models described so far only calculate the peak shape and resolution of the components inside the test tubes or the

number of theoretical plates. When the CCD process is executed to the point where all the tubes have been transferred with mobile phase transferred into i.e. when $n = p$, the process is known as “fundamental distribution”. In this fundamental distribution process no component elutes, but when it is continued in the same manner mobile phase starts eluting from the last tube and carries the component out of the process with it. This is called “single withdrawal” and was first described by Craig and Craig [1956] and subsequently by many others.

Counter Double Current Distribution (CDCD) described by Post and Craig [1963] is a modified CCD process. In CDCD both liquid phases are transferred simultaneously between the tubes in opposite directions. The feed of the sample mixture enters the train of tubes in the middle. Post and Craig described that when both phases with component from one tube are moved out to the next tubes in opposite directions this initial tube ends up with no component in its phases. A schematic representation of this is shown in Figure 1-26.

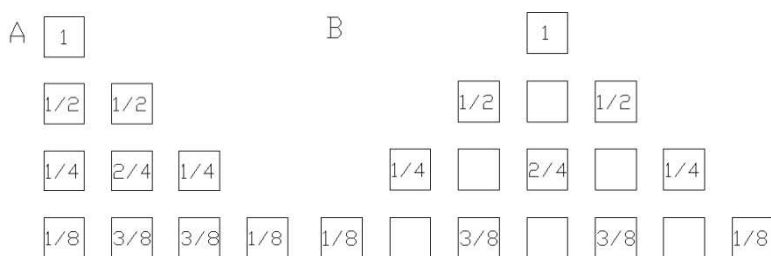


Figure 1-26: Distribution scheme for CCD (A) and CDCD (B). Adapted from Post and Craig [1963].

For CDCD it can be seen that the tubes alternate between those with component present and those without. When drawn in the form of a graph of the component in the tubes, the peaks would spike between the tubes. A device to perform CDCD separations was described by Post and Craig [1963] and model separations were performed with it so as to test the CDCD theory. These experiments showed that the transfers were not 100% perfect, i.e. a small amount of component

found its way into alternate tubes. Despite this, it was shown that the model separation corresponded closely with the calculated values obtained using the binominal expansion.

Approximately 5 years ago Sutherland and co-workers [2003] made a programme for Craig and Potts [1949] Eluting CCD model. This modelling program was written in Delphi 3 (a visual Pascal programming language for Microsoft Windows) and is called CHES, which stands for Chromatographic Experiment Simulation System. The interface of this modelling program is simple; the user enters the D-values of two components, the number of tubes, the number of steps and the retention of the stationary phase. When the program is run to calculate the separation this produces a graph showing the chromatogram of the eluted components and the components inside the coil in each phase. The program also calculates the peak position, peak height, peak width and the resolution between the two eluted peaks. By default the program runs in “step mode” where the peaks are displayed as they elute (the first eluting peak on the left and the second on the right), but this can be changed into “time mode” where the chromatogram will have a time/volume scale (with the first eluted peak on the left). In time mode the program calculates the number of theoretical plates (N) equivalent to the separation. A screenshot of the program separating two components with D-values of 0.5 and 2 in a column with stationary phase retention of 50% is shown in Figure 1-27. A new enhanced version with more functions is currently being created and will be released soon (J. De Folter, personal communication).

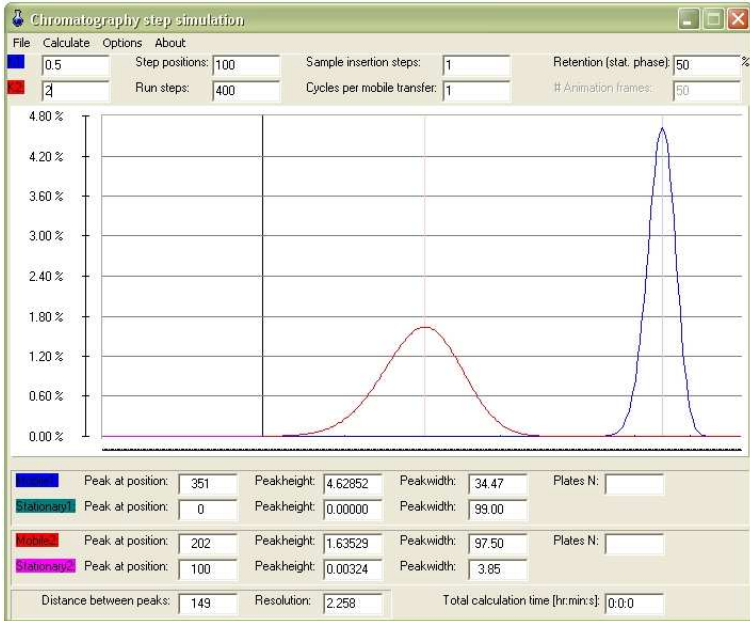


Figure 1-27: Screenshot of the CCD modelling program CHES separating two components with D -values of 0.5 and 2 with a stationary phase retention of 50%. [Sutherland et al. 2003]

Kostanian [2002] described two complex mathematical models on CCC using a chemical engineering approach for modelling of mass transfer processes. These two models (Figure 1-28) are the ideally mixed cell model and the diffusion longitudinal mixing model. Kostanian points out that in typical models, such as the Craig model, only the motion of the mobile phase is considered. For CCC this is not entirely valid given that the stationary phase is a liquid as well, and the dispersion of the solute in this phase should be included. Kostanian compares the two models to determine the effect of the liquid stationary phase.

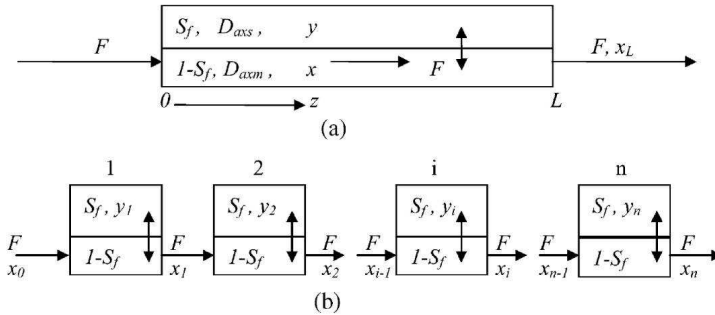


Figure 1-28: Schematic diagram of A) the diffusion longitudinal mixing model and B) the ideally mixed cells model. In the diagram S_f is the stationary phase retention, D_{axm} and D_{axs} are the diffusion coefficients in the mobile and stationary phase respectively, x and y are the substance concentration in the mobile and stationary phase respectively, F is the flow rate, L is the length of the coil and n is the number of cells in the model. [Kostanian 2002, Kostanian et al. 2004]

Kostanian and co-workers [2004] tested the cell model of longitudinal mixing introduced earlier by Kostanian [2002] and showed that the peak shape of a solute with a given D -value can be predicted from experimental data on other solutes.

1.4.4 Dual flow CCC

The origins of Dual flow CCC come from Foam CCC separations. Foam separations have been used to separate a variety of substances. In the mid 1970's Ito and Bowman [1976] described a new method for foam separation using a flow through centrifuge. Rhodamine B in a mixture with Lauryl Sulphate and a NaCl solution was successfully isolated using Nitrogen as the gas stream. This was the basis for Foam and Dual CCC separations. Later Ito [1985] described Foam CCC in detail using a Dual CCC system with a J-type centrifuge possessing a revolutionary radius of 20 cm. The coil consists of a 10 m long PTFE tube with a 2.6 mm internal diameter (ID) wound in two layers on a holder with a diameter of 12.5 cm. This gives a coil with a capacity of 50 ml and a Beta value (β) range of 0.32-0.34. There are five tubes, the feed and collection lines,

going to and fro from the coil as shown in Figure 1-29 and Figure 1-30.

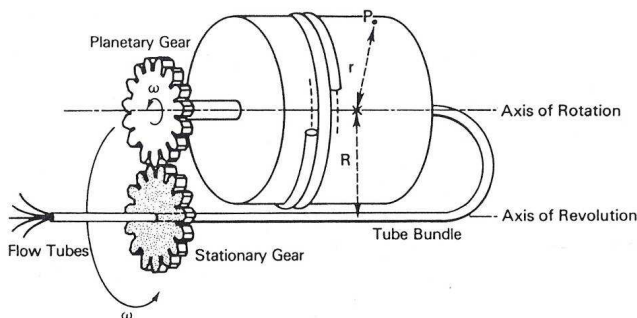


Figure 1-29: J-Type centrifuge with five flow tubes [Ito 1985]

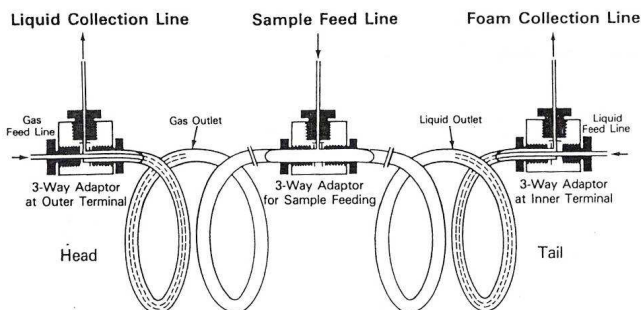


Figure 1-30: Layout of the five flow channels on the Foam CCC column [Ito 1985]

Foam CCC was applied for a separation of rhodamine B and Evans Blue and for a preliminary separation of bovine serum albumin (BSA) and sheep haemoglobin [Ito 1985]. Bhatnagar and Ito [1988] studied the effect of additives on the foam separation using the same centrifuge and coil that was used in an earlier study [Ito 1985]. Lee et al [1988] first described dual flow CCC using the same centrifuge but with a multilayer coil of PTFE tubing with a 1.6 mm ID and capacity of 400 ml. Again in common with the Foam CCC column in Figure 1-30 there are five flow channels, but the gas feed and foam

collection lines became the liquid feed and collection lines respectively. The phases are pumped into opposite directions through the coil. The flow of these phases is aided by the hydrodynamic and hydrostatic forces due on the liquids to the rotation. Sutherland [2000] showed that the light phase goes to the head and the heavy goes to the tail. This means that the heavy phase goes in at the head and the light phase goes in at the tail of the coil. The focus of Lee and co-workers [1988] study was on the separation of natural products and synthetic intermediates. These separations were performed at a rotational speed of 450 rpm and are shown in Table 1-7.

Table 1-7: Separations described by Lee et al [1988].

Sample	Phase System	Flow rate
Biphenyl (50 mg) Indole (30 mg) Indole-3-acetic acid (25 mg)	Pentane, Ethanol and Water (5:4:1)	1.5 ml/min for both phases
Synthetic Intermediates (250mg)	Hexane, Ethanol and Water (6:5:4)	2.0 ml/min for both phases
Steroid mixture of five components with various functional groups (120mg)	Hexane, Ethyl Acetate, Methanol, Water (6:5:5:5)	1.8 ml/min for both phases
Steroid mixture of nine components with identical tetracyclic ring skeletons (225mg)	Hexane, Ethyl Acetate, Methanol, Water (6:5:5:5)	1.8 ml/min for both phases

In later work Lee [1991, 1996] described three different Dual Flow CCC separations using a coil wound with 2.6 mm ID PTFE tubing and a capacity of 400 ml. The separations described are shown below and are all performed at the same flow rate of 2.0 ml/min.

Table 1-8: Separations described by Lee [1991, 1996]

Sample	Phase System
Crude ethanol extract of Schisandra rubriflora Rhed et Wils (125mg)	Hexane, Ethyl Acetate, Methanol, Water (6:5:5:5)
Mixture of Boswellic carterii extract (400mg)	Hexane, Ethanol, Water (6:5:1)
Crude [2-D-Penicillamine, 5-D-Penicillamine] enkephalin (DPDPE) (500mg)	n-Butanol (0.1% trifluoroacetic acid (TFA)), Water (0.1% TFA) (1:1)

Yuko Ito and co-workers [2006] reported on some new Dual Flow CCC research proposing a theory predicting the solute retention time of the components separated using DFCCC. For this theory it was assumed that the phases distribute evenly throughout the coil. The equation to calculate the solute retention time is given by:

$$t_R = \frac{D \cdot V_U + V_L}{Q_L - D \cdot Q_U} \quad \text{Equation 1-31}$$

According to this theory the direction of elution depends on the sign of the denominator. When it is positive the solute is carried by the lower phase from the head to the tail and when it is negative it is carried by the upper phase from the tail to the head of the coil. The solute remains in the coil when the denominator is zero, i.e. when $D \cdot Q_U = Q_L$. When $Q_U = Q_L$ the solute with a D-value of 1 will remain in the coil [Ito et al. 2006].

This theory was tested using several synthetic dyes and it was found that the actual solute retention time was different from the theoretical determined value. The research discussed in this thesis and in van den Heuvel and Sutherland [2007] (see Appendix VI) attempts to supply a reason for this difference.

1.4.5 Other “Continuous” techniques

There is another “continuous” chromatographic technique that is currently used by industry. This technique is called Simulated Moving Bed (SMB) chromatography (which originated from True Moving Bed (TMB)) and is mainly used for larger scale preparative or production separations [Barker and Ganetsos 1992]. SMB uses an array of solid phase support columns connected by switching valves to simulate the movement of the solid support in opposite direction from the mobile phase flow. The following figure shows a schematic four-zone SMB representation.

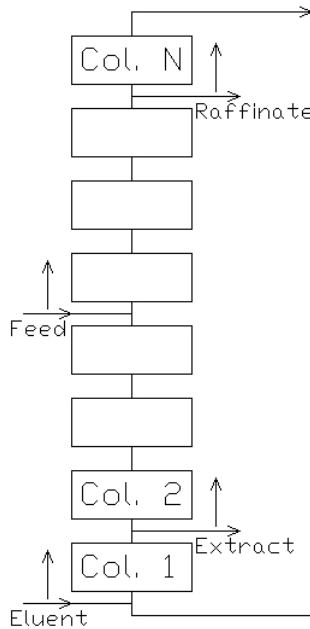


Figure 1-31: Schematic representation of a four-zone SMB system [Charton and Nicoud 1995].

To simulate the counter current flow, the feed, eluent, extract and raffinate lines are all moved one column forward in the fluid flow direction at fixed time intervals [Charton and Nicoud 1995]. In TMB both the liquid mobile phase and the solid stationary phase is moved.

This requires complicated installations and gives many complications.

1.5 Objectives of this thesis

The background and basic theories of Column Chromatography and CCC were introduced in this chapter. In both of these techniques there is a stationary phase in the column, which is either solid or liquid, and a liquid mobile phase which flows through it. The different interaction between components carried with the mobile phase causes them to be separated. In Dual Flow CCC, where both phases flow in opposite direction, the sample mixture is introduced in the centre of the coil and a component or a family of components is carried one direction while the remaining components are carried the opposite direction. This technique has been used with a gas/liquid phase systems (Foam CCC) and with liquid/liquid phase systems (Dual Flow CCC). Current scientific literature does not give any reason why Dual Flow CCC could not provide more efficient separations. To date, practical demonstrations of this have not been forthcoming. Accordingly, the main objective of this thesis has been to investigate the feasibility of Dual Flow CCC by performing retention studies and industrial relevant separations. At the outset of this project the following two research questions were raised:

- Is Dual Flow CCC (or CCCE) feasible and attractive for the pharmaceutical industry?
- What are the mechanics of Dual Flow CCC?

Chapter 2 Methods and Materials

2.1 Outline

This chapter describes the methods and the materials used for the experiments performed in this thesis. This is done in three sections, which each describing the equipment, how the equipment is set-up and the method for the series of experiments performed. In the first section, the preparation of the phase systems is described. The second section describes the set-up and the methods used for the photographic visualisation studies that were performed at Brunel University. The last section describes the set-up and the methods used for the application studies on the process scale CCCE centrifuge at Pfizer.

2.2 Preparation of Phase Systems

The phase systems used for the experiments described in this chapter are prepared by the following method which has been adapted from Wood [2002].

1. From the component ratio the amount of liquid needed for each component was calculated. For example, when the component ratio is 4/1/4 parts and a total of 9 L of solvent system is to be made up, 4 L of the first component would be used followed by 1 L of the second component and finally 4 L of the third component.
2. The required volume of each component was measured out in a separate clean measuring cylinder. These volumes were adjusted to the desired volume of each component with a pipette. When too much of a component was used, the component was disposed of in a waste container.
3. A large stainless steel or glass funnel was used to pour each component into the appropriate container. For example a 10 L aspiration flask. The funnel was removed and bung was placed in the opening of the flask. To ensure that both phases were mixed thoroughly the flask was carefully shaken.

4. The phase system was left for a minimum of 4 h to equilibrate before it was used. When the phases were equilibrated they were separated using a separating funnel into two separate containers. Before the separated phases were ready to be used they were degassed using a sonicator for a minimum of 0.5 h. After this the phase system was ready to be used.

If the composition of each phase is known, or can be easily worked out, it might be more beneficial to make the phases separate as the desired amount of each phase can be made and no unnecessary waste is created. The procedure for making the phases separately is the same as steps 1 to 4 above except that there will be no need to separate the phases.

2.3 Photographic rig set-up and Methods

The photographic rig was used for retention studies. This rig is built around a specially designed CCC centrifuge where the covers are made of Perspex and the coil is cantilevered forward so that the liquids inside the coil can be seen from outside the centrifuge. This centrifuge is called the Cantilever centrifuge. The volumes of the liquids were determined at equilibrium and pictures of the liquids in the coil at equilibrium were made to study the phase distribution. Parts of the set-up and method described in this section were previously published in a special issue of *Journal of Chromatography A* related to the conference proceedings of CCC 2006 [van den Heuvel and Sutherland 2007].

2.3.1 Experimental CCCE Centrifuge

The experimental CCCE coil is installed in a special centrifuge. This centrifuge has both the axis for the coil and the counterbalance extended so that the coil and the counterbalance can be seen through the Perspex front cover. Visualisation of the liquids inside the coil is possible because the spiral CCCE coil also has a Perspex front cover and the tubes are transparent. Special dyes, Sudan Blue and Procion Brilliant Yellow described by Wood [2002], are used to create a contrast between the two liquid phases. The rotating coil was visualised using stroboscopic light (with a stroboscope 15kA from Strobe Automation Ltd.) triggered to the rotation of the rotor of

the centrifuge. This created a still image of the coil at the top position which was photographed with an Olympus SP-500 digital camera.

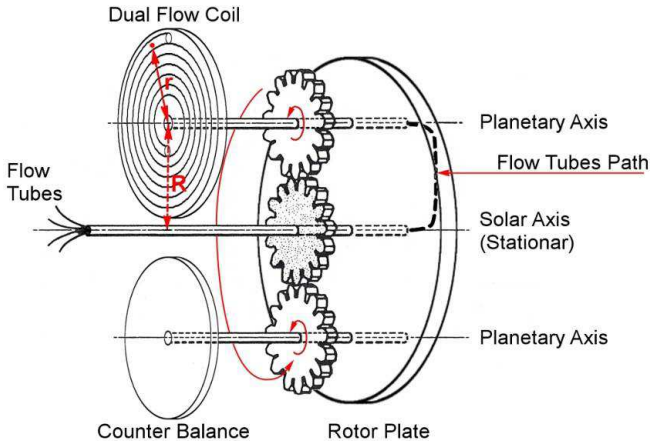


Figure 2-1: Schematic diagram of the Cantilever centrifuge showing the special Dual Flow coil, the counterbalance and the path of the flow tubes. [van den Heuvel and Sutherland 2007]

The CCCE coil is made of 2.2 m clear PTFE tubing with an internal diameter of 5 mm. This tubing is wound on an aluminium disk in 5.5 loops to create a spiral coil with an internal volume of 42 ml. The distance between the planetary axis and centre of rotation (R) is 101.6 mm (4 inch) and the β -value (Equation 1-4) of the coil on this centrifuge ranges from 0.55 to 0.85. At each end of the coil special end fittings with two connections each allow the inlet and outlet for each end to be connected. These special end fittings allow the inlet tube to be extended into the coil for one complete turn at the centre (35 cm) and half a turn at the periphery (25 cm). A schematic diagram of the special centrifuge with the CCCE coil installed is shown in Figure 2-1.

2.3.2 Experimental Rig Set-up

The tubes emerging from the centrifuge are connected to pumps and valves. Two pumps, one Knauer K-1800 with 250 ml heads and one

Dynamax SD-1 with 200 ml heads, were used for pumping upper and lower phase respectively through the coil and the system. On/Off Valves and Four way/Two channel valves from Upchurch were used to connect the pumps to the centrifuge and to direct the liquid flow along the desired path. Figure 2-2 shows the connection between the coil, pumps and valves which are shown in the run position.

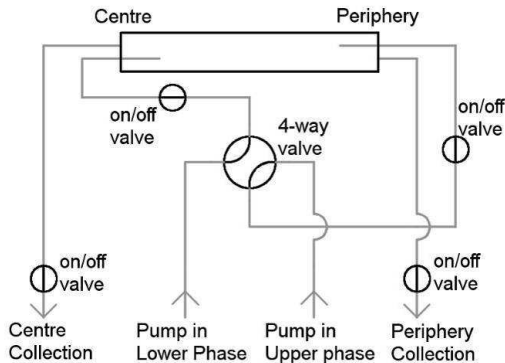


Figure 2-2: Schematic set-up of the CCCE centrifuge with the two pumps and valves connected. The valve position shown is for the set-up in dual flow run mode. [van den Heuvel and Sutherland 2007]

The set-up was built in a dark room to ensure only the stroboscopic light would illuminate the coil and the photographs would be as clear as possible.

The phase systems used for the retention experiments on the photographic CCCE rig are the 4A, 4B and 4C phase systems (described in Table 1-3). Both the upper and the lower phase of these phase systems were dyed to increase the contrast between them. The upper phase was dyed with Sudan Blue and the lower phase with Procion Brilliant Yellow. The dye system for this phase system was established and described by Wood [2002].



Figure 2-3: Dyed phase system.

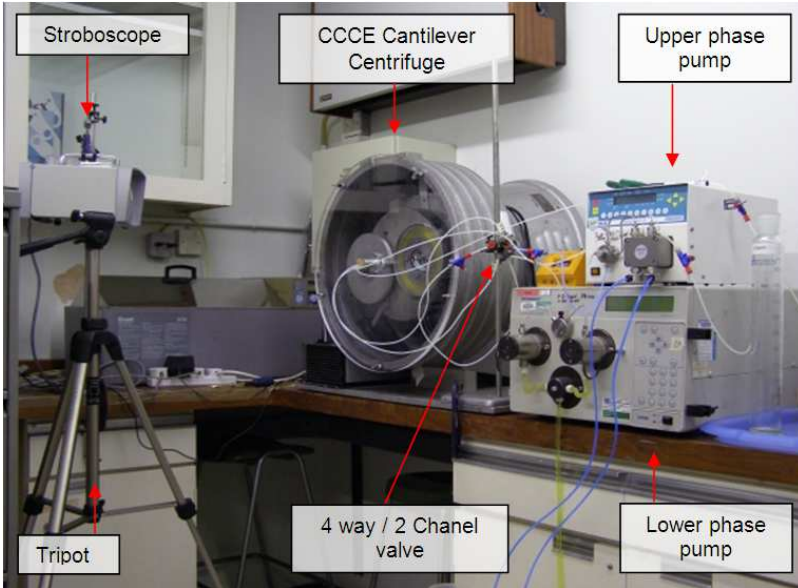


Figure 2-4: Photograph of the set-up of the CCCE cantilever centrifuge in the dark room.

2.3.3 Method used on the Photographic rig

For all the experimental procedures the coil was rotated at 1000 rpm in the clockwise direction. Clockwise rotation places the head of the coil at the centre and the tail at the periphery [Sutherland et al. 2000].

To prepare for the experiment, the coil was filled, while stationary, with lower phase by pumping the phase in from periphery to centre. When the coil was almost full with lower phase, the coil was rotated in a clockwise direction to push the remaining air out. To ensure all leads were full with lower phase the on/off valves were opened to allow the remaining air and lower phase to flow through. When no more air could be expelled the flow was stopped and the on/off valves closed.

At the start of the experiment both the upper and lower phase were pumped into the filled coil simultaneously while the centrifuge was spinning in the clockwise direction. The blue upper phase was

pumped from the peripheral tail to the central head and the yellow lower phase was pumped from the central head to the peripheral tail. The eluted phases from the coil were collected in two cylinders, one from the centre and one from the periphery. The stroboscopic light allowed the liquids inside the coil to be photographed and studied. When the liquids inside the coil were visibly equilibrated (i.e. when the transition between the upper and lower phase is not moving any more), the phase distribution was recorded with the digital camera, after which the experiment was stopped. The amount of upper and lower phase displaced from each end of the coil was measured.

To prepare the coil for the next experiment, the upper phase in the coil and system was replaced with lower phase. The upper phase was removed from the coil by pumping lower phase from tail to head through the spinning coil. The eluent was collected in a clean cylinder to determine the amount of upper phase in the coil and system from which the volume ratio of phases in the coil could be determined. After this the next experiment was started.

Each experiment, with the same flow rate combination, was repeated for different time durations to establish whether equilibrium was reached inside the coil. When the measured amount of mobile phase in the coil at the end of each experiment was the same, equilibrium was judged to be reached.

To investigate the relationship between flow rate and phase ratio inside the coil different flow rate combinations were used. The flow rates used for the experiments ranged from 0 ml/min to 200 ml/min for both phases.

2.3.4 Photograph Analysis Method

The photographs that were taken during the experiments were measured to determine the location of the transition area. This was done by placing a scaled circular mask (see Figure 2-5) on the picture and rotating it so the screws and the flying leads hole on the coil line-up with the lines on the mask. By doing this the start of the coil at the centre lines-up with the start line on the mask. Using the scale on the mask the number of loops filled with upper phase was determined by first counting the number of completely filled loops

from the centre and adding to this the part of coil filled with upper phase. An example of this is shown in Figure 2-6.

When the number of loops filled with upper phase has been determined this is used to calculate the length and the volume of that section of the coil. The spiral starts at the centre with a half circle with a radius of 51.5 mm followed by quarter circles with the radii increasing with 1.5 mm.

The length of each quarter section is calculated from the radius and is a quarter of the circumference of a circle with that radius (Equation 2-1).

$$L_{\text{quarter section}} = \frac{1}{4} \cdot 2 \cdot \pi \cdot R_{\text{quarter section}} \quad \text{Equation 2-1}$$

The length and the radius of the quarter section are both in [mm].

To obtain the length of the coil section filled with upper phase the length of each quarter section with upper phase is added together. The volume of the coil section is calculated from the length of the coil section multiplied by the area of the coil (calculated from the coil diameter which is 5 mm as described in Section 2.3). This is shown in Equation 2-2.

$$V_{\text{coil section}} = L_{\text{coil section}} \cdot \frac{1}{4} \cdot \pi \cdot D_{\text{coil}}^2 \quad \text{Equation 2-2}$$

Where the length of the coil section is in [cm] and the diameter of the coil tube is changed to [cm] to give the volume of the coil section in [ml].

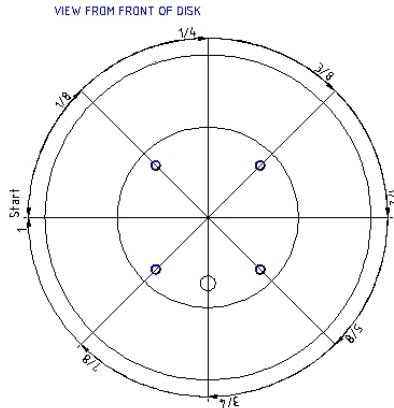


Figure 2-5: Mask which was applied to the photographs to determine the number of loops filled with the upper phase.

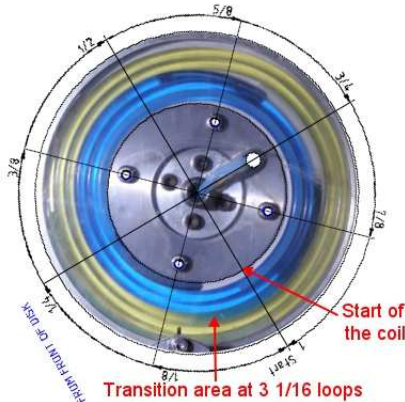


Figure 2-6: Example of the measurement of the number of loops filled with upper phase using the graduated circular mask. When the mask is lined-up with the screws on the coil the start of the coil is lined-up with the start line. Counting the loops from this point to the transition area gives in this case 3 1/16 loops. Note that the clear part in the picture is the location where the main coil goes behind the plate to the centre connection.

The quarters of the coil with their corresponding radii and the calculated length are shown in Table 2-1. The increasing length of

the coil section in [mm] and the volume of the coil section are also shown.

Table 2-1: Conversion table to calculate the length of coil filled with upper phase with quarter circle intervals.

Loops from centre	Quarter section		Length of coil section from the centre (mm)	Calculated Volume (ml)
	Radius (mm)	Length (mm)		
1/4	51.5	81	81	1.6
1/2	51.5	81	162	3.2
3/4	53.0	83	245	4.8
1	54.5	86	331	6.5
1 1/4	56.0	88	419	8.2
1 1/2	57.5	90	509	10.0
1 3/4	59.0	93	602	11.8
2	60.5	95	697	13.7
2 1/4	62.0	97	794	15.6
2 1/2	63.5	100	894	17.5
2 3/4	65.0	102	996	19.6
3	66.5	104	1100	21.6
3 1/4	68.0	107	1207	23.7
3 1/2	69.5	109	1316	25.8
3 3/4	71.0	112	1428	28.0
4	72.5	114	1542	30.3
4 1/4	74.0	116	1658	32.6
4 1/2	75.5	119	1777	34.9
4 3/4	77.0	121	1898	37.3
5	78.5	123	2021	39.7
5 1/4	80.0	126	2146	42.1
5 1/2	81.5	128	2275	44.7

The table above was extended to 1/8th coil sections and from this a graph was drawn plotting the relationship between the number of loops and the length of the coil section (Figure 2-7).

The equation from the trend line which is used to calculate the length of the coil filled with upper phase from the measured number of loops from the start of the coil to the interface.

$$L_{\text{coil section}} = 1.86 \cdot \text{Loops}^2 + 31.12 \cdot \text{Loops} \quad \text{Equation 2-3}$$

The volume of this coil section was calculated using Equation 2-2.

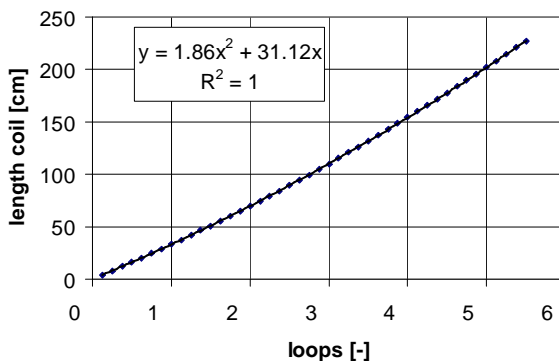


Figure 2-7: Graph showing the relationship between the number of loops with the coil length and showing the trend line with equations which fits the relationship. Microsoft Excel® is used to fit a trend line and equation for this relationship.

2.4 Applications study at Pfizer

This section describes the set-up and method used for the phase system selection and the separations performed at the Pfizer labs in Sandwich in Kent, UK. An industrial sample was separated using the CCCE rotor. Parts of the set-up and method described in this section are being prepared for publication in the Journal of Chromatography A.

2.4.1 Phase System Selection

Mixtures of compounds to be separated on a CCC centrifuge, also referred to as “the sample mixture”, were first analysed using a fast HPLC method. After identifying the components on the HPLC chromatogram the sample mixture was screened to identify the ideal phase system for separation. The screening method tests the mixture in different phase systems, which consist of a selection of commonly used solvents at different ratios. In order to identify the ideal phase system for a dynamic separation, the distribution of each component over the phases of each phase system was determined. For the purpose of this experiment the D-value was defined as the concentration of the one component in the organic phase over the concentration of that component in the aqueous phase (Equation 2-4). Both upper and lower phase of each screening phase system were analysed using HPLC as described in section 2.4.5. The volume of both the upper and lower phase injected into the HPLC system was 5 μ l. The calculated area of one component on the HPLC chromatogram corresponds to the concentration of that component, and because they are the same for the upper and lower phase the areas can be used to calculate the D-value. The equation for the D-value (Equation 2-4) then becomes:

$$D_{org/aq} = \frac{C_{org}}{C_{aq}} = \frac{Peak Area_{org}}{Peak Area_{aq}} \quad \text{Equation 2-4}$$

The optimum operating condition for normal isocratic CCC is when the target component in the mixture (whether it is an Active Pharmaceutical Ingredient (API) or contaminant) has a D-value = 1. To establish the phase system that would give a D-value = 1 for the target component, the results from the screen are put into a statistical package. This statistical software uses the compositions of the phase systems of the screen and the D-values of the target component in the phase systems of the screen. When the phase system that gives a D-value of one for the target component is calculated, this phase system will need to be made up and the D-values of all the other components in the mixture need to be measured to confirm the right distribution of values. The further the

D-values of the components in the mixture are apart the better the phase system will work for a CCC separation.

To find a suitable phase system for a liquid-liquid extraction using a DFCCC centrifuge the mixture was also run through the basic screen and the D-values were calculated. The D-values were analysed manually and compared on value and the difference between them. Ideally, binary mixtures have one very high D-value (above $D=1$) and one very low D-value (below $D=1$). For complex mixtures the D-values should be evenly distributed around $D=1$ with the first component very low ($D < 1$) and the last component very high ($D > 1$). The distribution of these D-values is important because the expected place where the DFCCC separation cuts is around the $D=1$ value, but this will depend on the flow rates and the volumes of each phase retained inside the coil.

The basic screen (as detailed in

A series of phase systems across the hydrophobicity range were developed around 2000 and described by Sutherland and co-workers [2000, 2001]. These phase systems are also made up of heptane, EtOAc, MeOH and water, are well characterised and have been used in many different projects and applications at the Brunel Institute for Bioengineering (BIB). Table 1-3 shows the composition and other characteristics of this phase system series.

Table 1-4) uses Heptane, EtOAc (Ethyl Acetate), DCM (Dichloromethane), Methanol and Water. Each phase system consists of four components (two in the organic phase and two in the aqueous phase). Nine phase systems consisting of Heptane, EtOAc, Methanol and Water and another nine of Heptane, DCM, Methanol and Water. In each set of nine phase systems there are two the same to test repeatability. All the EtOAc phase systems in the basic screen have the organic phase as upper phase. For the DCM phase systems where the amount of DCM is small the organic phase is the upper layer, but where there is more DCM the organic phase is the lower layer (

A series of phase systems across the hydrophobicity range were developed around 2000 and described by Sutherland and co-workers [2000, 2001]. These phase systems are also made up of heptane, EtOAc, MeOH and water, are well characterised and have been used in many different projects and applications at the Brunel Institute for Bioengineering (BIB). Table 1-3 shows the composition and other characteristics of this phase system series.

Table 1-4). An extended screen, which consists of a larger range of solvents (listed in Table 1-5), can be used when the solvents in the basic screen do not give sufficient selectivity or give solubility problems. The phase systems in the extended screen consist of four components of equal volume: two components from the aqueous side of Table 1-5 (water and another component) and two components from the organic side of the table (Heptane or Toluene and another component). In this way every possible combination is made which gives 40 different phase systems.

The screen of solvent phase systems is either made manually using a pipette or automatically using an auto-sampler. Both methods make up the phase systems in 2 ml HPLC vials. The mixture is manually put into the vials before the phase systems are made into them. After the phase systems are made into the vials they are capped and undergo a mixing cycle after which both layers are analysed on HPLC. The results of each layer (area of the peaks) are put in a spreadsheet to calculate the D-value using Equation 2-4. The protocol is detailed in Appendix V.

2.4.2 Process size CCCE Coil

A schematic diagram of the dual-flow coil with its connections illustrated was shown in Figure 1-30. The separations were performed on a specially built CCCE. This coil has six layers of PTFE tubing with a 5 mm internal diameter and a total volume of 625 ml. At the tube ends, special terminals (Figure 2-8) allow the coil to have both an inlet and outlet on each end.

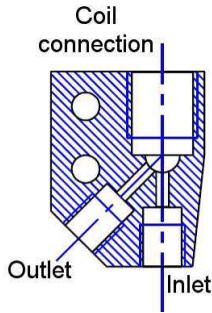


Figure 2-8: AutoCAD drawing of the end terminal which allows for the Dual Flow connection.

At the middle of the coil, between layer three and layer four, a sample inlet is connected through a “T-junction”. Through the special terminals at the ends of the coil the inlet tubes are extend for 1000 mm into the coil to prevent the introduced phase from flowing back out at the same side (backflow) [Ito 1985]. The tube is wound in six layers on a spool with a radius of 56 mm. This gives a radius of 59 mm at the inner layer and a radius of 91.5 mm at the outer layer. The radius from the solar axis to the planetary axis is 110 mm. This gives a β -value range across the layers from centre to periphery of 0.54 to 0.83 (where the β -value is the ratio of the radial distance on the planetary coil, r to the distance between the planetary axis and the centre of rotation, R).

2.4.3 Experimental set-up at Pfizer

There were two process scale CCCE coils present in the planetary gear centrifuge. One of the two CCCE coils was set-up for separation with three pumps, two computer controlled valves and some manual valves. A schematic layout of the operating system is given in Figure 2-9. Valves A – E are on/off valves and were switched to block lines to prevent the coil from leaking when not used. At the end of each run when the coil was not in use these valves were closed. To select the direction in which the phases are pumped, valve F (a 4-way/2- channel valve) was used. To ensure no mistakes were made (for good practice) valve F was switched into the “running position” after use (so the lower phase went towards

electronic valve 1). To prime the pumps the electronically actuated valves (valve 1 and 2) were switched to allow the stream to go to waste instead of into the coil. Figure 2-9 shows the schematic set-up of the DFCCC centrifuge, the valves and the pumps. The valves show the set-up in “run mode”; the phases go into the correct ends of the coil for the separation and the sample flows into the centre of the coil.

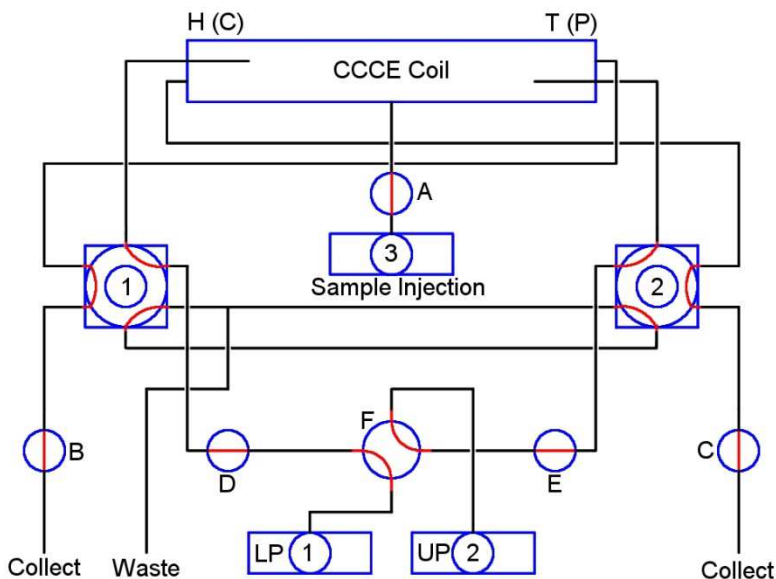


Figure 2-9: Schematic drawing of the CCCE set-up with the valves and pumps. The positions of the valves are in running condition. In the diagram the H is the head end of the coil at the centre (C), the T is the tail end of the coil at the peripheral (P), A to E are on/off valves, F is a four way/two channel valve, valves 1 and 2 are the six way electronic actuated valves and pumps 1 to 3 are the pumps for the phases and the sample.

2.4.4 Four protocols for the CCCE separations

Four protocols (detailed in Appendix V) were used for the preparation and the running of the DFCCC centrifuge. Before a Dual Flow extraction could be performed the pumps needed to be primed with the right phase system (protocol 1) and the coil needed to be

filled with the lower phase (protocol 2). After the DFCCC separation (protocol 3) the coil needs to be refilled with fresh lower phase (protocol 4). Of each fraction collected during the DFCCC separation a sample (of 1 ml) was taken for HPLC analysis. The HPLC results show areas representing the amount of compound in the injected volume (5 μ l). These areas were put into a spreadsheet to reconstruct a chromatogram of the DFCCC separation. The spreadsheet was programmed to normalise the results so all the peaks on the chromatogram have the same height. Normalisation was done by dividing all the areas of each compound by the maximum area of that compound.

The four protocols in Appendix V are:

1. **Priming of the pumps;** where the pumps are primed and prepared for the CCCE separation.
2. **Preparation of the coil;** where the coil is filled with lower phase from peripheral tail to central head.
3. **CCCE extraction;** where the extraction of a sample mixture is performed and fractions are collected after the equilibration of the phases in the coil at the desired flow rates.
4. **Refilling of the coil with lower phase at the end of the run;** where the coil is refilled with lower phase ready for the next experiment, while pushing out the coil contents to determine the phase ratio inside the coil.

2.4.5 HPLC analysis of the sample mixtures and the fractions

The HPLC that was used for the analysis of the sample mixtures before and after the separations is an Agilent 1200 unit. This unit is set-up to run in reverse phase mode at high flow rates to allow fast analysis. The following operating parameters were applied.

- Flow rate used was 5 ml/min.
- The two solvents for the gradient were Acetonitrile (MeCN) and Water with 0.1% Tri-fluoro-acetic-acid (TFA). The gradient was from 5% MeCN to 95% MeCN over a time of 1.7 minutes and 0.3 minutes hold at the end.

- Injection volume was 5 μl .
- The column used was a Zorbax Stable Bond SB C_{18} with dimensions of 4.6 x 150 mm and a particle size of 1.8 μm . This column was used at a temperature of 75°C to allow high flow through.
- Wavelength for the optical detection was 220 nm.

The samples mixtures that were analysed were diluted to get an approximate concentration of 1 mg/ml. Fractions collected from the separation however were put directly onto the HPLC for analysis.

2.4.6 Mass balance procedure

A mass balance consists of two parts. The first part is where the amount of component injected into the system is determined and the second part is where the amount of component eluting from the system is determined. These two measures should be the same when there is 100% recovery.

To determine the amount of component injected into the system the concentration of the sample mixture and the volume injected will need to be determined. The concentration of the prepared sample mixture was determined by drying down a fixed volume using a “Buchi R-205” rotary evaporator with the “Buchi B-490” heating bath and measuring the mass of the dried components. Dividing the dried components by the volume that was dried down gives the concentration of the sample mixture. The volume injected was determined by subtracting the final volume from the initial volume. The following equation shows how this calculation is done.

$$C_{\text{sample}} = \frac{m_{\text{dried down}}}{V_{\text{original volume}}} \quad \text{Equation 2-5}$$

$$m_{\text{injected}} = C_{\text{sample}} \cdot (V_{\text{initial}} - V_{\text{final}}) \quad \text{Equation 2-6}$$

During the separation the phases eluting from the centre and the periphery were collected in fractions. All these fractions were analysed by HPLC (as detailed in Section 2.4.5) and the relative amount of components present in each fraction was determined from this HPLC analysis. The fractions from the centre outlet with components present according to the HPLC analysis were pooled together and the fractions from the periphery outlet with components present were pooled together. These two batches of liquid were dried down using the “Buchi” rotary evaporator to determine the mass of the components. The coil contents collected when executing protocol 4 (Appendix V) was also dried down to determine the mass of the components that was still in the coil at the end of the experiment.

The following parameters could contribute to an error in the mass balance of the separation. The HPLC samples that were created to analyse the collected fractions were not recovered and dried down for the mass balance. Only the fractions that had components present according to the HPLC analysis were used and dried down for the mass balance. It is possible that the HPLC analysis didn't pick up some of the components due to different wave lengths or undetectable low level. The coil refill procedure (protocol 4) does not empty the system completely, but refreshes the phase in the coil. This could result in components staying behind in the coil.

Chapter 3 Theory and Models of CCCE

3.1 Outline

This chapter consists of three main sections. The first section describes a proposed calculation for the phase distribution inside the Dual Flow CCC coil. The second section describes the original CCD model and the third section describes the Dual Flow CCD (DFCCD or Continuous Counter-current Distribution CCCD) model. The CCD model is based on the CCD models described in the literature review. In this CCD model the elution of the components from the distribution is described and simplified. The DFCCD model uses the same basics as the CCD model and the similarities and differences are pointed out.

3.2 Phase distribution in the Coil

3.2.1 Calculations to determine the transition area

The results of the initial visualisation studies discussed in Chapter 4 and van den Heuvel and Sutherland [2007] show that the phases are not equally distributed through the coil. This means that at equilibrium there will be a cross over area in the coil where the phase distribution switches between mainly upper phase to mainly lower phase. In Figure 3-1 the schematic drawing of the phase distribution is shown. This figure shows that at the head in part UP there is mainly upper phase (yellow) in the coil and that at the tail in part LP there is mainly lower phase (green) in the coil. The position of the transition area (L_U) is dependant on the flow rates of the upper and lower phases.

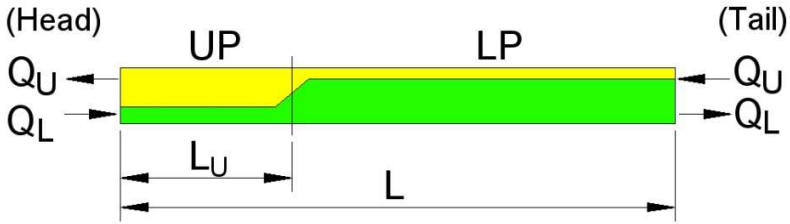


Figure 3-1: Schematic diagram of the phase distribution in the Dual Flow CCC coil.

The proposed calculation is that with the gradients from the isocratic Normal and Reverse phase mode operations and the volume distribution at the end of the coil the position of the transition area can be calculated. For the Normal and Reverse phase mode the Du-plot relationships are derived from Equation 1-10 with negative gradient values (B) and become as follows.

$$S_f(\text{Rev.}) = B_L \cdot \sqrt{Q_L} + 1 = \%UP(R) \quad \text{Equation 3-1}$$

$$S_f(\text{Nor.}) = B_U \cdot \sqrt{Q_U} + 1 = \%LP(N) \quad \text{Equation 3-2}$$

The percentage of the coil that seems to be occupied by the upper phase and the percentage that is actually occupied with the upper phase are calculated with the following equations.

$$\%L_U = \frac{L_U}{L} \quad \text{Equation 3-3}$$

$$\%V_U = \frac{V_U}{V_C} \quad \text{Equation 3-4}$$

The total volume of upper phase in the coil is the sum of the upper phase in both parts of the coil.

$$\%V_U = \%UP(R) \cdot \%L_U + (1 - \%LP(N)) \cdot (1 - \%L_U)$$

Using this definition, the equation to calculate the position of the transition area is derived as follows.

$$\%V_U = \%UP(R) \cdot \%L_U + 1 - \%L_U - \%LP(N) + \%LP(N) \cdot \%L_U$$

$$\%V_U + \%LP(N) - 1 = \%L_U (\%UP(R) + \%LP(N) - 1)$$

$$\%L_U = \frac{\%V_U + \%LP(N) - 1}{\%UP(R) + \%LP(N) - 1} \quad \text{Equation 3-5}$$

$$\%L_U = \frac{\%V_U + B_U \cdot \sqrt{Q_U}}{B_L \cdot \sqrt{Q_L} + B_U \cdot \sqrt{Q_U} + 1} \quad \text{Equation 3-6}$$

3.3 Original CCD model

3.3.1 Theory

The Distribution ratio used for the development of the theory is defined as the concentration of the component in the stationary phase over the concentration in the mobile phase ($D_{S/M}$). It is assumed that the D-value is a constant at a given temperature and does not vary with concentration or other factors.

$$D_{S/M} = \frac{C_S}{C_M} \quad \text{Equation 1-3}$$

The concentration is defined as the mass (m) of the compound over the Volume (V) which it is dissolved in.

$$C = \frac{m}{V} \quad \text{Equation 3-7}$$

Assuming all solute has dissolved the total mass of the compound in a tube (m_{TOT}) is the sum of the mass of the compound in the stationary phase (m_S) and the mobile phase (m_M).

$$m_{TOT} = m_S + m_M \quad \text{Equation 3-8}$$

The total volume of the coil or tube (V_C) is the sum of the volume of the stationary phase (V_S) and the mobile phase (V_M).

$$V_C = V_S + V_M \quad \text{Equation 3-9}$$

The ratio of the two volumes in the coil or the tube is defined as the volume of the stationary phase over the volume of the mobile phase.

$$X_{S/M} = \frac{V_S}{V_M} \quad \text{Equation 3-10}$$

The stationary phase retention (defined in Equation 1-9) relates to the volume ratio as is shown in the following two equations.

$$\begin{aligned} S_f &= \frac{V_S}{V_C} = \frac{V_S}{V_S + V_M} \\ &= \frac{X_{S/M} \cdot V_M}{X_{S/M} \cdot V_M + V_M} = \frac{X_{S/M}}{X_{S/M} + 1} \end{aligned} \quad \text{Equation 3-11}$$

$$\begin{aligned} X_{S/M} &= \frac{V_S}{V_M} = \frac{V_S}{V_C - V_S} \\ &= \frac{S_f \cdot V_C}{V_C - S_f \cdot V_C} = \frac{S_f}{1 - S_f} \end{aligned} \quad \text{Equation 3-12}$$

Combining the volume ratio with the distribution ratio and the definition of the concentration gives the ratio of the mass of the component in the stationary phase with the mass in the mobile phase. This is shown in the following equations.

$$\begin{aligned} X_{S/M} &= \frac{m_S}{m_M} \cdot \frac{C_M}{C_S} \\ &= \frac{m_S}{m_M} \cdot \frac{C_M}{D_{S/M} \cdot C_M} = \frac{m_S}{m_M \cdot D_{S/M}} \\ \frac{m_S}{m_M} &= X_{S/M} \cdot D_{S/M} \end{aligned} \quad \text{Equation 3-13}$$

When the D-value is calculated as the concentration of the component in the mobile phase over the concentration in the stationary phase, the volume ratio X should be calculated as the volume of the mobile phase over the volume of the stationary phase. This way all the m subscripts should be replaced with the s subscripts and vice versa. The results of this are shown in the following equations.

$$D_{M/S} = \frac{C_M}{C_S} \quad \text{Equation 3-14}$$

$$\frac{m_M}{m_S} = X_{M/S} \cdot D_{M/S} \quad \text{Equation 3-15}$$

$$\frac{m_S}{m_M} = \frac{1}{X_{M/S} \cdot D_{M/S}}$$

Combining Equation 3-8 with Equation 3-13 gives two equations which express the mass of the component in the mobile phase and the mass of the component in the stationary phase after one mixing and settling step. These two equations are as follows.

$$m_{TOT} = m_M \cdot X_{S/M} \cdot D_{S/M} + m_M$$

$$m_{TOT} = m_M \cdot (X_{S/M} \cdot D_{S/M} + 1)$$

$$m_M = \frac{m_{TOT}}{(X_{S/M} \cdot D_{S/M} + 1)} \quad \text{Equation 3-16}$$

$$m_{TOT} = m_S + \frac{m_S}{X_{S/M} \cdot D_{S/M}}$$

$$m_S = \frac{m_{TOT} \cdot X_{S/M} \cdot D_{S/M}}{(X_{S/M} \cdot D_{S/M} + 1)} \quad \text{Equation 3-17}$$

The amount of component moved with the mobile phase and staying behind with the stationary phase is calculated using these two

equations. When all the mobile phase is moved from one tube to the next, the above equation for the mass of the component in the mobile phase can be used without any adjustments. However, when a part of the mobile phase (%V_M) is moved from one tube to the next, the equation for the mass in the mobile phase will need to be adjusted accordingly. The following figure illustrates transfers in five tubes.

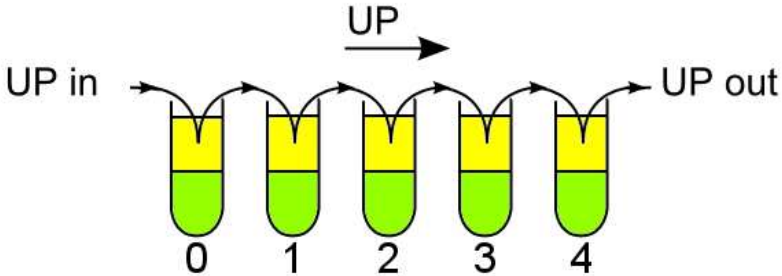


Figure 3-2: Movement of the mobile (upper) phase in five tubes (P=5). An amount of mobile phase is moved to the next tube and an amount of mobile phase stays in the tube. The first tube (0) receives fresh mobile phase and the mobile phase leaving the last tube (4) goes to collection.

As discussed in the literature review, the calculation of the fraction of a component in the tubes has been described by [Martin and Synge 1941] and [Williamson and Craig 1947]. Martin and Synge referred to the distribution of a component in a series of test tubes over a number of steps as the binominal expansion, (Y + Z)ⁿ. In the binominal expansion Z is considered the fraction transferred in the upper phase and Y the fraction transferred or staying in the lower phase. Equation 3-16 and Equation 3-17 written as the binominal expansion becomes as follows.

$$\left[\frac{X_{S/M} \cdot D_{S/M}}{X_{S/M} \cdot D_{S/M} + 1} + \frac{1}{X_{S/M} \cdot D_{S/M} + 1} \right]^n = 1 \quad \text{Equation 3-18}$$

The binomial theorem is applied to this equation to find an equation describing the quantity of the component in every tube (p) at any step (n) of the separation. Numbering of both the tubes and steps

starts at 0 and runs to p-1 and n-1 respectively. For the previous equation this becomes as follows.

$$MF_{n,p} = \frac{n!}{(n-p)! \cdot p!} \cdot \left(\frac{X_{S/M} \cdot D_{S/M}}{X_{S/M} \cdot D_{S/M} + 1} \right)^{n-p} \cdot \left(\frac{1}{X_{S/M} \cdot D_{S/M} + 1} \right)^p \quad \text{Equation 3-19}$$

This equation is simplified into the following equation.

$$MF_{n,p} = \frac{n!}{(n-p)! \cdot p!} \cdot \left(\frac{X_{S/M} \cdot D_{S/M}}{X_{S/M} \cdot D_{S/M} + 1} \right)^n \cdot \left(\frac{1}{X_{S/M} \cdot D_{S/M}} \right)^p \quad \text{Equation 3-20}$$

As described in the literature review, the equation following from the binominal theorem can be approximated using the normal distribution equation [Williamson and Craig 1947]. The normal distribution equation, which was defined in Equation 1-23, gives the following approximation for Equation 3-20.

$$MF_{n,p} = \frac{1}{\sqrt{\pi \cdot A}} \cdot e^{-((p-p_{MAX})^2/A)} \quad \text{Equation 3-21}$$

Where:

$$A = 2n \cdot \frac{X_{S/M} \cdot D_{S/M}}{(X_{S/M} \cdot D_{S/M} + 1)^2}$$

$$p_{MAX} = n \cdot \frac{X_{S/M} \cdot D_{S/M}}{X_{S/M} \cdot D_{S/M} + 1} \quad \text{Equation 3-22}$$

In this equation p_{MAX} is the tube number with the largest amount of component in also referred to as the location of the top of the peak.

As is shown in the literature review the approximation of the binominal expansion theorem is a valid approximation for the calculation of the fraction of component inside the tubes.

3.3.1.1 Single Withdrawal

The theory described so far only considers the fraction or the mass of the component inside the tubes. The single withdrawal theory [Craig and Craig 1956] is applied to the binominal expansion theory to describe the fraction of the component eluting from the CCD process. At a certain step (n), the fraction eluting from the CCD process is calculated from the previous step (n-1) at the last tube (P-1). The total number of tubes is P and the first tube number is 0, therefore the last tube number is P-1. So the fraction at a certain step (n) is the fraction of the previous step in the last tube multiplied by the fraction eluting in the mobile phase. The calculations for this are as follows.

$$MF_n^{out} = MF_{n-1, P-1} \cdot \left(\frac{1}{X_{S/M} \cdot D_{S/M} + 1} \right) \quad \text{Equation 3-23}$$

$$MF_n^{out} = MF_{n-1, P-1} \cdot \left(\frac{X_{S/M} \cdot D_{S/M}}{X_{S/M} \cdot D_{S/M} + 1} \right) \cdot \left(\frac{1}{X_{S/M} \cdot D_{S/M}} \right) =$$

$$\frac{(n-1)!}{(n-1-(P-1))!(P-1)!} \cdot \left(\frac{X_{S/M} \cdot D_{S/M}}{X_{S/M} \cdot D_{S/M} + 1} \right)^{n-1} \cdot$$

$$\left(\frac{X_{S/M} \cdot D_{S/M}}{X_{S/M} \cdot D_{S/M} + 1} \right) \cdot \left(\frac{1}{X_{S/M} \cdot D_{S/M}} \right)^{P-1} \cdot \left(\frac{1}{X_{S/M} \cdot D_{S/M}} \right)$$

$$MF_n^{out} = \frac{(n-1)!}{(n-P)! \cdot (P-1)!}$$

Equation 3-24

$$\left(\frac{X_{S/M} \cdot D_{S/M}}{X_{S/M} \cdot D_{S/M} + 1} \right)^n \cdot \left(\frac{1}{X_{S/M} \cdot D_{S/M}} \right)^P$$

This equation, based on the single withdrawal of the binomial expansion, can also be approximated using the normal distribution principle. The normal distribution equation used is the same as is described in the literature review (Equation 1-23). The location of the fraction is now the step number (n), the tube number at the maximum fraction (μ), and the standard deviation (σ) are as follows.

$$\mu = P + X_{S/M} \cdot D_{S/M} \cdot (P-1)$$

Equation 3-25

$$\sigma = \sqrt{n \cdot X_{S/M} \cdot D_{S/M}}$$

Equation 3-26

Combining these two equations with the standard deviation equation shown in the literature review (Equation 1-23 on page 54) gives the approximation for the fraction of the component eluting from the test tube train which is as follows.

$$MF_n^{out} = \frac{1}{\sqrt{2 \cdot \pi \cdot n \cdot X_{S/M} \cdot D_{S/M}}} \cdot e^{AA}$$

Equation 3-27

Where:

$$AA = - \frac{(n - (P + X_{S/M} \cdot D_{S/M} \cdot (P-1)))^2}{2 \cdot n \cdot X_{S/M} \cdot D_{S/M}}$$

The equations for normal CCD separations, developed in this section, are compared in a Microsoft Excel spreadsheet. This is shown in the following section.

3.3.2 Model in Excel

Table 3-1: CCD separation with 5 tubes and 25 steps. The D-value is 1 and the volume ratio of the upper and lower phase in the tubes is 1. For each step all the upper phase is moved to the next tube.

Step (n)	Tube (p)					OUT
	0	1	2	3	4	
0	100.00	0.00	0.00	0.00	0.00	0.00
1	50.00	50.00	0.00	0.00	0.00	0.00
2	25.00	50.00	25.00	0.00	0.00	0.00
3	12.50	37.50	37.50	12.50	0.00	0.00
4	6.25	25.00	37.50	25.00	6.25	0.00
5	3.13	15.63	31.25	31.25	15.63	3.13
6	1.56	9.38	23.44	31.25	23.44	7.81
7	0.78	5.47	16.41	27.34	27.34	11.72
8	0.39	3.13	10.94	21.88	27.34	13.67
9	0.20	1.76	7.03	16.41	24.61	13.67
10	0.10	0.98	4.39	11.72	20.51	12.30
11	0.05	0.54	2.69	8.06	16.11	10.25
12	0.02	0.29	1.61	5.37	12.08	8.06
13	0.01	0.16	0.95	3.49	8.73	6.04
14	0.01	0.09	0.56	2.22	6.11	4.36
15	0.00	0.05	0.32	1.39	4.17	3.05
16	0.00	0.02	0.18	0.85	2.78	2.08
17	0.00	0.01	0.10	0.52	1.82	1.39
18	0.00	0.01	0.06	0.31	1.17	0.91
19	0.00	0.00	0.03	0.18	0.74	0.58
20	0.00	0.00	0.02	0.11	0.46	0.37
21	0.00	0.00	0.01	0.06	0.29	0.23
22	0.00	0.00	0.01	0.04	0.17	0.14
23	0.00	0.00	0.00	0.02	0.11	0.09
24	0.00	0.00	0.00	0.01	0.06	0.05

In the Excel model, it is assumed that the mixing and settling steps are ideal and are exactly as the theory described in the previous section. A model separation process is built up in a Microsoft Excel spreadsheet using Equation 3-16 and Equation 3-17. This model mimics a CCD process where the number of test tubes (p) and the mixing and settling steps (n) can be kept the same as in a real CCD process and the mass in every tube is calculated iteratively. The following table shows the results of the use of these equations. In each step all the upper phase is moved from tube p to tube $p+1$, the D -value of the component is 1 and the volume ratio ($X_{S/M}$) is set to 1.

In the first tube ($r=0$) and at the first step ($n=0$) the input mass is displayed. If at each time all the mobile upper phase is moved to the next tube the following equations are valid.

For $p = 0$ and for $n \geq 1$

$$M_{n,0} = \frac{M_{n-1,0} \cdot X_{S/M} \cdot D_{S/M}}{X_{S/M} \cdot D_{S/M} + 1} \quad \text{Equation 3-28}$$

For $p \geq 1$ and for $n \geq 1$

$$M_{n,p} = \frac{M_{n-1,r} \cdot X_{S/M} \cdot D_{S/M}}{X_{S/M} \cdot D_{S/M} + 1} + \frac{M_{n-1,r-1}}{X_{S/M} \cdot D_{S/M} + 1} \quad \text{Equation 3-29}$$

For the output for $n \geq 1$

$$M_{n,Out} = \frac{M_{n-1,r \max}}{X_{S/M} \cdot D_{S/M} + 1} \quad \text{Equation 3-30}$$

The distribution of components within the test tubes can be calculated with the Excel model (using Equation 3-16 and Equation 3-17). For a CCD process with a train of 100 tubes, the distribution of a series of components is calculated and is shown in Figure 3-3. The iterative excel model is used to generate the following two

graphs. Both graphs show the same separation of the same components, the first graph shows the distribution of the components inside the tubes after 100 mixing and settling steps and the second graph shows the elution of these components.

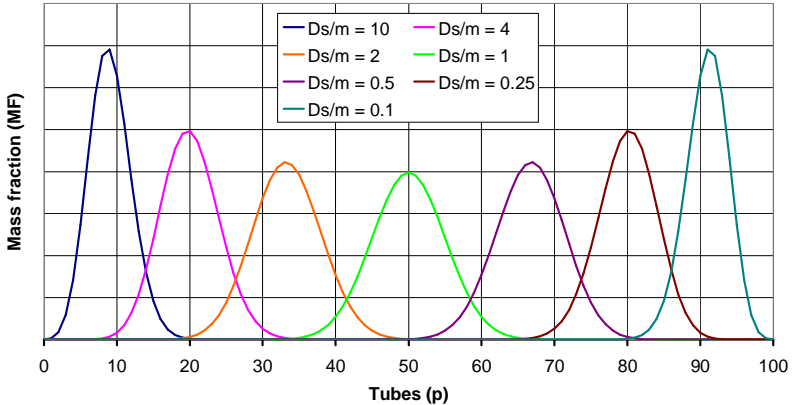


Figure 3-3: Theoretical distribution of 7 components in a CCD process inside the tubes after 100 mixing and settling steps. This is calculated using the iterative model with 100 tubes in Microsoft Excel.

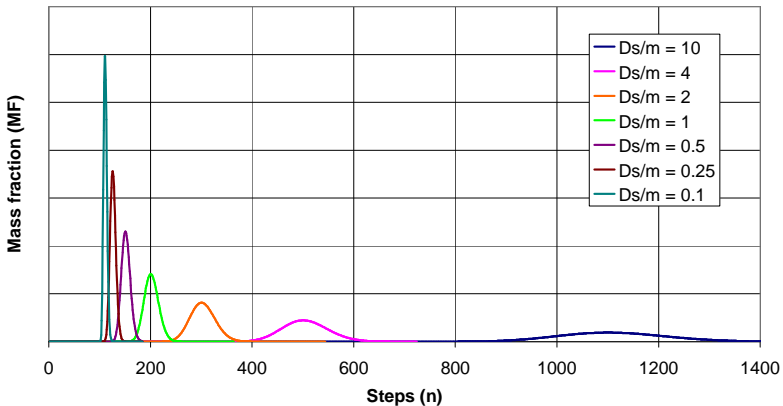


Figure 3-4: Theoretical CCD process showing the elution of 7 components at stationary phase retention of 50%. This is calculated using the iterative model with 100 tubes in Microsoft Excel.

Equation 3-29 is basically the binominal expansion equation explained in the literature review and in the previous section. As is shown, from this binominal expansion one equation (Equation 3-24) can be made to calculate the fraction of the component in each tube. The available modelling programs like Microsoft Excel and MathCAD 13 can not cope with large factorial numbers. A factorial larger than 170 seems to be the limit. This means that the approximation using the normal distribution equation would be a good alternative providing the calculated fraction corresponds with the result from the CCD test tube model.

The following graph shows the comparison of the three ways to calculate the fraction of the component eluting from the CCD process.

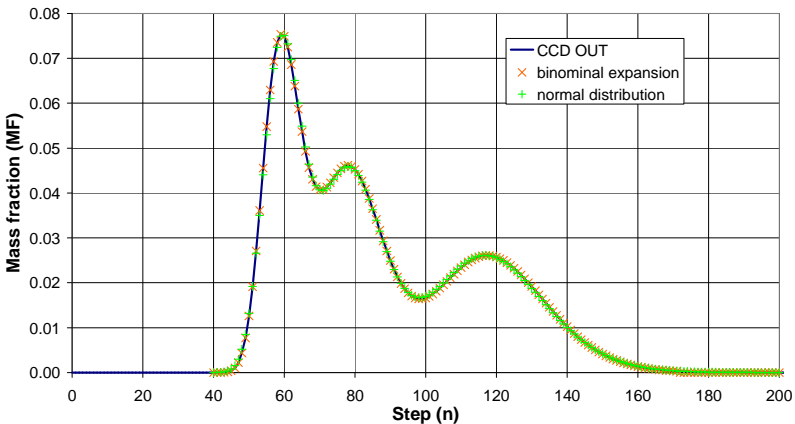


Figure 3-5: Comparison of the three different ways of calculating the fraction of the components eluting from the CCD process. The solid blue line is the fraction eluting from the CCD tube model, the orange cross (x) is the elution calculated with the binominal expansion equation and the green cross (+) is the fraction calculated using the normal distribution approximation.

This graph shows that the approximation with the normal distribution equation gives a good representation of the fraction eluting from the CCD process.

3.4 Continuous Dual Flow CCD model

3.4.1 Theory

Dual Flow CCD (DFCCD) is a CCD process where both liquid phases are simultaneously transferred in opposite directions. As mentioned in the literature review an apparatus for this technique was described by Post and Craig in 1963 and was described as Counter Double Current Distribution (CDCD). The theory of the DFCCD model and the Continuous DFCCD model uses almost the same equations as the Original CCD model. In the CCD model only one phase was moved along and in the DFCCD models both phases are moved along. And in the DFCCD model there is no mobile and stationary phase and therefore these phases are identified as upper and lower respectively. This means that the Distribution Ratio ($D_{s/m}$) and the volume ratio ($X_{s/m}$) need to be redefined. The stationary phase in the CCD process becomes the lower phase in the DFCCD process and the mobile phase becomes the upper phase. The definition of the D-value and the phase ratio becomes as follows.

$$D_{L/U} = \frac{C_L}{C_U} \quad \text{Equation 3-31}$$

$$X_{L/U} = \frac{V_L}{V_U} \quad \text{Equation 3-32}$$

These two equations are comparable with Equation 1-2 and Equation 3-10. This means that the equations that determine the amount of component carried in the upper phase and in the lower phase also are comparable with Equation 3-16 and Equation 3-17 and become as follows.

$$m_U = \frac{m_{tot}}{X_{L/U} \cdot D_{L/U} + 1} \quad \text{Equation 3-33}$$

$$m_L = \frac{m_{tot} \cdot X_{L/U} \cdot D_{L/U}}{X_{L/U} \cdot D_{L/U} + 1} \quad \text{Equation 3-34}$$

As in the original CCD model when all the phase is moved from one tube to the previous the equations can be applied without any

modification. When a percentage of one or both phases is moved this needs to be multiplied by the appropriate fraction. The amount in the remaining phase is calculated by multiplying the equation with the percentage of phase that stays behind in the tube. The previous two equations can be rewritten into the following form:

$$m_{U(n,p)} = \%V_U \cdot \frac{m_{tot} \cdot F_{(n-1,p-1)}}{X_{L/U} \cdot D_{L/U} + 1} +$$

Equation 3-35

$$(1 - \%V_U) \cdot \frac{m_{tot} \cdot F_{(n-1,p)}}{X_{L/U} \cdot D_{L/U} + 1}$$

$$m_{L(n,p)} = \%V_L \cdot \frac{m_{tot} \cdot F_{(n-1,p+1)} \cdot X_{L/U} \cdot D_{L/U}}{X_{L/U} \cdot D_{L/U} + 1} +$$

Equation 3-36

$$(1 - \%V_L) \cdot \frac{m_{tot} \cdot F_{(n-1,p)} \cdot X_{L/U} \cdot D_{L/U}}{X_{L/U} \cdot D_{L/U} + 1}$$

Where %V_U is the percentage of upper phase in the tube (p) that is moved to the next tube (p+1) and %V_L is the percentage of lower phase in the tube (p) that is moved to the next tube (p-1).

The following diagram shows the transfer of the liquids between nine tubes and the two inlets and the two outlets.

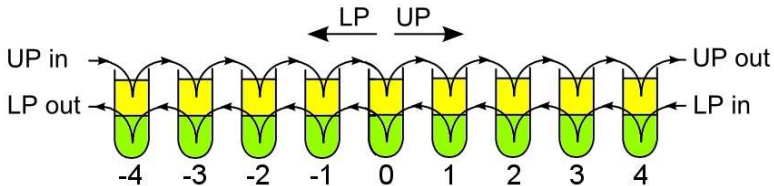


Figure 3-6: Dual Flow CCD process showing the movement of both phases in five tubes. An amount of the upper and lower phase is moved in opposite directions and the remaining amount of each phase stays in the tubes.

In the diagram the upper phase transfers to the right with increasing tube number and the lower phase is transferred to the left with decreasing tube number.

When all the phase is transferred to the next tube, the fraction of the component in the tubes of the DFCCD process can be compared with the fraction in the tubes of the CCD process. The following two tables show the fractions of the component distributed in the CCD process and the fractions of the component in the DFCCD process respectively. For both tables $D_{L/U}=1$ and $X_{L/U}=1$.

Table 3-2: CCD process where $D_{L/U}=1$, $X_{L/U}=1$ and all the mobile phase is moved on to the next tube.

		$p_{CCD} =$				
$n =$	0	1	2	3	4	
0	1	0	0	0	0	
1	0.5	0.5	0	0	0	
2	0.25	0.5	0.25	0	0	
3	0.125	0.375	0.375	0.125	0	
4	0.063	0.25	0.375	0.25	0.063	

Table 3-3: DFCCD process where $D_{L/U}=1$, $X_{L/U}=1$ and all the phase is moved to the next tube. The upper phase travels to the right and the lower phase travels to the left.

		$p_{DFCCD} =$								
$n =$	-4	-3	-2	-1	0	1	2	3	4	
0	0	0	0	0	1	0	0	0	0	
1	0	0	0	0.5	0	0.5	0	0	0	
2	0	0	0.25	0	0.5	0	0.25	0	0	
3	0	0.125	0	0.375	0	0.375	0	0.125	0	
4	0.063	0	0.25	0	0.375	0	0.25	0	0.063	

When both phases containing component are moved out of a tube and new phase is moved into the tube (containing no component), there is no component left in that tube. This is only valid for the DFCCD process when all the upper phase is moved to the next tube

in one direction and all the lower phase is moved to the next tube in the other direction. Until $n=p$, the fractions calculated in the DFCCD process are exactly the same as the fractions calculated in the CCD process as can be seen by comparing Table 3-2 with Table 3-3. This was shown by Post and Craig as is discussed in the literature review on page 52.

3.4.2 Model in Excel

The adapted equations are put into a Microsoft Excel spreadsheet to create a DFCCD process which iteratively calculates the mass of the component in each tube. In the same way as the Original CCD process the mixing and settling steps and volume ratios can be kept the same as a real DFCCD process. The following table shows the result of the iterative calculations of a DFCCD process. This process has nine tubes, the mass of the component shown has a D-value of one, the volume ratio (V_L / V_U) is one and all the phase is moved between the tubes. According to the results of the calculations in the table in every other tube there is no component left in the tube. This is due to the fact that at every transfer all of both the upper and lower phase is moved out of the tube into the next tube.

Table 3-4: Results from the Excel Dual Flow CCD model where the D-value of the component is one, the volume ratio is one and at every transfer all of the phase is moved to the next tube.

Step (n)	LP OUT	Tube (p)									UP OUT
		-4	-3	-2	-1	0	1	2	3	4	
0	0.00	0.00	0.00	0.00	0.00	100.00	0.00	0.00	0.00	0.00	0.00
1	0.00	0.00	0.00	0.00	50.00	0.00	50.00	0.00	0.00	0.00	0.00
2	0.00	0.00	0.00	25.00	0.00	50.00	0.00	25.00	0.00	0.00	0.00
3	0.00	0.00	12.50	0.00	37.50	0.00	37.50	0.00	12.50	0.00	0.00
4	0.00	6.25	0.00	25.00	0.00	37.50	0.00	25.00	0.00	6.25	0.00
5	3.13	0.00	15.63	0.00	31.25	0.00	31.25	0.00	15.63	0.00	3.13
6	0.00	7.81	0.00	23.44	0.00	31.25	0.00	23.44	0.00	7.81	0.00
7	3.91	0.00	15.63	0.00	27.34	0.00	27.34	0.00	15.63	0.00	3.91
8	0.00	7.81	0.00	21.48	0.00	27.34	0.00	21.48	0.00	7.81	0.00
9	3.91	0.00	14.65	0.00	24.41	0.00	24.41	0.00	14.65	0.00	3.91
10	0.00	7.32	0.00	19.53	0.00	24.41	0.00	19.53	0.00	7.32	0.00
11	3.66	0.00	13.43	0.00	21.97	0.00	21.97	0.00	13.43	0.00	3.66
12	0.00	6.71	0.00	17.70	0.00	21.97	0.00	17.70	0.00	6.71	0.00
13	3.36	0.00	12.21	0.00	19.84	0.00	19.84	0.00	12.21	0.00	3.36
14	0.00	6.10	0.00	16.02	0.00	19.84	0.00	16.02	0.00	6.10	0.00
15	3.05	0.00	11.06	0.00	17.93	0.00	17.93	0.00	11.06	0.00	3.05
16	0.00	5.53	0.00	14.50	0.00	17.93	0.00	14.50	0.00	5.53	0.00
17	2.77	0.00	10.01	0.00	16.21	0.00	16.21	0.00	10.01	0.00	2.77
18	0.00	5.01	0.00	13.11	0.00	16.21	0.00	13.11	0.00	5.01	0.00
19	2.50	0.00	9.06	0.00	14.66	0.00	14.66	0.00	9.06	0.00	2.50
20	0.00	4.53	0.00	11.86	0.00	14.66	0.00	11.86	0.00	4.53	0.00
21	2.26	0.00	8.20	0.00	13.26	0.00	13.26	0.00	8.20	0.00	2.26
22	0.00	4.10	0.00	10.73	0.00	13.26	0.00	10.73	0.00	4.10	0.00
23	2.05	0.00	7.41	0.00	12.00	0.00	12.00	0.00	7.41	0.00	2.05
24	0.00	3.71	0.00	9.70	0.00	12.00	0.00	9.70	0.00	3.71	0.00

The D-value of the component used in this example is one, and from the table can be seen that this component distributes evenly over the tubes. This means that the component does not elute on one of the sides, but will spread evenly over the tubes and eventually elute at the same time at both sides.

A model of 101 tubes is made in an Excel spreadsheet where seven components (the same D-values as for the 100 tube Original CCD model which is shown in Figure 3-3 and Figure 3-4) are separated. For each transfer all the phase is moved from the tube to the next and the phase ratio in each tube is one. The distribution of the components in the tubes shows the overall Gaussian peaks as the 100 tube Original CCD model, but the peaks are spiking (shown in the following figure). This is, as shown in the table with the nine tube

separation, due to the fact that at every transfer all of both phases is moved from the tube and no component is left in that tube.

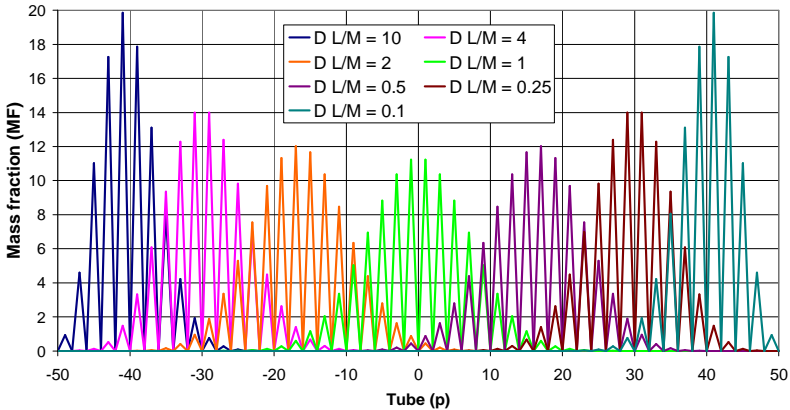


Figure 3-7: Distribution of the components in the tubes after 50 steps in a 101 tube Dual Flow CCD model. The volume ratio (X) is one and at each transfer all the phase is moved to the next tube.

The distribution of the DFCCD process shown in Figure 3-7 is very similar to the distribution of the CCD process which was shown in Figure 3-3. Note that the x-axis scales have the same total number of tubes but are numbered differently. Both processes have 100 tubes, but the DFCCD process only needs 50 steps (compared to 100 for the CCD process) to achieve the same distribution. When the process is continued the components will start to elute from both ends of the process. The elution patterns for these two outlet streams are shown in Figure 3-8 and Figure 3-9.

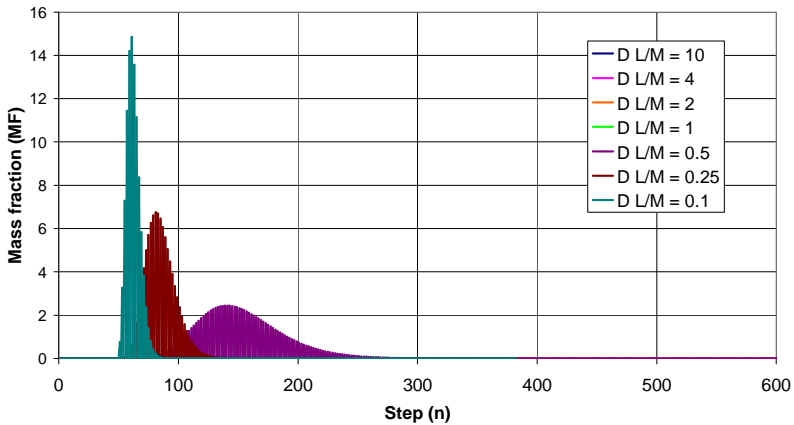


Figure 3-8: Chromatogram of the components eluting in the upper phase from the 101 tube Dual Flow CCD model.

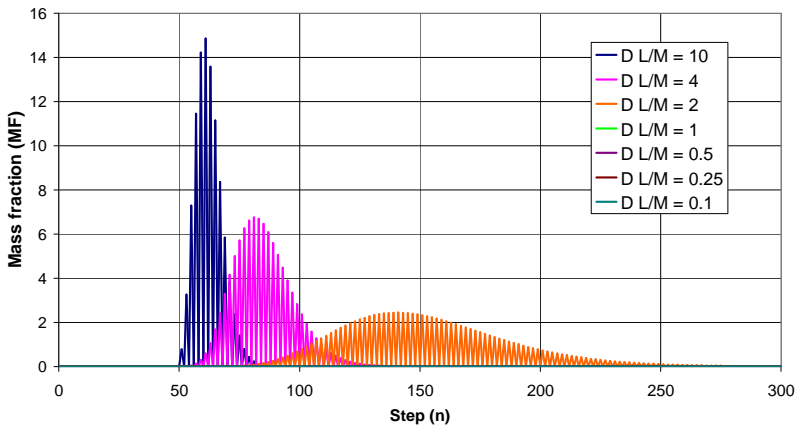


Figure 3-9: Chromatogram of the components eluting in the lower phase from the 101 tube Dual Flow CCD model.

When at each transfer only 50% of the phase is moved to the next tube, the distribution of the components in the tubes is as follows.

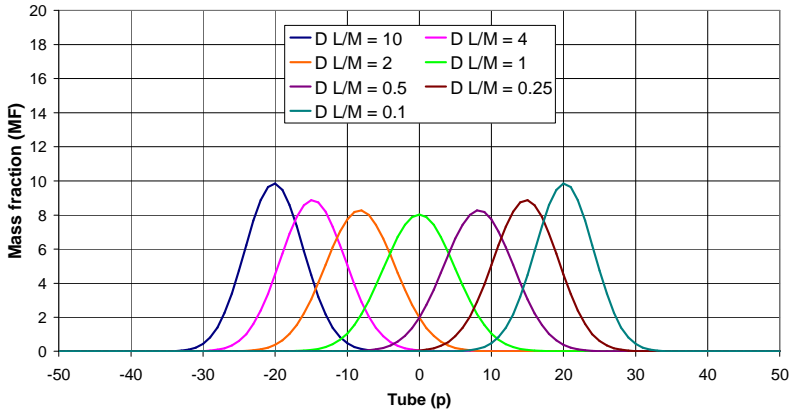


Figure 3-10: Distribution of the components in the tubes after 50 steps in a 101 tube Dual Flow CCD model. The volume ratio (X) is one and at each transfer 50% of each phase is moved to the next tube.

The lines are now smooth, but the distribution of the components is only half as far developed in the 50 steps as it was in the same number of steps when all the phase was transferred in Figure 3-7. This means that the elution of the components also needs twice as many steps when only 50% of each phase is transferred (Figure 3-11 and Figure 3-12). However, when comparing the chromatograms on elution volume, the separations with 100% and 50% moved are exactly the same. The peaks are lower for the prediction where 50% is moved compared to the peaks where 100% is moved each step. This is because the peaks are spread over more steps for the model where 50% is moved and in the model where 100% is moved the peaks are made of spikes in which all the component needs to elute.

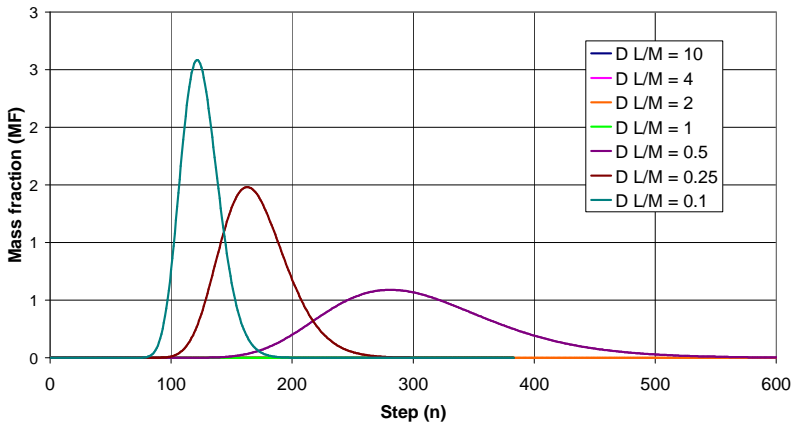


Figure 3-11: Chromatogram of the components eluting in the upper phase from the 101 tube Dual Flow CCD model where 50% of phase is transferred at each step.

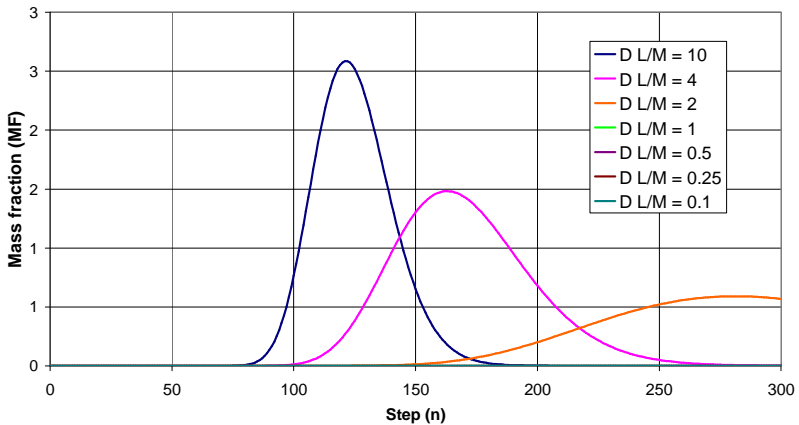


Figure 3-12: Chromatogram of the components eluting in the lower phase from the 101 tube Dual Flow CCD model where 50% of phase is transferred at each step.

3.5 Discussion and Conclusion

3.5.1 Discussion

The elution from the CCD model in the first part of this chapter is based on the single withdrawal theory [Craig and Craig 1956] (described in section 3.3.1.1). This theory is further developed with an estimation using the normal distribution equation. Both the original CCD model and the binominal expansion correspond well with the normal distribution estimation. This equation could be incorporated into a stand alone programme to predict the elution from the CCC separations.

The DFCCD model described in the second part of this chapter is a model with several limitations due to the fact it has been made in Excel. The main limitations of the DFCCD model in Excel are as follows:

- The tube numbers can not be changed easily in the excel model as the calculations in the model are done iteratively in separate cells as was shown in Table 3-4. Each component is calculated on a separate spreadsheet and the results from these spreadsheets are collated on a graph. For models with a lot of tubes or a lot of components the Excel file is very big and uses a lot of computer memory for its iterations. For example a model with 41 tubes, seven components and 850 steps uses 45 Mb.
- The volume distribution in the coil, which was observed to be not equal throughout the coil [van den Heuvel and Sutherland 2007], is not incorporated into the model. The volume distribution in the model and the elution predictions is important as was shown by Ito [2006] where the theory based on equal volume distribution did not match experimental data. It was not incorporated because a more advanced model (not an Excel spreadsheet) was required. One drawback of including the volume distribution into the model will be the extra input variables and complication it will add. These variables (volume distribution at the head and tail of the coil and the location of the transition area) are not known and will need to be calculated or estimated as not

many CCC devices allow photographic studies to determine some of these variables.

- Continuous injection is not built into the model. During continuous injection the location of the peaks is not important as they will be continuous also. For the model it is therefore not important to include continuous injection as all the important information can be extracted from a single sample injection.

Apart from these limitations in the model most things can be adjusted and set. These variables are as follows:

- The total volume of phase in each tube can be set. This way the total volume of the model can be set equal or similar to the CCCE coil volume.
- The volume ratio of the phases in the tube can be set. Together with the total volume of phase in each tube the volume of each phase is calculated. These volumes on the main data spreadsheet are automatically updated on the individual component spreadsheets.
- The percentage of each phase moved on at each step can be adjusted. As is shown in this chapter, and discussed in the literature review, when 100% of each phase is moved to the next tube every other tube contains component resulting in a spiky chromatogram. When a percentage of phase is moved there will be component in every tube and the spikes are smoothed out.

The CCD model in the first part of this chapter provides the basics and foundation for the DFCCD model in the second part of the chapter. This CCCD model has been well described in the literature and validated by Sutherland et al. [2003] using experimental data.

3.5.2 Conclusion

The DFCCD model described in this chapter is a versatile model that is useful for the initial predictions and understanding of the dual flow process. However, for advanced DFCCD modelling and separation

prediction the model needs some improvements. The first obvious improvement would be to make the tube numbers adjustable and to create a standalone programme that would do the iterative calculations.

Chapter 4 Experiments on the Photographic rig

4.1 Outline

This chapter describes the results of the experiments done on the experimental “cantilever” coil planet centrifuge described in the methods and materials chapter (section 2.3). There were two studies performed on this setup. The first study was a **visualisation study** where the unique feature was the stroboscopic photography to study the fluid dynamics and phase behaviour inside the coil under different flow rate conditions. The second study was a **retention study** where the effect of different flow rate combinations on the volumes of phase retained in the coil was systematically studied.

4.2 Visualisation studies

This part consists of four sections: aims, experiments performed, the results obtained and discussion. Parts of the results described in this chapter were presented at the international CCC 2006 conference in Washington DC. The results were subsequently published in a special issue of the Journal of Chromatography A in volume 1151 devoted to Counter-current Chromatography. A reprint of this publication is attached in Appendix VI.

4.2.1 Aim

The aim of the experiments on the photographic rig was to investigate how the phases behave inside the spinning coil under dual flow conditions. This included a visual study of the phases involving stroboscopic light and photography and a retention study where volumes of the phases inside the coil at equilibrium were established. These two parts will together give some idea of the behaviour of the phases inside a CCCE centrifuge and how this would affect the separation.

4.2.2 Experiments Performed

The 4B phase system, which consists of Heptane, Ethyl Acetate, Methanol and Water with the ratios 1.4:0.6:1.0:1.0 (described by [Sutherland et al. 2000] and discussed in section 1.4.2), was used for the visualisation studies on the photographic set-up. For increased

contrast during the visualisation the upper phase was dyed with Sudan Blue and the lower phase with Brilliant Yellow. The flow rates for both phases ranged between 0 ml/min and 200 ml/min and each flow rate combination was used at least two times for different time durations.

4.2.3 Results

4.2.3.1 Visualisation

The images taken and flow situations observed showed that with different flow rates the fluids inside the coil behaved and distributed differently. The situations observed ranged from a coil mainly filled with yellow lower phase and the blue upper phase flowing past on the inner side of the tubing (Figure 4-1A) to a coil which was mainly filled with upper phase and the lower phase flowed past along the outer side of the tubing (Figure 4-1B).

When the lower phase flow rate is equal to or greater than the upper phase flow rate the coil is mainly filled with the lower phase.

When the upper phase flow rate is significantly higher than the lower phase flow rate the coil is mainly filled with upper phase.

For certain flow rate combinations the lower (heavy) phase occupies most of the outer loops of the coil while the upper (lighter) phase occupies most of the inner loops (Figure 4-1C).

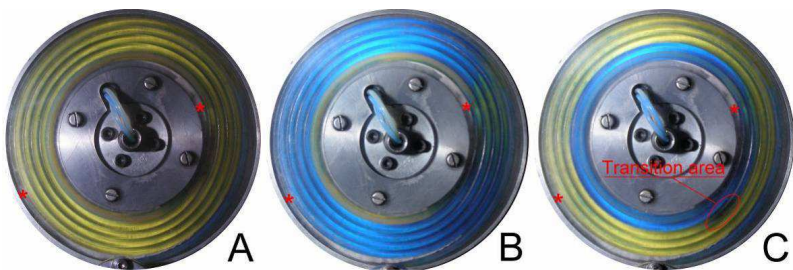


Figure 4-1: Pictures of the coil spinning at 1000 rpm with 4B phase system and the phases at equilibrium at (A): 50 ml/min for both the upper and lower phase; (B) 150 ml/min for the upper phase and 50 ml/min lower phase flow rates; and (C) 85 ml/min for the upper phase flow rate and 10 ml/min for the lower phase flow rate. The red asterisks mark the location of the coil terminals.

The position of the transition area is dependent on the flow rate combinations, phase system and temperature.

4.2.3.2 Phase ratio

For each experiment the amount of upper phase inside the coil and system was measured. As described in the method section this was done by refilling the coil with lower phase prior to every experiment and collecting the effluent to determine the displaced volume of lower phase so that the volume of the upper phase inside the coil could be calculated. This value was used then to determine the percentage of lower phase inside the coil.

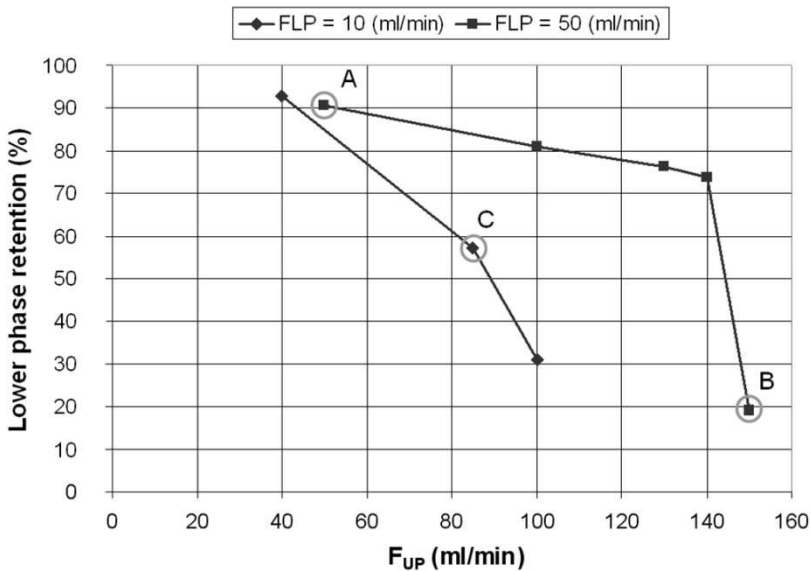


Figure 4-2: Effect of flow rate on the percentage of lower phase inside the coil. The lines in the graph show the phase system 4B at lower phase flow rates of 10 ml/min and at 50 ml/min. The marked points correspond to the pictures illustrated in Figure 4-1.

Figure 4-2 shows the percentage of lower phase in the coil as a function of the upper phase flow rate for two different lower phase flow rates (10 and 50 ml/min). When the lower phase flow rate was 10 ml/min, increasing the upper phase flow rate from 40 to 85 to 100 ml/min decreased the percentage of lower phase in the coil. When the lower phase flow rate was 50 ml/min, increasing the upper phase flow rate from 50 through 100, 130, 140 to 150 ml/min also decreased the percentage of lower phase in the coil. Initially the decrease in the percentage of lower phase shows a linear relationship with the increasing upper phase flow rate. After the upper phase flow rate of 140 ml/min this shows a significant drop.

4.2.4 Discussion

During the experiments it was noted that with certain flow rate combinations the lower phase that initially occupied the coil was partly replaced by the upper phase flowing in. Due to the rotation the heavy lower phase naturally wants to go to the tail of the coil and the light upper phase naturally wants to go to the head [Sutherland et al. 2000]. The study of the behaviour of the phases flowing against each other through the coil shows that the phases do not distribute equally throughout the coil. The phase distribution can be compared with the modes of operation for normal single phase flow (isocratic) CCC. These modes are normal phase mode and reverse phase mode. For normal phase mode the organic (upper) phase is mobile and generally occupies a small volume inside the coil while the aqueous (lower) phase is stationary. For reverse phase the aqueous (lower) phase is mobile and generally occupies a small volume inside the coil. At the head of the dual-flow coil the phases are distributed similar to reverse phase mode and at the tail of the coil the phases distribute similar to normal phase mode. In between these two modes there is a transition area that appears at different locations in the coil for different flow rate combinations. This is shown schematically in Figure 4-3.

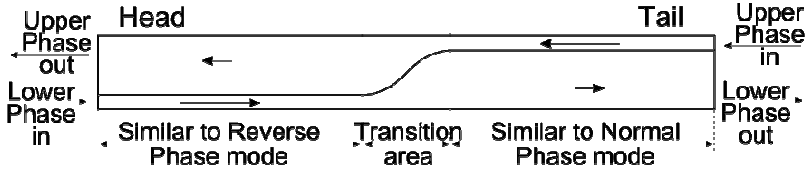


Figure 4-3: Stretched out dual-flow coil with the observed phase distribution.

The position of the transition area is dependant on the flow rates of both the phases, the physical properties of the phase system used and the rotational speed of the coil. When the flow rate of the lower phase is equal to the flow rate of the upper phase the transition area will be nearer the head of the coil. This means that the lower phase occupies a larger volume inside the coil than the upper phase. This is due to the denser and more viscous nature of the lower phase. To achieve equal volumes of upper and lower phase in the coil and a transition area in the centre of the coil the flow rate of the upper phase needs to be higher than the flow rate of the lower phase. In Figure 4-1(A) the transition area is located at the centre outlet. The blue that can be seen at the periphery is the inlet tube filled with upper phase. Any other blue seen in Figure 4-1(A) are the mixing waves occurring due to the rotation. Figure 4-1(B) has the transition area located at the periphery outlet. The yellow at the centre of the coil is the inlet tube filled with lower phase. A small amount of yellow can be seen to the right of Figure 4-1(B).

Ito et al. [2006] assume in the dual-flow theory that the phases distribute equally throughout the coil. However, the observations from this study suggest this is not the case. The distribution of the phases inside the coil appears to be more complex than initially thought and suggested. Phase distributions and linear flow rates vary radically in different areas of the coil, as shown in Figure 4-1(C). The distribution of the phases in the coil and the position of the transition area appear to be related to the physical properties of the phases and their flow rates – the exact relationship will require a much more detailed study. Separations in dual-flow coils will be influenced by the location of the transition area and the distribution of the phases inside the coil.

4.2.5 Conclusion of initial visualisation studies

The initial observations from this study appear to contradict the logical assumptions made by Ito et al. [2006] in a publication where a theory of DFCCC was proposed. Phase systems flowing through a dual-flow coil appear not to distribute evenly along the length of the coil. The majority of the heavy phase collects at the tail and the majority of the light phase collects at the head of the coil. This complicates the proposed theory on DFCCC as it affects the assumptions on which the theory is based. Understanding the relationship between the phase retention in the coil, the flow rates of the phases and the position of the interface would be a step forward in the development of the DFCCC theory. The studies to gain an understanding into the behaviour of the phases in the coil both in isocratic CCC and in Dual Flow CCC are described in the following parts of the chapter.

4.3 Normal and Reverse phase mode

To understand the behaviour of the phases in the coil under Dual Flow conditions the behaviour of the phases in the coil in the two isocratic CCC modes are studied. These two modes are the Normal phase mode where the upper (non-polar and organic) phase is mobile and the Reverse phase mode where the lower (polar and aqueous) phase is mobile. The experimental method used for this section was described in the methods chapter (section 2.3).

4.3.1 Aim

The aim of these experiments was to investigate the behaviour of the phases in the coil in isocratic CCC modes. Du et al. [1999] described the linear relationship of the square root of the mobile phase flow rate and the stationary phase retention in the coil. Later, Wood [2002] described the connection between the linear relationships and the viscosity of the mobile phases across the two isocratic modes for one phase system in one coil. In this study these

linear relationships are established and compared with the viscosity ratio.

4.3.2 Experiments Performed

The methods and the set-up for the experiments performed are described in the methods chapter (section 2.3). These methods are for Dual Flow CCC but for Normal and Reverse phase CCC one of the flow rates was zero and the other flow rate ranged between 10 ml/min and 200 ml/min. Each flow rate was tested twice for each mode of operation to ensure repeatability. The experiments were performed using the 4A, 4B and 4C phase systems.

4.3.3 Results and Analysis

The following three figures (Figure 4-4, Figure 4-5 and Figure 4-6) show the Du-plots for the normal and reverse phase mode for the three phase systems tested. In the Du-plot for the 4A phase system can be seen that in reverse phase mode the stationary phase retention is higher and decreases slower than in the normal phase mode. This is unexpected as for the other two phase systems (4B and 4C) the normal phase mode has higher stationary phase retention and decreases slower. Also when the slopes are compared with the viscosity as was suggested by Wood [2002] and described in section 1.3.2.2:

$$\frac{B_{LP}}{B_{UP}} = \sqrt{\frac{\mu_{LP}}{\mu_{UP}}} \quad \text{Equation 1-15}$$

This does not entirely match as shown from the slopes and the calculations shown in the following table.

Table 4-1: The physical properties data (density, interfacial tension and viscosity), Du-plot gradients and the calculations are taken from Wood [2002].

	4A (1 st)	4A (2 nd)	4B	4C
Density				
ρ_{UP} (kg·m ⁻³)	679	679	708	833
ρ_{LP} (kg·m ⁻³)	947	947	938	931
Interfacial Tension				
Γ (mN·m ⁻¹)	17.8	17.8	6.2	1.1
Viscosity				
μ_{UP} (mN·s·m ⁻²)	0.36	0.36	0.35	0.42
μ_{LP} (mN·s·m ⁻²)	1.36	1.36	1.35	1.35
B_{UP}	-0.0175	-0.0149	-0.0045	-0.0346
(R ²)	(0.9985)	(0.9937)	(1)	(0.9973)
B_{LP}	-0.0215	-0.0202	-0.0076	-0.0596
(R ²)	(0.9988)	(0.9945)	(1)	(0.9974)
$\sqrt{\frac{\mu_{LP}}{\mu_{UP}}}$	1.9437	1.9437	1.9639	1.7928
$\frac{B_{LP}}{B_{UP}}$	1.2286	1.3557	1.6889	1.7225

The linear part of the slopes, which is usually the first part of the slope with the lower flow rates, was used to calculate the gradient of the slope. For the 4A phase system the Du-plot is repeated with lower flow rates because the Du-plot with the higher flow rates showed the slope for the normal phase mode below the slope of the reverse phase mode. This unexpected behaviour could not be explained and therefore the Du-plot experiments were repeated with lower flow rates. The results of both experiments are shown in Figure 4-4 and included in the table above. The 4C gradients and the viscosities of the 4C phase system show the closest relationship. Phase system 4B follows and the phase system 4A shows the worst relationship. Even the repeat of the 4A phase system does not give a good relationship. It is interesting to note that the 4C relationship, which is closest, is the one with the lowest interfacial tension and the lowest density difference.

Experiments on the Photographic rig

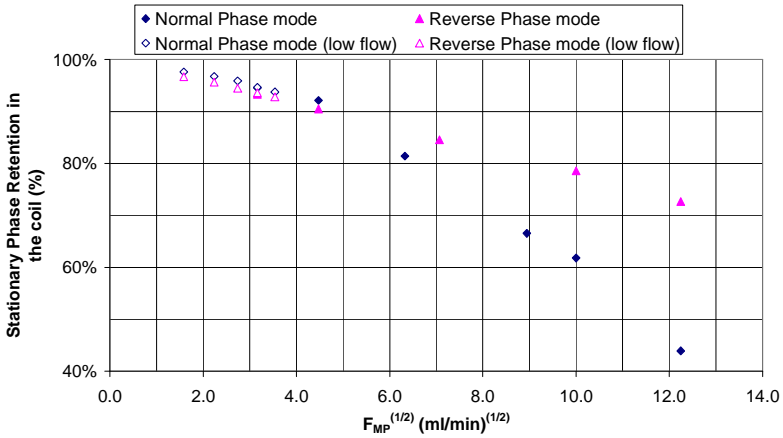


Figure 4-4: Du plot of the Normal and Reverse phase mode for the 4A phase system in the 5mm ID bore DFCCC coil at 1000 rpm.

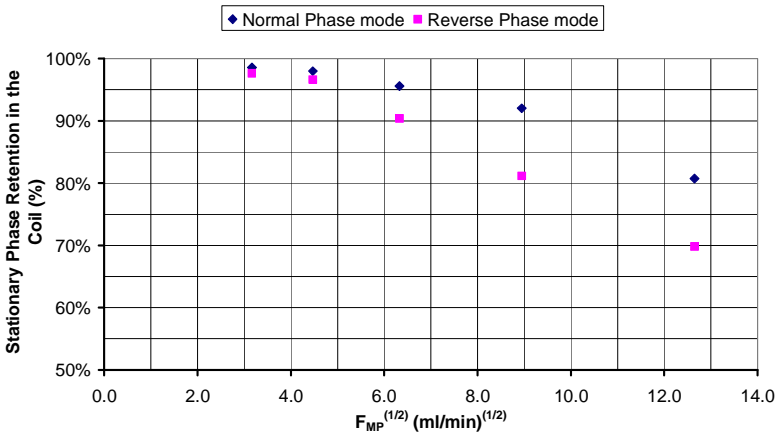


Figure 4-5: Du plot of the Normal and Reverse phase mode for the 4B phase system in the 5mm ID bore DFCCC coil at 1000 rpm.

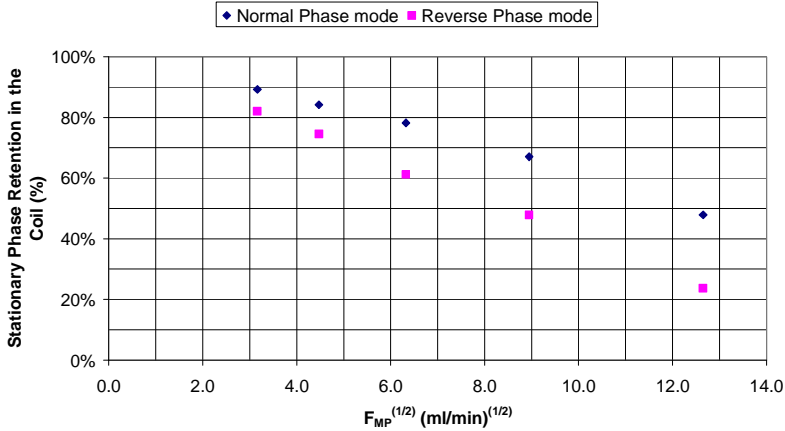


Figure 4-6: Du plot of the Normal and Reverse phase mode for the 4C phase system in the 5mm ID bore DFCCC coil at 1000 rpm.

4.3.4 Discussion and Conclusion

The Du-plots were determined and the gradients of the slopes were extracted using Excel trend lines. With these gradients the relationship suggested by Wood [2002] was tested. For the 4C phase system the relationship was the best and for the 4A phase system the relationship was the worst. The first set of data for the 4A phase system was unexpected and unexplainable. It might have been an error in the making of the phase system or the addition of the dye that changed the composition and the physical properties which caused the stationary phase retention to behave the way it did. The second Du-plot for the 4A phase system showed better correlation between the gradients and the viscosity.

4.4 Retention study on the Photographic rig

This part describes the systematic retention study conducted on the photographic rig. The two main sections describe the experiments performed and the analysis of the results from these experiments.

The experimental and analysis methods with the experiments and their results are described in the methods chapter (section 2.3.4).

4.4.1 Aim

The aim of the experiments was to gain understanding of the behaviour of the phases in the coil and to identify the effect of the flow rates and the starting condition on the volume of the phases in the coil and the position of the transition area. Another aim of the experiments was to identify the flow rates and/or starting conditions that would give a phase distribution of 50%/50% in the coil with the transition area in the centre of the coil as this is thought to be the ideal operating condition.

4.4.2 Experiments Performed

The experiments were conducted on the photographic rig which was used for the visualisation study described in section 4.2 and the 4A phase system was used. For each experiment the phases were recorded photographically while they flowed through the coil. Photos were taken at two points; a) when the phases are flowing and at equilibrium in the coil and b) when the flow has stopped. The procedures described for the visualisation study (in section 2.3) are the same as the procedures used for the retention studies.

Two flow rates were chosen (one high and one low) for the upper and lower phase to make four combinations as a base for the experiment. For the high limit 50 ml/min was chosen and for the low limit 10 ml/min was chosen. These two flow rates give the four following combinations; 10/10, 50/10, 50/10 and 50/50 (upper phase/lower phase). Three starting conditions of the coil contents were chosen. These starting conditions are 0%, 50% and 100% upper phase in the coil. In addition to the twelve different experimental conditions two more flow rate combinations were chosen (30/30 and 40/20) to be used with the initial coil contents of 50% upper phase. This gives a total of fourteen experimental conditions which are shown in Figure 4-7. The analysis of the obtained photographs is described in section 2.3.4.

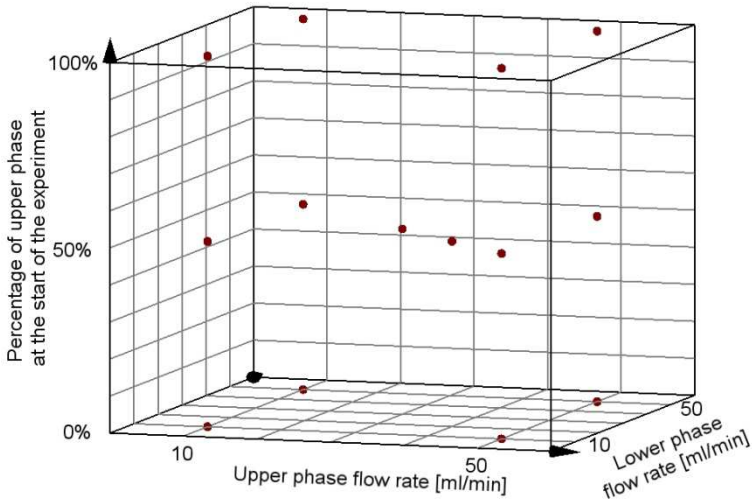


Figure 4-7: Showing the fourteen experimental conditions within the limits of 10 and 50 ml/min for the upper and lower phase flow rate and 0 and 100 % of the percentage upper phase in the coil at the start of the experiment

4.4.3 Results and Analysis

The raw data obtained from the experiments described in the previous section is shown in **Error! Reference source not found.** and is discussed and analysed in this section.

The total system volume for the upper phase is 47 ml. This includes the coil and in and outlet leads for the upper phase. The coil volume was measured to be 42 ml. Therefore the extra coil volume for the upper phase is 5 ml. The total system volume for the lower phase was also 47 ml with a dead volume of 5 ml, but this is not used as the upper phase is measured and used to determine the phase ratio in the coil. With the dead volume the measured upper phase volumes at the end of the experiment were adapted to get a true value for the upper phase in the coil. These values are shown in the following table with the calculated percentage of the coil that is occupied with the upper phase.

Experiments on the Photographic rig

Table 4-2: Data with the six flow rate combinations. The volumes are corrected for the extra coil volume and the percentage of the upper phase in the coil is calculated (V_{UP}/V_{COIL}).

F_{UP} (ml/min)	F_{LP} (ml/min)	% UP in the coil at start	Average V_{UP} (ml)	$V_{UP} -$ V_{EXTRA} (ml)	% V_{UP} in the coil
10	10	0 %	21.67	16.67	39.68 %
50	10	0 %	41.00	36.00	85.71 %
10	50	0 %	6.00	1.00	2.38 %
50	50	0 %	10.33	5.33	12.70 %

10	10	50 %	19.00	14.00	33.33 %
50	10	50 %	46.50	41.50	98.81 %
10	50	50 %	5.25	0.25	0.60 %
50	50	50 %	9.25	4.25	10.12 %

10	10	100 %	21.00	16.00	38.10 %
50	10	100 %	43.33	38.33	91.27 %
10	50	100 %	6.25	1.25	2.98 %
50	50	100 %	9.75	4.75	11.31 %

30	30	50 %	8.50	3.50	8.33%
40	20	50 %	29.50	24.50	58.33%

4.4.3.1 The effect of the starting condition on the phase distribution

The first analysis of the data is to determine the effect of the starting condition on the volume of the phases in the coil at equilibrium. To examine this, the average of the measured volume of upper phase in the coil is shown at each flow rate combination and at each starting condition (Figure 4-8).

Also in this graph is shown the average of the volume of upper phase for each flow rate combination across the starting conditions with the standard deviation (as error bars) of these measurements. The average values of the volume of upper phase in the coil and the calculated standard deviations between the experiments with the different starting conditions are shown in Table 4-3.

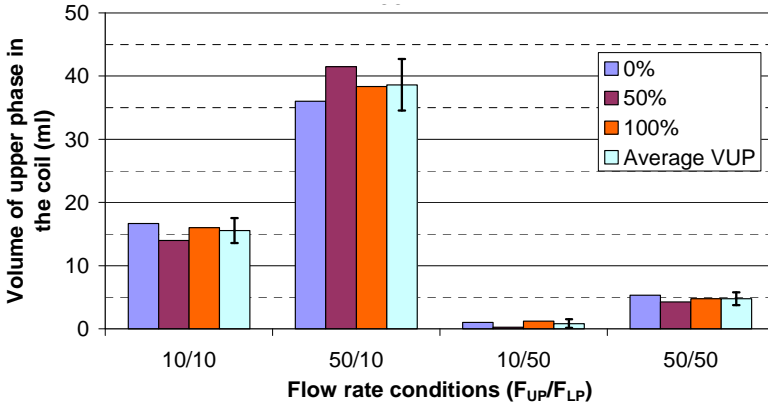


Figure 4-8: Average of the measured volume of the upper phase in the coil at each flow rate combination and at the different starting phase distributions in the coil.

In the graph can be seen that there is no significant difference in the upper phase volume of a given flow rate condition for the different phase distributions in the coil at the start of the experiments. This means that the volume of the upper phase in the coil at equilibrium is independent of the starting conditions, i.e. whether the coil is filled with upper phase, lower phase or a mixture of the two.

Table 4-3: Mean upper phase volume across the starting conditions with the standard deviation and the percentage of upper phase in the coil.

FUP/FLP	Mean V_{UP} (ml)	STDEV (ml)	% VUP in the coil
10/10	15.56	1.976	37.04%
50/10	38.61	4.077	91.93%
10/50	0.83	0.683	1.98%
50/50	4.78	1.029	11.38%

4.4.3.2 Statistical analysis of the data

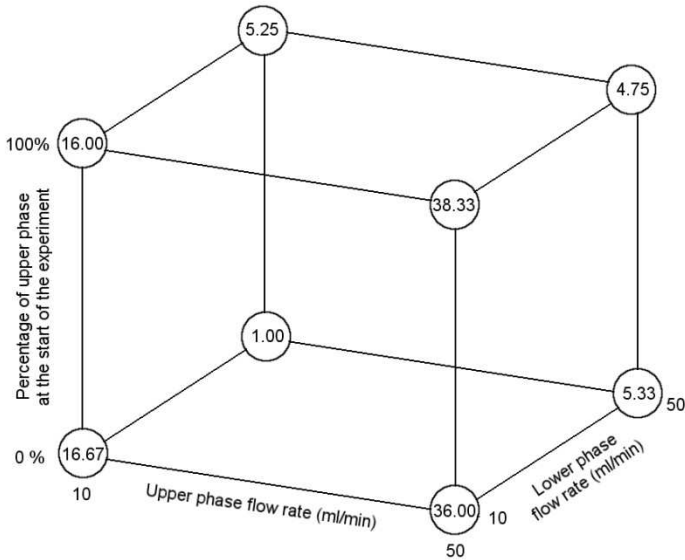


Figure 4-9: 2³ factorial design of the retention study experiment showing the 8 points measured with the average results of the volume of upper phase in the coil at equilibrium

The observations described in the previous section are confirmed when the results of the retention experiments are analysed using the 2³ factorial experimental design principle [Box et al. 1978]. This design has three variables (which are the flow rates for both the upper and lower phase and the phase in the coil at the start of the experiment) with each two values (10 ml/min and 50 ml/min for the flow rates and either upper or lower phase in the coil at the start of the experiment). The effect of the variables on the volume of upper phase in the coil is studied and the results from the experiments related to this design are shown in Figure 4-9 (the raw data is listed in Appendix VIII). In Appendix VIII the calculations with the analysis of this experimental design are shown. The effect of each variable is

calculated and the effect of interacting variables is calculated. The further the result is away from zero the greater the effect of this variable or the variable interaction.

With the results shown in the figure the effects of the variables and the interactions between them is calculated and these are shown in Table 4-4. As an example the calculation for the effect of the upper phase flow rate is as follows.

$$\begin{aligned} \text{Effect } F_{UP} &= \frac{36.00 + 5.33 + 38.33 + 4.75}{4} - \\ &\frac{16.67 + 1.00 + 16.00 + 1.25}{4} = 12.38 \end{aligned} \quad \text{Equation 4-1}$$

The large number calculated (12.38) means that the flow rate of the upper phase has a great effect on the upper phase volume in the coil.

An example of the calculation for the two factor interaction between the two flow rates is as follows.

$$\begin{aligned} \text{Effect } F_{UP} \times F_{LP} &= \frac{16.67 + 16.00 + 5.33 + 4.75}{4} - \\ &\frac{36.00 + 38.33 + 1.00 + 1.25}{4} = -8.46 \end{aligned} \quad \text{Equation 4-2}$$

The equations and an image explaining these calculations including the three factor interaction calculation are shown in Appendix VIII. The effects and interactions are calculated from averages of at least two experiments. The results from these independent experiments are used to calculate the standard error (also shown in Appendix VIII).

From the main effect of the starting phase in the coil and the interactions of the starting phase with the flow rates, it can be concluded that whether the coil is filled with upper or lower phase at the start of the experiment this does not have any effect on the equilibrium of the phases in the coil. The lower phase flow rate has

almost twice as big an effect on the upper phase volume in the coil than the upper phase flow rate. However, according to this analysis they both have a great effect on the upper phase in the coil.

Table 4-4: Calculated effects and standard errors for the 2³ factorial design of the retention study on the photographic rig

Effect	Estimate +/- standard error		
Main Effects = average(+) - average(-)			
F _{UP}	12.38	+/-	1.54
F _{LP}	-23.67	+/-	1.54
% UP	-0.33	+/-	1.54
Two factor interactions			
F _{UP} x F _{LP}	-8.46	+/-	1.54
F _{UP} x %UP	0.54	+/-	1.54
%UP x F _{LP}	-0.50	+/-	1.54
Three factor interactions			
F _{UP} x F _{LP} x %UP	-0.96	+/-	1.54

4.4.3.3 Ideal operating conditions analysis

It is assumed that the ideal running condition in the coil would be the flow rates when there is 50% upper phase in the coil. Ratios around this 50% like between 40% and 60% upper phase in the coil could also be ideal running conditions, but the 50% ratio is used here for the further calculations. To find this flow rate or these flow rates Figure 4-10 is used. In this figure the percentage of upper phase in the coil is shown with their flow rates. At the point of 50% upper phase in the coil a surface is drawn to show the aimed level. The point at 40/20 (which means 40 ml/min for the upper phase and 20 ml/min for the lower phase) is not included in the calculations as this point is aimed to be found. Lines are drawn as an approximation of

curves between points 30/30 and 50/10, 10/50 and 50/10 and between 50/50 and 50/10 to calculate the flow rate combination between these two points where the percentage of upper phase in the coil is 50%.

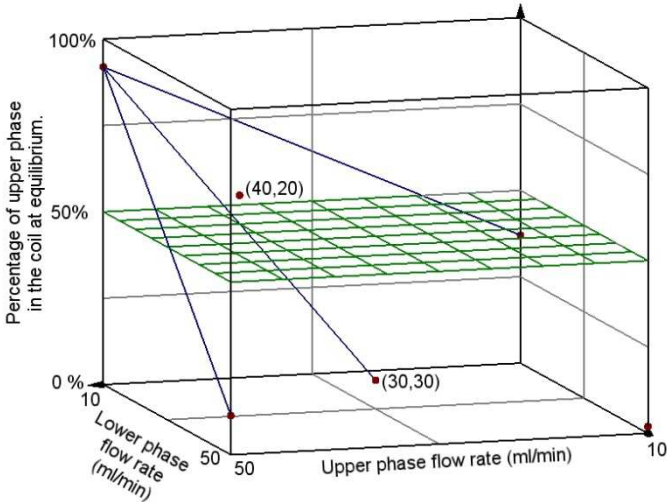


Figure 4-10: Percentage of upper phase in the coil against the flow rate. The lines between some of the points are used to calculate some ideal flow rate for 50% upper phase in the coil at equilibrium.

The main equation used for the calculations to determine this flow rate is as follows.

$$\mathbf{r}(t) = \mathbf{a} + t \cdot (\mathbf{b} - \mathbf{a}) \quad \text{Equation 4-3}$$

Where: **a** is one of the two points indicated as a vector
b is the other point indicated as a vector
r(t) is the vector at “t” between points **a** and **b**

The calculations are then as follows:

$$\begin{pmatrix} F_{UP} \\ F_{LP} \\ 50\% \end{pmatrix} (t) = \begin{pmatrix} 30 \\ 30 \\ 8\% \end{pmatrix} + t \cdot \left(\begin{pmatrix} 50 \\ 10 \\ 92\% \end{pmatrix} - \begin{pmatrix} 30 \\ 30 \\ 8\% \end{pmatrix} \right)$$

The value of “t” was calculated as follows:

$$50\% = 8\% + t \cdot (92\% - 8\%)$$

$$t = \frac{50\% - 8\%}{92\% - 8\%} = 0.498$$

And with the value “t” the values of the flow rates “F_{UP}” and “F_{LP}” were calculated as shown in the following calculations.

$$F_{UP} = 30 + 0.498 \cdot (50 - 30) = 39.9 \text{ (ml/min)}$$

$$F_{LP} = 30 + 0.498 \cdot (10 - 30) = 20.0 \text{ (ml/min)}$$

At the experimental point 40/20 there was 58.3% of upper phase in the coil.

Another point near the 50% surface is the point with the flow rates 10/10. These flow rates resulted in 37.04% upper phase in the coil at equilibrium. With the 10/10 and 50/10 flow rates and their volume percentages in the coil another point that would result in 50% upper phase in the coil can be calculated. These calculations are as follows.

$$\begin{pmatrix} F_{UP} \\ F_{LP} \\ 50\% \end{pmatrix} (t) = \begin{pmatrix} 10 \\ 10 \\ 37\% \end{pmatrix} + t \cdot \left(\begin{pmatrix} 50 \\ 10 \\ 92\% \end{pmatrix} - \begin{pmatrix} 10 \\ 10 \\ 37\% \end{pmatrix} \right)$$

$$t = \frac{50\% - 37\%}{92\% - 37\%} = 0.236$$

$$F_{UP} = 10 + 0.236 \cdot 40 = 19.44 \text{ (ml/min)}$$

$$F_{LP} = 10 + 0.236 \cdot 0 = 10 \text{ (ml/min)}$$

The two calculated points suggest that the flow rate of the upper phase should be twice as high as the flow rate of the lower phase. This was also suggested by the statistical analysis which showed that the effect of the lower phase flow rate is almost twice as big as the effect of the upper phase flow rate (Table 4-4). It is also interesting to point out that the square root of the lower phase viscosity over the upper phase viscosity is 2.

The intercept between the surface and the third line and the intercept between the surface and the 10/10 and 30/30 point are calculated in the same way as the previous two intercepts. These intercepts are plotted in Figure 4-11 and show a linear relationship for the flow rates up to 40 ml/min for the upper phase and 20 ml/min for the lower phase. The values of the intercepts calculated for all four lines are shown Table 4-5.

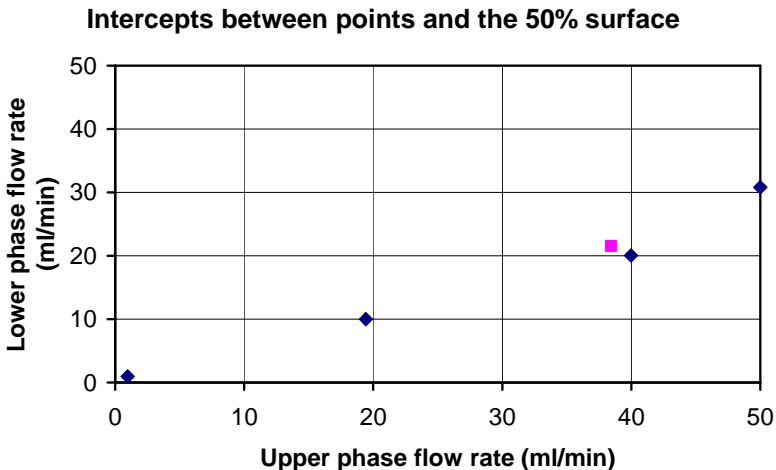


Figure 4-11: The blue diamonds show the intercepts between the lines (between the points shown in Figure 4-10) and the 50% surface. The pink square shows the intercept between the line between point 40/20 and 30/30 and the 50% surface.

Experiments on the Photographic rig

Table 4-5: Two points used for the calculation of the intercepts and the results of the four intercepts with the 50% surface.

Point 1			
Data	F UP (ml/min)	F LP (ml/min)	V UP (ml)
1	10	10	37.04
2	30	30	8.33
3	50	50	11.38
4	10	10	37.04

Point 2			
Data	F UP (ml/min)	F LP (ml/min)	V UP (ml)
1	50	10	91.93
2	50	10	91.93
3	50	10	91.93
4	30	30	8.33

Calculated		
Data	F UP (ml/min)	F LP (ml/min)
1	19.44	10.00
2	39.97	20.03
3	50.00	30.82
4	0.97	0.97

The point 40/20 was tested but not used for the calculations as mentioned before (on page 127). According to the calculations the point 40/20 should give a percentage of upper phase in the coil of 50%, however, the experiments showed that the percentage for this point was 58.33%. As was said before, the line between the two points used for the calculations was assumed to be linear. This point however, shows that this is not the case as the predicted flow rate gave a percentage which is higher than desired. When the point 40/20 is used with the point 30/30 to predict the flow rates that would

give a 50% volume distribution in the coil the result is 38.43/21.57 (shown in Figure 4-11).

4.4.3.4 Analysis of the number of loops filled with upper phase

The number of loops filled with upper phase measured from the photographs taken during the experiments is converted into percentages of the coil length which is shown in Table 4-6. This means that they now also represent the percentage of the coil occupied with upper phase. At two points during the experiments photographs were taken, at equilibrium with flow and without flow at the end. The length of these two points was calculated and transferred to the percentage of the coil.





Table 4-6: Percentage of upper phase in the coil with their flow rates measured in two different ways. The volume collected at the end of the experiment and graphically.

F_{UP} (ml/min)	F_{LP} (ml/min)	Percentage of upper phase in the coil calculated from the:		
		Volume	Length measured	
			During	End
10	50	1.98%	1.72%	5.25%
30	30	8.33%	5.25%	10.72%
50	50	11.38%	8.29%	14.34%
<hr style="border-top: 1px dashed black;"/>				
10	10	37.04%	37.37%	37.30%
40	20	58.33%	58.54%	56.73%
50	10	91.93%	91.77%	85.42%

In Table 4-7 four pictures are shown of two different experiments. For each experiment there are two pictures, one of the coil during the experiment when the phases are at equilibrium and one at the end of the experiment when the pumps were stopped. The two experiments shown are the 50/10 experiment with 100% upper phase at the start of the experiment and the 40/20 experiment with 50% upper phase in the coil at the start of the experiment. Results

from the measurements done on the photographs are listed in **Error! Reference source not found.**

Table 4-7: Two picture sets of two experiments with one picture of the coil during the experiment and one picture at the end of the experiment.

	During the experiment at equilibrium.	At the end of the experiment when the flows were stopped.
$F_{UP}=50$ (ml/min)		
$F_{LP}=10$ (ml/min)		
$V_{UP}=100\%$		
$F_{UP}=40$ (ml/min)		
$F_{LP}=20$ (ml/min)		
$V_{UP}=50\%$		

In the table can be seen that there is a difference between the percentage of coil with upper phase “during” the experiment (when the phases were flowing) and at the “end” of the experiment (when the flows were stopped). When there is a small amount of upper phase in the coil the percentage at the end is larger than during and when the coil is almost filled with upper phase this is the reverse. While the phases are flowing there is lower phase next to the upper phase and upper phase next to the lower phase. When the flow stops all the upper phase collects at the head of the coil at the centre and all the lower phase collects at the tail of the coil at the periphery. This is graphically shown in Figure 4-12.

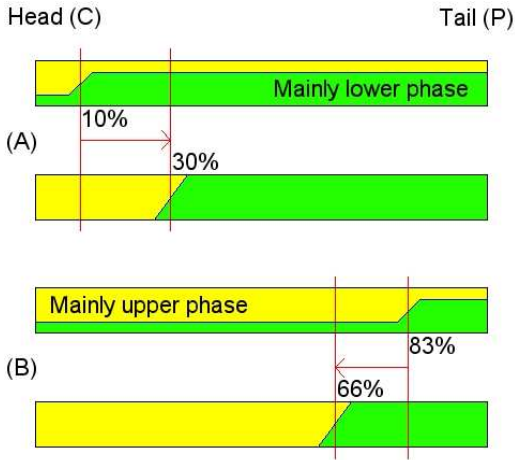


Figure 4-12: Volume distribution between the two observed points in the experiments. For both (A) and (B) the top coil shows the phases flowing and the bottom of the two shows the phases stopped. (A) has mainly lower phase in the system and shows that the observed percentage of upper phase increases. (B) has mainly upper phase in the coil and shows that the observed percentage of upper phase decreases.

In Table 4-6 can also be seen that there is a difference between the percentage of coil filled with upper phase calculated from the measured volume and calculated from the measured distance at the end of the experiment. This difference has two causes. The first cause is the (yellow) lower phase next to the (blue) upper phase when the distance is measured. Because the blue phase is darker than the yellow phase only the blue phase is observed and not the thin line of yellow next to it. This explains why more upper phase is measured than there actually is and has the most effect on the measurements when there is a small amount of upper phase in the coil. The second cause is the calculation from the number of loops to the percentage of upper phase occupying the coil. When there is a larger amount of upper phase the distance indicates there is less upper phase in the coil than there actually is. This difference is due to the calculations as from the number of loops the percentage of coil occupied by upper phase is calculated as if the coil is a straight tube. This however is not the case and due to the bending of the tube the

internal volume becomes less. The two measurements show a linear relationship when they are plotted against each other (Figure 4-13) which could be used for correction of the measurements in the future.

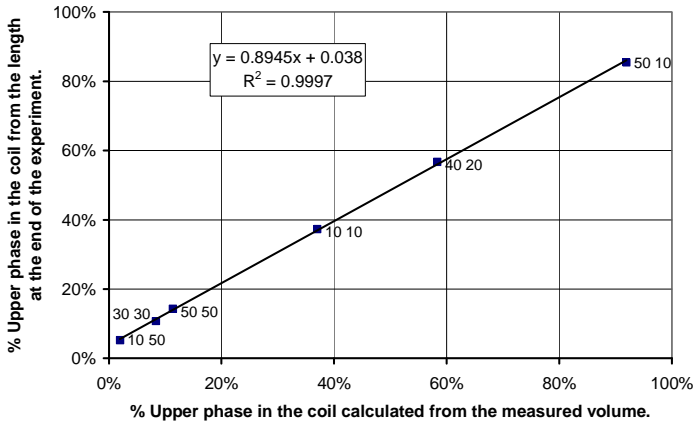


Figure 4-13: Percentage of upper phase in the coil determined from the number of loops at the end of the experiment versus determined from the measured volume.

With the calculations proposed in section 3.2 the length of the coil which appears to be occupied with the upper phase during the experiment (or the location of the transition area) could be calculated. The location of the transition area calculated can then be compared with the location calculated from the photographs. In Table 4-8 the calculated values are listed with the flow rates of the experiments. The gradients used are the 4A gradients from the repeated experiments with the lower flow rates and are listed in Table 4-1. In the table can be seen that there is a difference between the location of the transition area calculated from the photograph and using the calculations proposed in Chapter 3. When there is a small amount of upper phase in the coil, the difference between the location calculated from the photograph and the in Chapter 3 proposed calculations is around 7%. The difference is around -6% when the coil is almost filled with upper phase (high

percentage of upper phase in the coil) and the difference is +/- 1% when the coil is half filled with upper phase.

Table 4-8: Calculated values for the position of the transition area using the photograph and the in Chapter 3 proposed calculations (Equation 3-5). The values for the gradients (B) are taken from Table 4-1.

F_{UP}/F_{LP} (ml/min)	%LP (N)	%UP (R)	$\%V_{UP}$	Photo %X	Calc. %X	Diff %X
10/50	95.3%	85.7%	2.0%	1.7%	-3.4%	5.1%
30/30	91.8%	88.9%	8.3%	5.3%	0.2%	5.0%
50/50	89.5%	85.7%	11.4%	8.3%	1.1%	7.2%
10/10	95.3%	93.6%	37.0%	37.4%	36.4%	1.0%
40/20	90.6%	91.0%	58.3%	58.5%	60.0%	-1.4%
50/10	89.4%	93.6%	91.9%	91.8%	98.0%	-6.2%

There are several possible reasons for the difference between the location of the transition area calculated using the photograph and the proposed calculations in Chapter 3. The first one would be that for the proposed calculations there is assumed that the phases in the coil at the head end behave as in reverse phase mode and at the tail end behave as in normal phase mode. However, for the normal and reverse phase mode there is one phase stationary and one mobile and this is not the case in the dual flow coil. Another reason for the difference would be that there is an error in the determined gradients from the Du-plots. The ratio of the gradients is not the same as the square root of the ratio of the viscosities of the phases, which was suggested to be the same by Wood [2002]. This indicates that there could be an error in the gradients from the Du-plots. Flatter Du-plots which would mean smaller gradients would give a calculated position of the transition area from the method in Chapter 3 closer to the position calculated from the photograph. It is also possible that there is an error in the position calculated from the photograph and/or in the percentage of upper phase in the coil, however the negative position calculated by the in Chapter 3 proposed calculations must be due to either these calculations or the gradients from the Du-plots.

4.4.4 Discussion of Results

As is shown from the results, the initial conditions of the phases filling the coil do not influence the final volume of upper phase in the coil. This would be reasonable to assume as both phases enter and leave the coil during the experiment, but it has now been shown experimentally. During a separation, this could prove to be very useful for the following reasons. 1) The extra volume of one or both phases introduced when the sample is injected will be corrected by the flowing phases and their equilibrium. 2) Stripping caused by some sample mixtures in normal CCC will not occur in DFCCC as both phases are continuously refreshed.

The ideal operating condition of the DFCCC centrifuge in terms of the phase volume distribution in the coil depends entirely on the required separation parameters. For these experiments this optimum condition is assumed to be around 50%. It is obvious that the separation is affected by the volume distribution and the flow rates, but how these two relate is not very clear. From the statistical analysis it is clear that the lower phase flow rate has a larger effect on the volume distribution in the coil than the upper phase. However, they both seem to have a large effect on the volume distribution in the coil. A different statistical method could be used to determine the effect of both flow rates on the volume distribution in the coil at equilibrium.

From the results it was not straightforward to predict the operating conditions that would give a 50% volume ratio in the coil. Drawing a straight line as an estimation gave a good indication of the flow rates that would result in a coil being filled with approximately 50% upper phase. However, the relationship between the flow rates and the upper phase in the coil is not linear but is likely to be more complex. To find this relationship more flow rates between the flow rates tested should be used like the 40/20 point which is shown in Figure 4-11. This would give a better view of the shape of this relationship and would allow a mathematical programme to calculate it.

The number of loops measured on the photographs corresponds with the amount of upper phase in the coil. This is due to the experimental nature of the set-up and the error in the calculation

from these loops to the volume or percentage. The linear relationship between the real and calculated percentage are most likely due to the inlet tubes in either end of the coil which make the phase in the coil seem more than there actually is. This explains why there is more upper phase in the coil according to the photographs when there is only a small amount of upper phase in the coil. Improvement of the photographs using better lighting and better imaging equipment would allow for better precision in the study of the behaviour of the phases inside the coil. Better lighting and more rapid photographs would result in sharper images where the phase distribution throughout the coil can be determined. A video or a series of high-speed photographs of the phases reaching equilibrium inside the coil would also be useful in gaining a greater understanding of the development of the complex hydrodynamic equilibrium between the phases and may allow an analysis of response to changes of any of the system variables like flow.

The prediction of the location of the transition area in the coil using the calculations proposed in Chapter 3 seems to be more complex than thought initially. The Du-plot gradients which are used for the calculations are not reliable as they do not correspond with the viscosity of the phases as was proposed by Wood [2002]. These Du-plot gradients are used for the calculations and this might explain why there is a difference between the location determined from the Du-plot gradients and from the photographs.

4.5 Conclusions

From the visualisation studies, it can be concluded that the balance of the phases flowing through the coil at equilibrium is complex. It was shown that the phases were not evenly distributed through the coil as was suggested by Ito and co-workers [2006]. The volumes of upper and lower phase and how they are distributed does influence the separation. Therefore, it is important to understand the relationship between the flow rates and the phase distribution.

The systematic retention study on the photographic rig has shown that the initial volume distribution in the coil (whether 100% upper phase or 100% lower phase or a mixture of the two) does not influence the volume distribution at equilibrium. This could have benefits when separations are performed on the DFCCC centrifuge

as the equilibrium in the coil will restore itself if it would become disrupted by injected sample mixtures. The retention studies showed that the effect of the lower phase flow rate on the volume of upper phase in the coil is twice as big as the effect of the upper phase flow rate. The photographic results should be improved to gain more understanding of the hydrodynamics inside the coil. With better lighting and higher-speed cameras or video recordings sharper images could be obtained and the location of the interface could be determined with more accuracy. A coil where the tubing is visible from terminal to terminal would also give more accurate measurements. Sharper images with more detail would also allow the volume distribution on either side of the interface to be determined.

Chapter 5 Applications study at Pfizer Ltd

5.1 Outline

This chapter describes the results of the application studies done on the CCCE centrifuge at the Pfizer R&D Laboratories in Sandwich in Kent. The methods used for the experiments described in this chapter are discussed in section 2.4.4. This chapter consists of four sections. The first two sections describe the aim of the experiments and what experiments were done to fulfil this aim. Part three describe the results of these experiments followed by part four, the discussion.

5.2 Aim

The aim of the experiments was to prove that CCCE would be able to continuously separate components from each other. Another aim was to gain understanding into the mechanism of the separation and how the separation is influenced by the flow rates of the phases.

5.3 Sample mixture screening

5.3.1 Screening Experiments

The experiments performed at the R&D Labs at Pfizer firstly involved screening experiments, where the sample mixture of components to be separated was tested against a range of phase systems. The screening method is detailed in section 2.4.1. As described after the experiments were performed, the phases were analysed and from the analysis the D-values were calculated. There were several sample mixtures tested across the basic screen which are all discussed in the results section of this chapter. It was preferred to have the D-values of the components spread around $D=1$ as this is the expected D-value where the components are split between elution from one end of the coil or the other. A range of D-values was preferred as this would give an idea of how the elution of the components behaves with the flow rates of the phases. The sample mixture chosen to use was a mixture with seven main components and a range of D-values on either side of $D=1$ (from 0.4 to 25).

5.3.2 Screening Results

5.3.2.1 Project Pfizer-A

This mixture has two components (Figure 5-1), one target compound (A) and one non-target (dimer) (B), and was screened by Dr. Stephane Dubant at Pfizer. Reasonable selectivity was achieved whilst screening using the basic screen. The EtOAc-I phase system gives D-values of 1.27 and 0.04 for peak A and B respectively and this is the largest difference between the D-values of the components around the D=1 value. The following figure shows the HPLC chromatogram of the mixture dissolved in methanol with the components labelled.

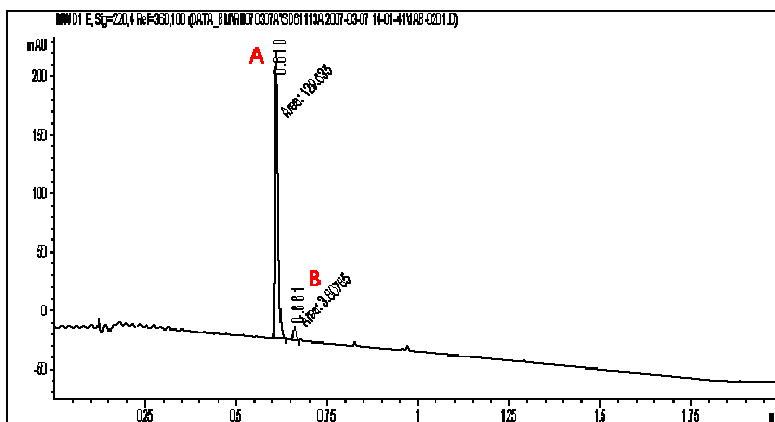


Figure 5-1: HPLC chromatogram of project Pfizer-A dissolved into methanol. The HPLC method is described in section 2.4.5.

5.3.2.2 Project Pfizer-B

This dried down mixture again has two main components labelled A and B (Figure 5-2). They had the same selectivity no matter what phase system was used. Both the basic and extended screens (Table 1-4 and the solvents from Table 1-5) have been tried and do not give any selectivity suitable for separation. For the D-values below D=4 the difference between the D-values of component A and

B ranged from 0.68 for the highest D-values to 0.01 for the lowest D-values. Due to time constraints, it was decided to drop this mixture from the test programme rather than trying to find alternative phase systems. The following HPLC chromatogram of the mixture dissolved in methanol shows the two main peaks A and B.

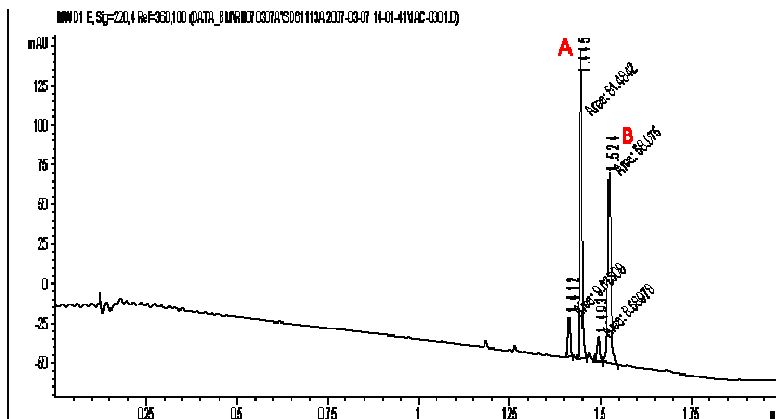


Figure 5-2: HPLC chromatogram of project Pfizer-B dissolved into methanol. The HPLC method is described in section 2.4.5.

5.3.2.3 Project Pfizer-C

This is a liquor that comes straight from a reaction. There are seven main peaks and these components are dissolved in a water/ isopropanol mixture. The basic screen has been tried and seems to give a wide range of D-values for the components. Initially EtOAc-C was identified as a good phase system for the CCCE separation, because for this phase system one component (D2) has a D-value below $D=1$ and the rest is above this D-value. However, the first separation showed that the components only eluted from one side of the coil (described in 5.4.1). From this it was decided that D-values of the seven components should be spread more and phase system EtOAc-F was chosen. For EtOAc-F the D-values are 0.44, 0.42, 0.66, 8.00, 0.71, 16.44 and 24.63 for peaks 1 to 7 respectively (identified in Figure 5-3). The complete results of the basic screen are shown in Table 5-1. Chromatograms of the upper and lower

phase of EtOAc-F are shown in Figure 5-4 and Figure 5-5. The following HPLC chromatogram (Figure 5-3) of the liquor diluted with methanol (50/50) shows the seven main peaks labelled 1 to 7.

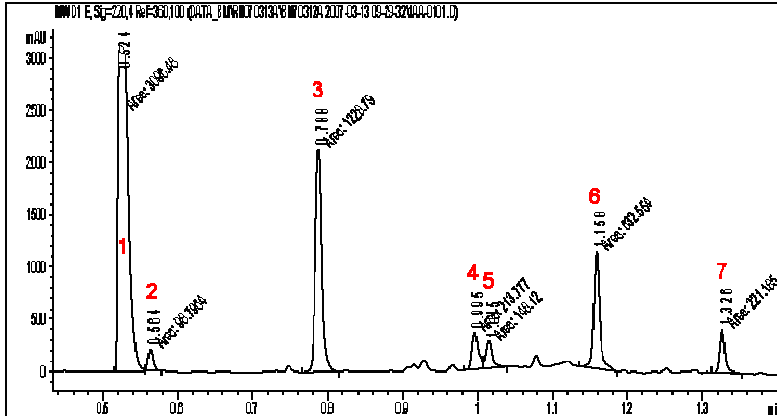


Figure 5-3: HPLC chromatogram of liquor from project Pfizer-C diluted with methanol. The HPLC method is described in section 2.4.5.

From the values of the D and E phase systems in Table 5-1 the reliability of the results can be worked out. The average of the D-values of the components in phase systems D and E is calculated and used to calculate the error in the D-value. This error ranges from 2% to 14% for all the components in the two different phase systems except for component D3 in the DCM phase system which has an error of 25%. It is thought that this error is due to an experimental error. The results from this table, however, were used as a guideline for the selection of the ideal phase system. An idea of how the D-values of the components were divided and their approximate values was required, not the exact D-values.

Table 5-1: Distribution ratio results from the basic screen on project Pfizer-C. The two EtOAc phase systems used later in the CCCE centrifuge are shaded dark grey. Phase systems D and E which have the same composition are shaded light grey.

	D1	D2	D3	D4	D5	D6	D7
EtOAc							
A	0.28	0.24	0.42	2.76	0.31	5.09	6.92
B	0.16	0.25	0.32	7.27	0.39	12.3	14.2
C	1.28	0.54	1.85	2.96	2.02	4.78	5.65
D	1.29	0.81	2.68	13.8	3.23	26.8	39.1
E	1.07	0.63	2.03	11.0	2.44	23.6	41.0
F	0.44	0.42	0.66	8.00	0.71	16.4	24.6
G	20.0	0.39	52.4	89.4	68.8	353.2	124.7
H	8.67	2.92	25.7	80.4	64.2	373.9	131.1
I	1.95	1.55	5.43	87.3	15.0	253.6	136.9
DCM							
A	22.7	0.63	0.94	0.26	0.63	0.13	0.11
B	0.06	0.64	0.22	1.83	0.41	2.82	4.36
C	0.01	20.3	50.1	42.4	55.6	289.5	69.7
D	0.01	11.9	17.7	47.9	52.7	308.2	94.6
E	0.01	9.26	10.5	49.5	54.5	361.8	113.0
F	0.16	2.03	1.60	8.07	3.38	38.8	7.50
G	0.14	50.0	133.3	36.1	45.4	202.3	48.6
H	0.13	21.0	24.9	65.9	56.9	381.8	124.2
I	0.31	5.80	4.23	57.8	6.35	36.0	112.0

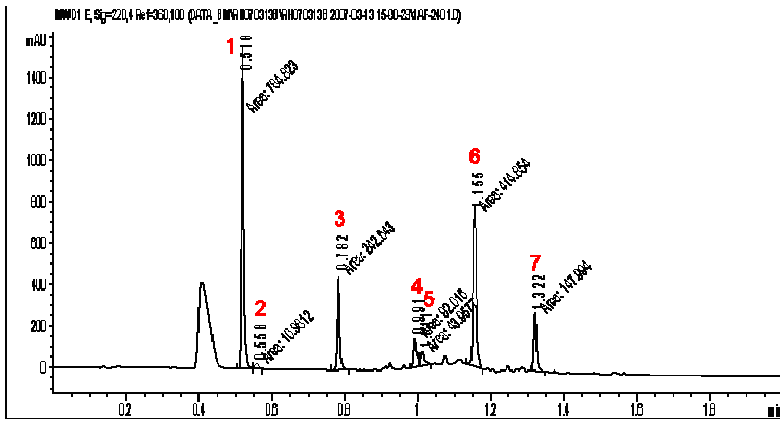


Figure 5-4: HPLC chromatogram of the upper phase partition of phase system EtOAc-F with the liquor from project Pfizer-C. The HPLC method is described in section 2.4.5.

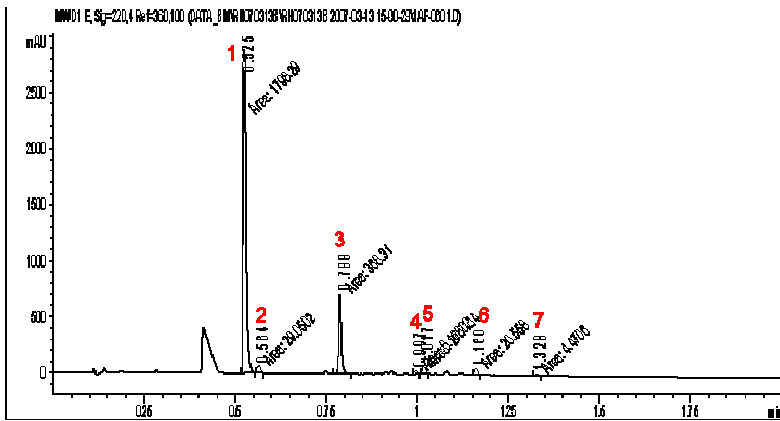


Figure 5-5: HPLC chromatogram of the lower phase partition of phase system EtOAc-F with the liquor from project Pfizer-C. The HPLC method is described in section 2.4.5.

5.3.2.4 Project Pfizer-D

This is a mixture with two main components of which 2 g was available for separation. Only the EtOAc part of the basic screen was tested and good selectivity was found. The screen results for EtOAc-D and EtOAc-E (which are the same phase systems and are shaded in Table 5-2) gave the best D-values for DFCCC. All the screen results are shown in the following table. The average D-values for the two screen results are 0.63 for A and 2.99 for B with HPLC retention time of 0.99 and 1.17 minutes respectively.

Table 5-2: Distribution ratio results of the Pfizer-D basic screen for the two main components with their HPLC elution time (note that the shaded phase systems have the same composition)

	A (0.99 min)	B (1.17 min)
EtOAc-A	0.096	0.294
EtOAc-B	0.038	0.095
EtOAc-C	1.930	8.238
EtOAc-D	0.636	3.157
EtOAc-E	0.623	2.823
EtOAc-F	0.222	1.344
EtOAc-G	28.322	187.459
EtOAc-H	10.952	127.601
EtOAc-I	2.681	9.239

The HPLC chromatograms corresponding to the screen results of EtOAc-D are shown in the following two figures.

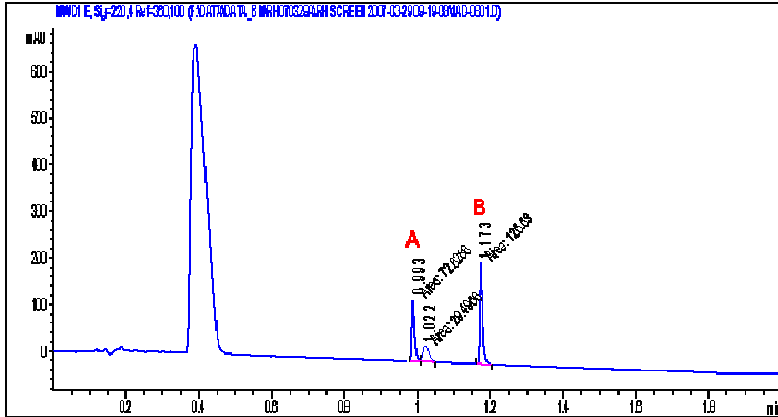


Figure 5-6: HPLC chromatogram of Pfizer-D in upper phase of EtOAc-D. The HPLC method is described in section 2.4.5.

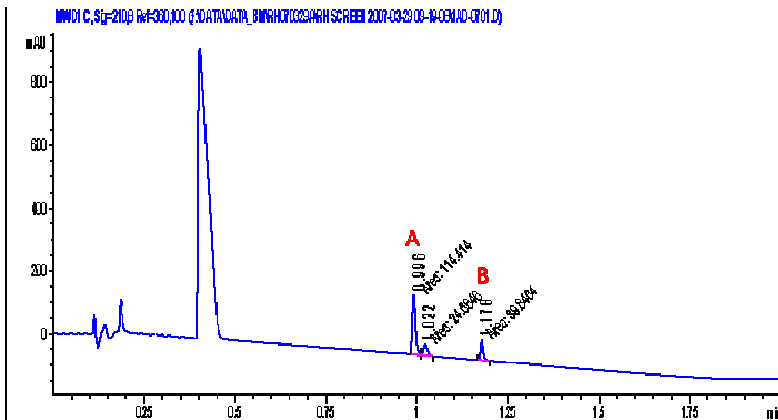


Figure 5-7: HPLC chromatogram of Pfizer-D in the lower phase of EtOAc-D. The HPLC method is described in section 2.4.5.

The error in the D-values in Table 5-2 was calculated from the D and E phase systems which have identical compositions. The highest error in these results is 6% which was deemed to be acceptable as the table is used as a guidance to see the difference in D-values and around which values they are.

5.3.3 Screening Results Discussion & Conclusions

Two of the four screened sample mixtures were chosen to be separated on the CCCE centrifuge. One mixture with multiple components was chosen to study the elution behaviour with different flow rates. The second mixture chosen is a binary sample mixture and the aim for this mixture is to separate the two components completely. Sample mixture Pfizer-C was chosen for the multiple component mixture to be used with phase system EtOAc-C initially and phase system EtOAc-F later. The choice for the binary mixture was between Pfizer-A and Pfizer-D as no suitable phase system was identified for sample mixture Pfizer-B. Pfizer-D was chosen to be separated on the CCCE centrifuge as the binary mixture because the D-values were further apart and not as near to $D=1$ as for Pfizer-A.

Table 5-3: Pfizer-D and Pfizer-A D-value comparison

	D-value of A	D-value of B
Pfizer-D in EtOAc-D	0.63	2.99
Pfizer-A in EtOAc-I	1.27	0.04

The screening method used proved to be a very useful application for the identification of the ideal phase system for a CCCE separation. As can be seen from the screening of mixture Pfizer-B, the screen does not always give a suitable phase system. To find a suitable phase system for this mixture a larger range of solvents could be used or the pH of the phases could be altered to achieve suitable selectivity. From the other applications however, it can be seen that the screening method used is an effective way to quickly find a suitable solvent phase system.

5.4 Sample Mixture Separations

5.4.1 Project Pfizer-C “Batch” separations:

For the first test separation, phase system EtOAc-C was used as initially it was thought that this phase system would be good for a CCCE separation. Initially the liquor was dried down to create a more concentrated sample to inject into the CCCE column. The

dried down sample however did not easily dissolve into the lower phase of phase system EtOAc-C. Slight precipitation occurred due to the high concentration of the sample. When injected into the centrifuge, the precipitation could cause the sample injection pump to block and not work properly so the amount of sample injected was unclear. The sample also precipitated when it reached the phase system in the coil presumably as some components were less soluble in the other phase. This precipitation collected in the sample injection tube and caused a blockage.

However, the analysis of the fractions collected in this first separation attempt did show that the components were eluting according to their D-values. At the centre of the coil where the upper phase eluted peak 6 and 7 eluted first (highest D-values), then peak 4, 5 and 3 eluted in that order and the final peak 1. Peak 2 was left in the coil and was recovered in the pump out. It seems likely that if the separation had been run for a longer period of time peak 2 would have eventually eluted from the periphery in the lower phase. From these results DFCCC seems a feasible option. The following figure shows the normalised chromatogram of the centre outlet (upper phase) constructed from the collected fraction.

Due to the problems of re-dissolving the dried down liquor it was decided that the pure liquor (sample components in the water / iso-propanol mixture) would be injected. Because for the EtOAc-C phase system only component 2 (which has a low concentration in the sample mixture) has a D-value below one a different phase system was chosen. The EtOAc-F phase system was tried as it also gave a good selectivity and would be able to separate the seven components into two groups according to the D-values. 10 ml of the liquor was injected into the coil on four separated occasions at different flow rate combinations. These flow rate combinations were 20/20, 20/30, 20/50 and 30/30 (LP/UP) as shown in Table 5-4.

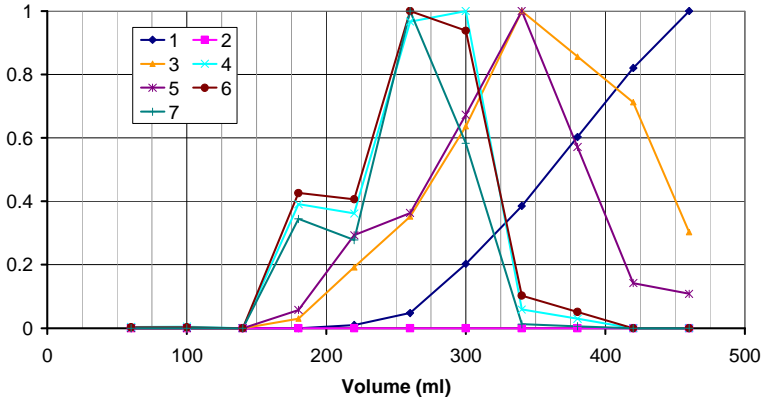


Figure 5-8: Reconstructed normalised chromatogram of the test separation using EtOAc-C on project Pfizer-C. The flow rates for the upper and lower phase were 20 ml/min. The chromatogram shows the analysed fractions from the centre outlet (UP)

Table 5-4: Flow rates of upper (UP) and lower phase (LP) and injected volume using EtOAc-F for the four "Batch" separations including the volume of upper phase in the coil at the end of the run.

Separation name	Flow rate [ml/min]		Volume [ml] sample	Volume end UP
	LP	UP		
B-1	20	20	10	30 ml
B-2	20	30	10	35 ml
B-3	20	50	10	245 ml
B-4	30	30	9.5	40 ml

The order and direction of elution of the seven peaks for the batch separations in project Pfizer-C are described in Table 5-5.

Table 5-5: Order and location of elution of the seven peaks using EtOAc-F in project Pfizer-C

Separation name	Order of elution	
	centre	periphery
B-1	4, 6 & 7 simultaneously	1 first followed by 2, 3 & 5 simultaneously
B-2	4, 5, 6 & 7 simultaneously	1 first followed by 2, 3 & 5 simultaneously
B-3	4, 5, 6 & 7 simultaneously followed by 3	1 first, 2 second and followed by 3 as last
B-4	4, 6 & 7 simultaneously	1 first, 2 second and followed by 3 & 5 simultaneously

Figure 5-9 and Figure 5-10 show chromatograms that show the normalised results of the separation B-4. The results from all the batch separations are shown in Appendix IX.

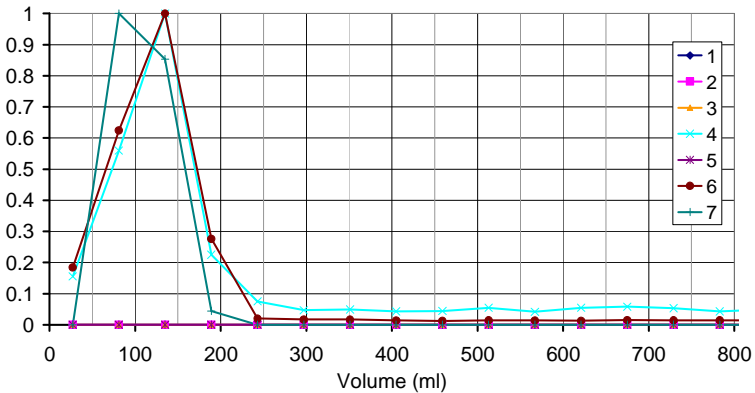


Figure 5-9: Normalised chromatogram of centre outlet (UP) of separation B-4 on project Pfizer-C

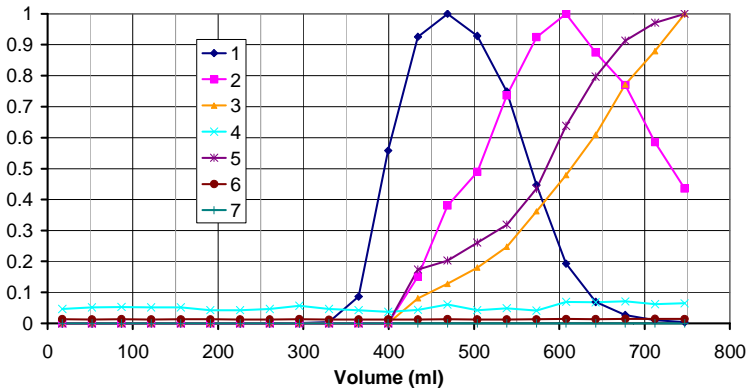


Figure 5-10: Normalised chromatogram of periphery outlet (LP) of separation B-4 on project Pfizer-C

Figure 5-11 and Figure 5-12 show HPLC chromatograms of fraction 3 from the centre (at 6 minutes and 135 ml), when all eluting peaks have developed, and fraction 17 from the periphery (at 25 minutes and 575 ml), when all peaks are developing or have developed, of separation B-4 on project Pfizer-C.

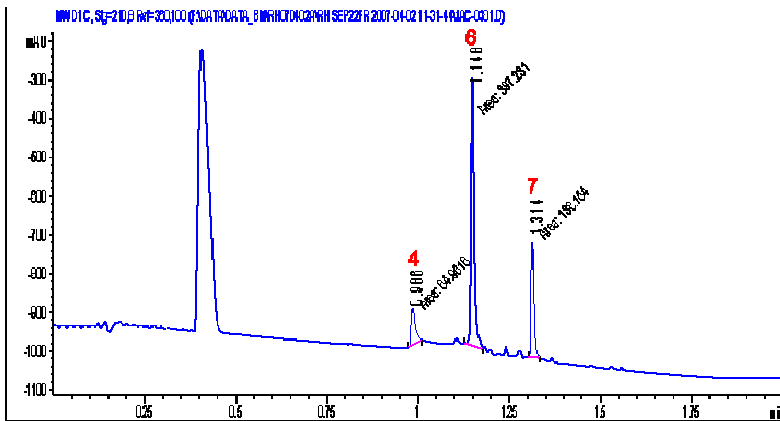


Figure 5-11: HPLC chromatogram of centre fraction 3 (3.5 min and 135 ml) of separation B-4 on project Pfizer-C. The HPLC method is described in section 2.4.5.

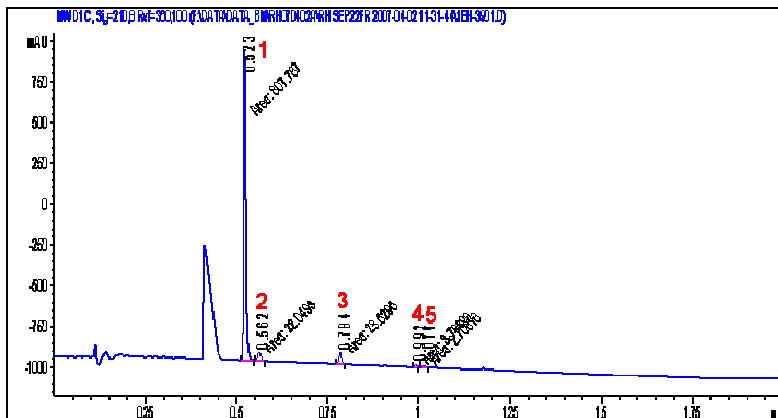


Figure 5-12: HPLC chromatogram of periphery fraction 17 (25 min and 575 ml) of separation B-4 on project Pfizer-C. The HPLC method is described in section 2.4.5.

In Figure 5-12 component 4 shows in the HPLC chromatogram. Analysis with a blank showed that this component was sticking on the HPLC column from previous analysis and has been eluting as a system peak in all the chromatograms.

On the last separation, B-4, a mass balance was performed to ensure that no sample was lost. 9.5 ml of the liquor was injected. The liquor was dried down again to determine the concentration. A volume of 20 ml gave a mass of 0.578 g sample – giving a concentration of 0.0289 g/ml. The injected volume of 9.5 ml gives a mass of about 0.275 g. The fractions were pooled together with the pump out volumes and dried down to give a total mass of 0.224 g. A recovery of 81.5% was achieved. A small amount (approximately 3%) of sample from the fractions is lost in the (1 ml) samples taken for HPLC analysis.

5.4.2 Project Pfizer-C “Continuous” separations (loading study)

The 30/30 flow rate was chosen to perform three continuous separations each at a different loading concentration. For each run

200 ml was injected in 40 minutes at a flow rate of 5 ml/min. All three runs were 90 minutes long. This allowed for a 50 minutes period for the compounds to elute after the continuous flow injection was stopped. The fractions were each collected for one and a half minute and were analysed using HPLC at the end of the run. Pure liquor was injected the first time (C-1), double concentration liquor the second time (C-2) and four times the original concentration was injected the third time (C-3). The following table shows the volumes and mass of the injections for all three runs.

Table 5-6: Volume and Mass of the three continuous injections

Separation name	Volume injected	Mass injected
C-1	192 ml	5.55 g
C-2	184 ml	9.75 g
C-3	170 ml	20.06 g

The injected volume decreased slightly as the sample concentration increased. This was because with the increasing concentration the viscosity of the sample increased and this had a negative effect on the pump and reduced its speed.

All the fractions from the separations were analysed and chromatograms were reconstructed from the results. They show continuous complete separations with peaks 1, 2, 3 and 5 eluted from the periphery in the lower phase and peaks 4, 6 and 7 eluted from the centre in the upper phase. Figure 5-13 shows the chromatogram of the centre outlet from separation C-2 and Figure 5-14 shows the periphery outlet from separation C-2.

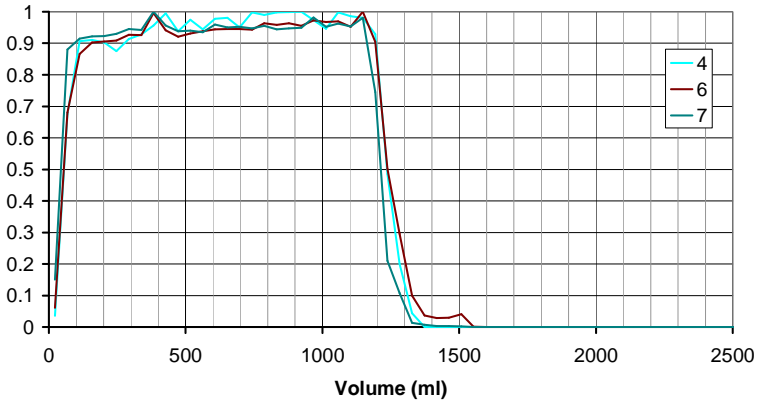


Figure 5-13: Chromatogram of the centre outlet (UP) of separation C-2 on project Pfizer-C

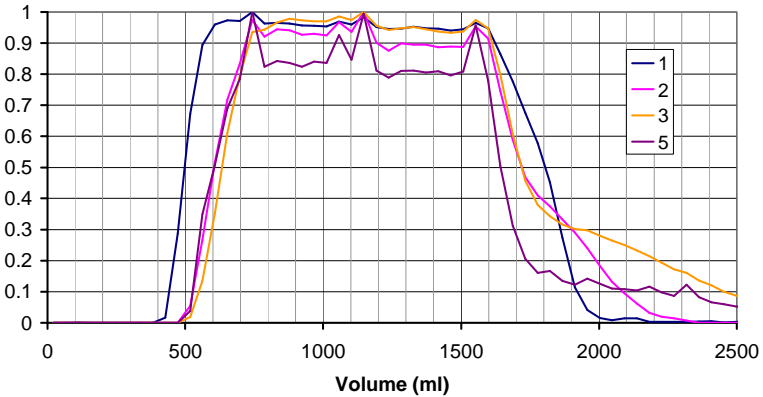


Figure 5-14: Chromatogram of periphery outlet (LP) of separation C-2 on project Pfizer-C

HPLC analysis of fractions 20 (at 30 minutes and 900 ml), when the peaks of all eluting components have fully developed, from both the centre and the periphery of separation C-2 on project Pfizer-C is shown in Figure 5-15 and Figure 5-16.

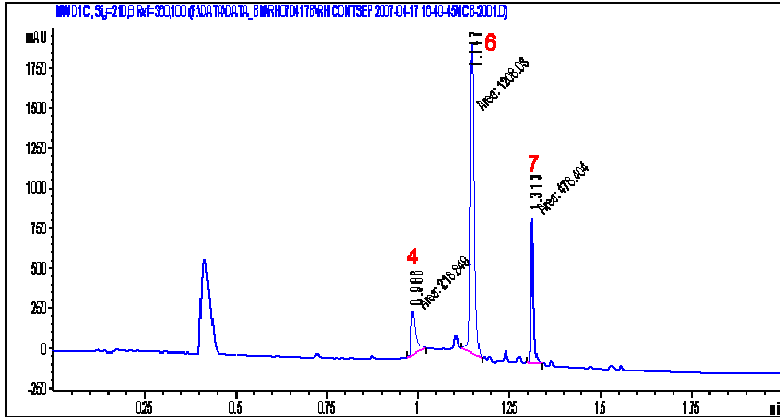


Figure 5-15: HPLC chromatogram of centre fraction 20 (30 minutes and 900 ml) of separation C-2 on project Pfizer-C. The HPLC method is described in section 2.4.5.

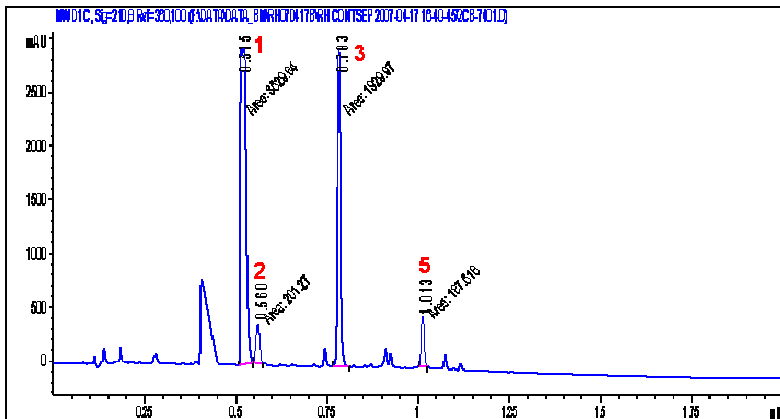


Figure 5-16: HPLC chromatogram of periphery fraction 20 (30 minutes and 900 ml) of separation C-2 on project Pfizer-C. The HPLC method is described in section 2.4.5.

The results of the continuous separations on project Pfizer-C are shown in Appendix X. The first separation (C-1) is used to perform

the mass balance. Fractions which contained compounds (according to the HPLC results) were dried down using a Buchi rotary evaporator. The remaining compounds from the centre, periphery and the Pump out with the total dried down mass are shown in the following table.

Table 5-7: Mass balance results for run C-1 on project Pfizer-C

Centre fractions 1 to 40 (the first 1800 ml)	1.272 g
Periphery fractions 10 to 60 (the last 2250 ml)	3.453 g
Pump Out	0.040 g
Total	4.765 g

The total amount of liquor injected was calculated to be 5.55 g. This means that 85.9% was recovered. The amount of materials lost in the 1ml samples taken for the HPLC analysis is estimated to account for 1% of the components. The remaining error is due to measurement errors and the unrecovered samples.

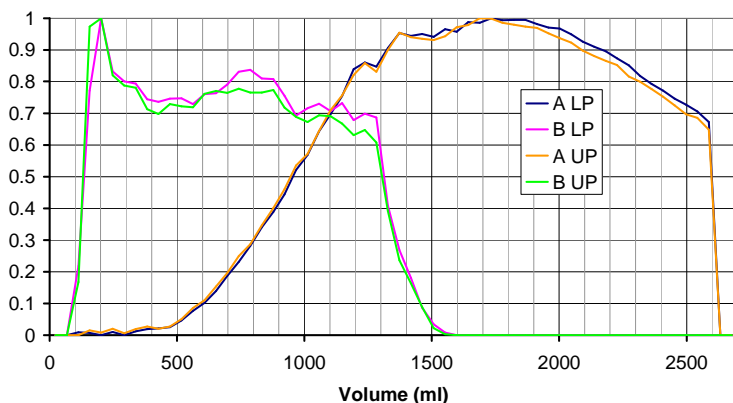
5.4.3 Project Pfizer-D “Continuous” separation

Two continuous separations were done on Pfizer-D. The first separation (C4) was done with upper and lower phase flow rate at 30 ml/min. Fractions of one and a half minutes each were collected for this separation. The second separation (C5) was done with the upper phase flow rate at 35 ml/min and the lower phase flow rate at 15 ml/min. For this separation fractions of two minutes each were collected. The following table shows the running conditions.

Table 5-8: Pfizer-D separations C-4 and C-5, flow rate and injected sample information

Separation name	Flow rate		Volume	Mass
	Upper phase	Lower phase	Sample	Sample
C-4	30 ml/min	30 ml/min	167 ml	1.66 g
C-5	35 ml/min	15 ml/min	182 ml	1.81 g

The volume of upper phase in the coil at equilibrium for the 30/30 flow rates was 38 ml. This gives a volume ratio X (V_{UP}/V_{LP}) of 0.0696. During the separations it was observed that a small percentage (about 10%) of the lower phase eluted with the upper phase at the head of the coil. This resulted in the actual lower phase flow rate from the outlet to be smaller than the flow rate at the inlet.

**Figure 5-17: Chromatogram of centre outlet (UP & LP) of the separation C-4 on Pfizer-D**

2 g of Pfizer-D was available to separate using DFCCC. For the first separation an amount of 1.992 g was weighed out and dissolved into 200 ml lower phase of EtOAc-D. This gave a cloudy mixture of which 167 ml was injected. The remaining sample was dried down and gave a mass of 0.409 g. The collected fractions were analysed

using HPLC and the reconstructed normalised chromatograms showed that both components eluted at the centre only (Figure 5-17). Fractions collected at the periphery didn't have any trace of the components.

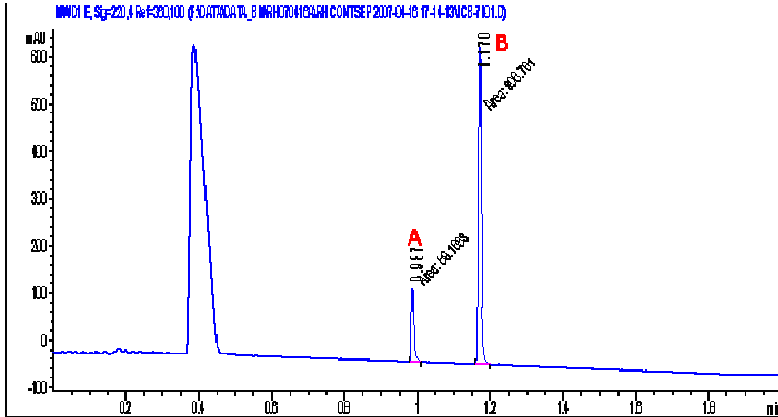


Figure 5-18: HPLC chromatogram of centre fraction 20 (30 minutes and 900 ml) of separation C-4 on Pfizer-D. The HPLC method is described in section 2.4.5.

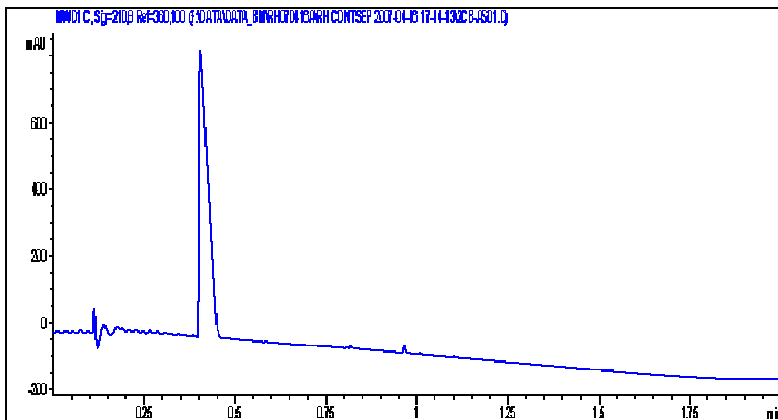


Figure 5-19: HPLC chromatogram of periphery fraction 20 (30 minutes and 900 ml) of separation C-4 on Pfizer-D. The HPLC method is described in section 2.4.5.

Figure 5-18 and Figure 5-19 show two HPLC chromatograms show the analysis of fraction 20 (at 30 minutes and 900 ml), when the peaks of the eluting components are developing or have developed, of the centre and the periphery respectively.

The fractions from separation C-4 were dried down and a mass of 1.414 g was recovered. Comparing this with the injected 1.66 g gives recovery of 85%.

The recovered Pfizer-D ($1.414 + 0.409 = 1.823$ g) and an additional 0.168 g Pfizer-D was dissolved again into 200 ml lower phase of the EtOAc-F phase system. After 40 minutes of separation C-5, just at the point where the sample injection stopped, the centrifuge was stopped due to time constraints (this was in the afternoon of the last day at the Pfizer labs). The collected fractions were analysed and the normalised reconstructed chromatograms for this separation are shown in Appendix XI. The remaining phases in the coil were pumped out and pooled together with the fractions for sample recovery. In separation C-4 nothing eluted from the periphery with the lower phase and in separation C-5 a very small amount of component A eluted from the periphery with the lower phase. Both components eluting from the centre with the upper phase from separation C-4 and C-5 are compared in Figure 5-20. In the figure can be seen that component B elutes with the same pattern for both flow rates, but starts off with a shallower slope for the 35/15 flow rates than for the 30/30 flow rates. Component A seems to be eluting faster and with a steeper slope for the 35/15 flow rates than for the 30/30 flow rates.

The fact that component A elutes faster with the upper phase at the centre and also elutes at the periphery with the lower phase could indicate that the 35/15 flow rates have improved the separation or that for that separation the initial concentration of component A was higher than for the 30/30 separation.

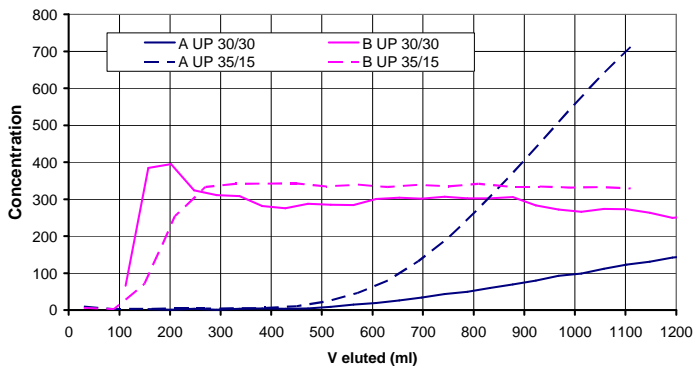


Figure 5-20: Reconstructed chromatogram for the components eluting from the centre outlet with the upper phase for separations C-4 and C-5 on Pfizer-D.

5.5 Separation results versus the DFCCD model

The D-values determined during the screening process are used in the DFCCD model to predict the elution of the components. For the prediction and the comparison with the real CCCE results the B-4 results and their corresponding D-values were chosen as this separation showed the components separated completely into two groups at equal flow rates. This was the project Pfizer-C with the EtOAc-F phase system. In the model, it was assumed that the phases are equally divided through the coil. The results were normalised to make each peak the same height and are plotted against the eluted volume to make the results from the prediction comparable with the CCCE results. The 41 tube model was used and the model was made to have the same total volume as the coil and the same upper phase volume as was in the coil at the end of the run. This gave the chromatograms shown in Figure 5-21 and Figure 5-22.

The components eluting in the upper phase in the real CCCE separation also elute in the upper phase in the DFCCD model and the components eluting in the lower phase in the CCCE separation elute in the lower phase in the DFCCD model. Figure 5-21 shows the upper phase elution from the model and it shows that the components elute faster with narrower peaks than in the CCCE separation. These three components start to elute at the same time

as the real CCCE separation. Figure 5-22 shows the lower phase elution from the model and it shows that the peaks of components 1, 3 and 5 elute at the same volume as in the CCCE separation. However, the peaks are much too broad and therefore start sooner and last longer than in the CCCE separation.

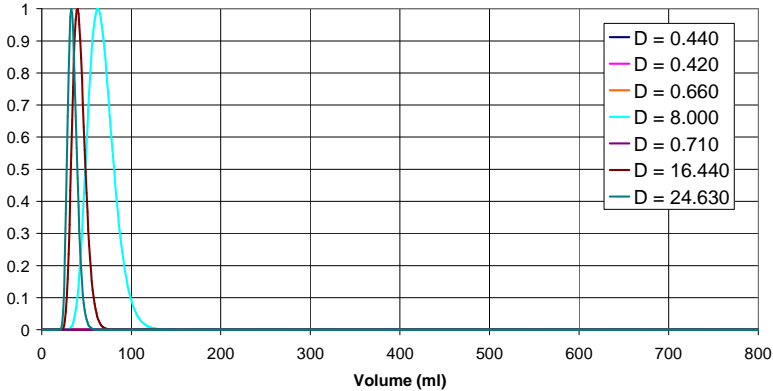


Figure 5-21: Chromatogram for the upper phase eluting from the 41 tube CCCE model with $V_{TOT} = 630$ ml and $X(V_{UP}/V_{LP}) = 0.0696$. At each transfer 1 ml of phase is moved to the next tube.

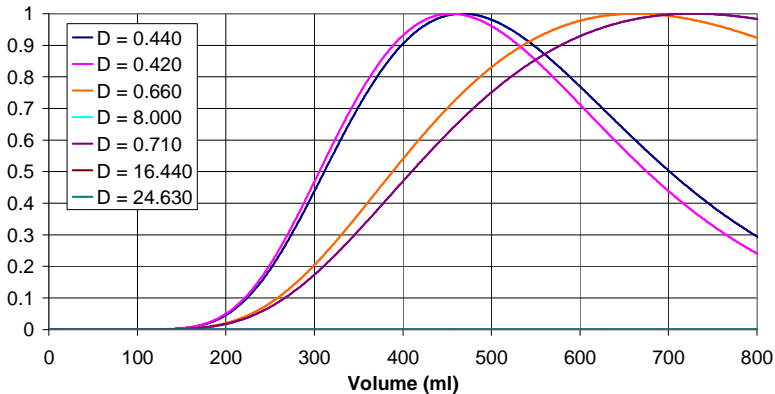


Figure 5-22: Chromatogram for the lower phase eluting from the 41 tube CCCE model with $V_{TOT} = 630$ ml and $X(V_{UP}/V_{LP}) = 0.0696$. At each transfer 1 ml of phase is moved to the next tube.

Another prediction is done on the Pfizer-D separation. The first separation is simulated as the whole elution pattern is known and the equilibrium volume in the coil is known. This equilibrium volume is kept the same in the model, but the flow rates are changed slightly for the model as in the real experiment (C-4), where the flow rates were the same, some of the lower phase eluted with the upper phase from the centre. The chromatogram for the centre outlet from the model is shown in Figure 5-23. In the figure can be seen that both components elute from the centre with the upper phase. The peaks are sharp and not continuous as this is not included in the model, but they start at the same time as the continuous C-4 separation and show the same slope for the peak front. This simulation of the continuous C-4 separation shows that the model works and is able to predict the elution of components when all the experimental conditions are known.

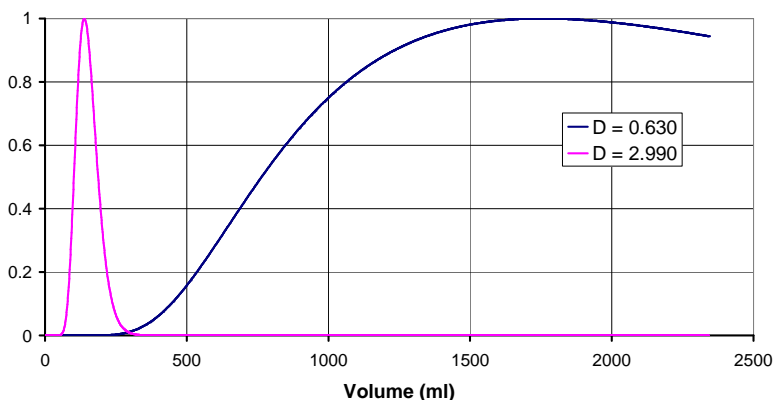


Figure 5-23: Chromatogram for the upper phase eluting from the 41 tube CCCE model with $V_{TOT} = 630$ ml and $X(V_{UP}/V_{LP}) = 0.0696$. At each transfer 0.9268 of upper phase and 0.5748 of lower phase is moved to the next tube.

When in the model both phases have the same flow rate the components are completely separated. This would mean that when in the CCCE separation the lower phase flow rate is increased the components of the binary mixture will be separated.

5.6 Discussion and Conclusions

5.6.1 Discussion

Batch separations B-1, B-2 and B-3 show clearly that changing the upper phase flow rate (and with this the amount of upper phase in the coil) influences which end of the coil each component elutes. The chromatograms show that the elution of peak 3 and 5 from either the centre or the periphery will depend on the upper phase flow rate. Comparing separation B-1 with B-4, where both flow rates are changed from 20 ml/min (B-1) to 30 ml/min (B-4), shows that the components elute sooner with higher flow rates at both the centre and the periphery (figures are shown in Appendix IX). All three continuous separations on project Pfizer-C (C-1, C-2 and C-3) show complete separation regardless of the loadings tried. A throughput of 30 g dried sample per hour was achieved on the last continuous separation (C-3). The importance of getting the right flow rates for the separation is shown with the two continuous separations on Reb-C (C-4 and C-5). With online analysis, the flow rates could be tuned until complete separation was established. This, however, would be a trial and error approach.

- DFCCC can separate binary mixtures or groups of components into two groups when the D-values are spread around $D=1$ in a continuous fashion.
- Dependant on the flow rate combination the components to separate will elute from either the centre or the periphery.
- Liquor that comes straight from a reaction can be separated continuously.
- The flow rate combination is very important to achieve complete separation.

The model used for the predictions described in Chapter 3 is tested here with real D-values and compared with real CCCE data. Results from this model, shown in the previous section, show that the model can be used for the prediction of CCCE separations. However, the model also highlights some prediction problems. The model works correctly concerning the location of elution, the components that eluted in the same phase both in the real CCCE separation and in the prediction using the model.

For the Pfizer-C project, the components eluting in the model in the upper phase eluted with peaks sharper than the CCCE separation and the components eluting with the lower phase eluted with broader peaks in the model than the CCCE separation.

Reasons for the difference between the DFCCD model separation and the CCCE separation could be the following.

- The phase distribution in the coil might have been very different from what was assumed in the DFCCD model. The model assumes the phases to be distributed evenly throughout the coil, but as was shown in Chapter 4 this is not the case. If there would be more upper phase near the end of the coil where the upper phase elutes the peaks would be broader.
- The solubility of the sample mixture had shown to be difficult when the sample mixture was prepared. The dried sample mixture did not dissolve in the phase system and was therefore used in the original liquid. It is possible that when the components entered the phase system this same solubility problem occurred inside the coil. If the components with a low D-value (which show a higher affinity for the lower phase) would be saturated in the little upper phase present in that part of the coil, they would be staying together more and this would result in narrower peaks. Solubility problems and non-linear D-values are not incorporated in the DFCCD model.

For the Pfizer-D project the model predicted the elution of the components correctly. However, the conditions of the experiment need to be interpreted and incorporated into the model for it to work. The continuous C-4 separation was performed with equal flow rates 30/30, but during the experiment some of the lower phase that should elute from the periphery eluted at the centre with the upper phase instead. This could not be incorporated in the model, but the reduction of the lower phase flow rate from the centre to the periphery was included which resulted in the separation shown. However, the model did show that increasing the lower phase flow rate (from what is shown in the previous section to equal flow rates) the two binary components were completely separated.

With some improvements the model will be a powerful tool for the prediction of the elution of the components. These improvements are mainly from the inclusion of the observed non-equal volume distribution and the eluting flow rates rather than the pumped flow rates. To make the model more adaptable and easier to use it would need to be built into a standalone program.

5.6.2 Conclusion

It can be concluded that the CCCE separations performed were successful as the sample mixture of project Pfizer-C was separated into two families of components. For the Pfizer-D project, however, the CCCE separation was not initially successful. When the flow ratio was changed from 1:1 to 2.3:1 UP:LP, it could be seen that A started to elute from both centre and periphery. Due to the time constraints at Pfizer, no more flow conditions could be tried, but increasing the ratio to about 4:1 would probably have resulted in a perfect elution profile with B eluting from the centre and A from the periphery. The DFCCD model has its limitations as was discussed in Chapter 3, but it has shown how the location of elution and the approximate location of the peaks can be predicted when the same volumes are used in the model as were measured at equilibrium in the CCCE coil. The flow rates used for the prediction however should be interpreted and adapted so they match the outlet flow rates rather than the pump flow rates.

Chapter 6 Discussions and Conclusions

6.1 Discussions

6.1.1 Model

The CCCD model described in this thesis has shown that it can be used for the prediction of CCCE separations. The CCCD model is based on the well established and validated CCD model [Sutherland 2003]. Even though it is a simple model, as the centrifuge parameters (like the coil dimensions and rotational speed) are not included, the predictions produced are very close to the separations achieved. These operating parameters are included in a dual flow CCC model proposed by Kostanian and Voshkin [2007]. However, Kostanian's model was not validated with any experimental data and it is unclear as to how it can be used for the prediction of the elution. This makes the CCCD model proposed in the thesis a better model as it is easier to use and backed up by experimental data.

6.1.2 Visualisation study

The visualisation study has shown that the phases are not equally divided throughout the coil [van den Heuvel and Sutherland 2007]. In the short spiral coil studied it was observed that the majority of the heavy phase collects at the peripheral tail of the coil and the majority of the light phase collects at the central head. This is a big step forward as before it was assumed that the phases were distributed equally throughout the coil [Ito 2006] and now for the first time this has been observed to be different. There were some limitations to this visualisation study. The first limitation was the visualisation equipment. The camera used for taking the pictures was limited to automatic focusing. Manual focussing would allow sharper and more consistent pictures. Only one stroboscope was used for the lighting, multiple stroboscopes would give better lighting and clearer pictures as the shadows from the angled lighting would be eliminated. With multiple stroboscopes there would be enough light for high-speed imaging equipment that could take images of every rotation and would allow the study of the waves and the establishment of

hydrodynamic equilibrium. This is the first time that DFCCC or CCCE has been successfully studied with stroboscopic visualisation. According to Wood [2002] the CCC centrifuge is a constant pressure pump. This would mean that the CCCE centrifuge is also a constant pressure pump and that the equilibrium (with the transition area) is due to a pressure balance inside the coil. This needs further investigation so that the behaviour of the phases and the equilibrium (with the transition area) can be predicted.

The calculations proposed in Chapter 3 are used to determine the location of the transition area in the coil using the gradients from the Du-plots and the total volumes of the phases in the coil. Calculations from the retention studies in Chapter 4 have shown that the position of the transition area determined using these calculations and determined from the photograph show a good correlation with a maximum difference of 7%. This maximum difference occurs when the transition area is near one of the ends of the coil and the difference is only 1% when the transition is in the centre of the coil. The gradients from the Du-plots of isocratic CCC with the 4A phase system were used for the calculations. According to Wood [2002] the gradients of the phases are related to the viscosities of the phases, however, for the Du-plots measured this was not the case. This might explain why there is a difference between the calculations from Chapter 3 and the calculations from the photographs.

6.1.3 Application study

6.1.3.1 Phase system selection

During the application study at the Pfizer laboratories it was found that the phase system selection was very important to the separation. Choosing a different phase system can result in a completely different separation. The phase system selection method (screen) developed at Pfizer by Dubant [2007] is for isocratic CCC separations (i.e. finding the $D=1$ point for a target component). Different solvent selection criteria were necessary for the CCCE separation i.e. the D -values of the components have to range either side of $D=1$. The phase systems used for the Pfizer screen were also used for the D -value determination for the CCCE separations. This showed that changing the phase systems changed the D -values

of the components in a predictable way. Hence it was relatively straightforward to adapt the Pfizer solvent selection criteria for CCCE.

6.1.3.2 The CCCE Separation

The CCCE separation has shown that a mixture of multiple components can be separated into two families for both “Batch” and “Continuous” operation. The “Batch” separations showed that some of the components in the multi-component mixture changed their elution location when the flow rate of the upper phase was changed. These components had their D-values slightly below the D=1 value. During the “Continuous” separations it was shown that for the mixture used the increase in concentration of the continuously injected sample did not influence the elution of the components. It is possible that the components with their D-values nearest to the D=1 value will overload when the concentration would be increased more. This would result in these components eluting from both sides of the coil. Therefore, the solvent selection process should take keep this in mind when the phase system is selected so the D-values are not too close to the D=1 value.

The two “Continuous” separations on the binary mixtures and the prediction using the CCCD model have shown that it is possible to separate the two components. They did not jet elute from opposite ends of the coil, but the peaks were separated. According to the D-values the two components should be separated when equal flow rates are used. Some of the lower phase eluted with the upper phase, causing the two eluting streams to have different flow rates (while the inlet flow rates were the same) and because of this the components eluted from the same side. This suggests that when the lower phase flow rate would be increased and the outlet flows are equal the two components will be separated.

6.1.3.3 CCCE predictions

The data from the CCCE separations was used to model the same separation using the CCCD model described in Chapter 3. The data

produced by the model showed good correlation with the real CCCE data. The components eluted from the same end of the coil in the model, just as they did from the CCCE separation. Also the predicted retention volumes were in the same region as the actual obtained retention volumes. The differences are most likely due to the phase distribution in the coil which was observed to be not equal throughout the coil (as described and discussed in Chapter 4) and this inequality was not included in the CCCD model. The model assumes the outlet and inlet flows to be the same, but in practice it was observed that there was some (~10%) elution of lower phase from the upper phase outlet. When the real flow rates were included in the model this resulted in the same chromatogram as that obtained during the separation. The model was not built to perform continuous separations as the peaks would just be broader, start at the same time as a single injection and end the same time after the end of the injection. It is more important to see where and when the components elute.

6.2 Conclusions

6.2.1 Advantages

- **Ease of operation**

It is a continuous technique that could be used either for a series of batch injections of different separations without having to refill the coil contents or continuously for one particular separation.

- **Predictability**

The CCCE separation is predictable. When the running conditions like the volume distribution in the coil and the flow rates through the coil are known the separation can be predicted using the CCCD model. More work is required to validate and tune the model, but this study has indicated that the CCCE separations can be reliably predicted using computational modelling techniques.

- **Potential for automation**

The continuous separation process lends itself to automation, with computer control of the peripheral

equipment that would allow separations to be performed with minimal operator intervention. The technology would then become comparable to the current chromatographic techniques (such as HPLC and SMB) that are well established in the pharmaceutical industry.

- **Potential for multistage automated processing**

Because CCCE can cope with crude sample materials as well as more defined component separation a number of CCCE centrifuges performing continuous separations could be connected together. This would allow a streamlined purification process from crude mixture to product(s).

6.2.2 Disadvantages

- **Complex fluid mechanics**

The fluid dynamics within the CCCE coil is more complex than conventional CCC. The position of the transition zone is very hard to predict because so many factors are responsible for the location and stability. For isocratic CCC it was shown by Wood [2002] that a coil planet centrifuge acts like a constant pressure pump. This could mean that the equilibrium of the interface is caused by a complex pressure balance. Small changes in pressure could therefore lead to major changes in performance.

- **Mechanical complexity**

The CCC or CCCE separation methods depend on a spinning coil centrifuge which is much more mechanically complex than conventional techniques such as HPLC. High speed moving parts and planetary gear action can be expensive to build and maintain.

- **Coil complexity**

Over and above the complexity inherent in the spinning coil centrifuge technique, the CCCE coil needs an additional sample inlet in the centre of the coil and two terminal connections at each end of the coil which make the coil more difficult (and expensive) to build. A complex flying lead system is also necessary, at each terminal and these fly leads are particularly prone to wear.

6.2.3 Summary

CCCE is a promising technology that would be ideal for the separation of binary mixtures (polishing step) or for the cleaning up of feed streams (purification step). This work has shown that a mixture of components can be separated into two families after the correct phase system was established. It was also shown that by using a CCD based model the separation can be predicted. The nature of the process, a continuous mode of operation, allows the technology to be automated for stand-alone operation or with multiple CCCE centrifuges.

6.3 Future Work

The visualisation study should be continued on an improved rig to gain an understanding of the fluid dynamics in a CCCE coil and to be able to find a relationship between the two flow rates and the volume distribution inside the coil. This improved experimental visualisation rig would include better lighting and high-speed imaging equipment together with a machine with better speed and temperature control and a new coil where 100% of the coil can be seen and studied. Also it will be important to monitor the pressure so that the relationship between pressure and the phase equilibrium can be understood. As it is suspected that the equilibrium in the coil is a sensitive pressure balance it might be beneficial to gain an understanding of the pressures inside the coil using small pressure transducers that could be mounted at regular intervals inside the new coil. More flow rates and different phase systems need to be tested using a systematic approach.

The phase system selection method could be simplified and automated. It would be very beneficial if the selection of the ideal phase system either for CCC or for a CCCE separation could be predicted through an automated process. This process could either be entirely theoretical or include some simple experiments followed by some calculations. The theoretical method would use the physical and chemical parameters of the sample mixture components. From these parameters the ideal phase system is calculated based on a large database of solvent and phase system data. The method based on a small number of simple experiments on the sample mixture will use the results from these experiments to

calculate the ideal phase system. These calculations will be done by a computer program which uses a statistical method of prediction.

The pilot-scale CCCE separation would be improved if an online analysis technique that could distinguish components was applied to each outlet. This would allow the separation to be monitored online and if required the flows adjusted to ensure the right components would elute from the right end. If the CCCE machine could be controlled using a computer it could be set-up with some electronic valves and a pump system that is also computer controlled to get a fully automated system. This system would then be able to run on its own with little or no attention from the operator.

The developed CCCD model needs to be validated using both the Liquid Handling Robot (LHR) and the CCCE centrifuge. Using the LHR a dual flow process can be simulated in a series of test tubes and with the CCCE centrifuge a model separation can be done to get data for the validation. Before the model is validated it will need to be improved to include the volume distribution inside the coil and to allow for a proportion of one phase to go in the wrong direction. The improved and validated model should then be developed into a stand alone program which will allow the user to predict CCCE separations without any additional software. Further work with the dual CCC model proposed by Kostanian would allow the two models to be compared and maybe combined.

6.4 Concluding Remarks

It is hoped that the research described in this thesis will be the first step towards understanding the hydrodynamics of CCCE, and that understanding the technique will encourage both the pharmaceutical industry and the academic world to use it for continuous separations. It is very encouraging that on the day before final submission of this thesis, Pfizer have asked if they can rent the CCCE centrifuge for testing the continuous CCC at the end of their continuous reactors as they are having trouble with the final isolation of their product. Further investigations combined with the research presented in this thesis will make CCCE a robust and predictable tool that can be used for a large variety of applications. It is therefore important that the momentum gained by this research is maintained and further research be initiated in the very near future.

Appendix I Locus of Coil Calculations

Calculations and Figure from Mathcad 13

$$R = 10$$

$$\Theta = 0,0.001 \cdot \pi \dots 2 \cdot \pi$$

$$x(\Theta, \beta) = R \cdot (\cos(\Theta) + \beta \cdot \cos(2 \cdot \Theta))$$

$$y(\Theta, \beta) = R \cdot (\sin(\Theta) + \beta \cdot \sin(2 \cdot \Theta))$$

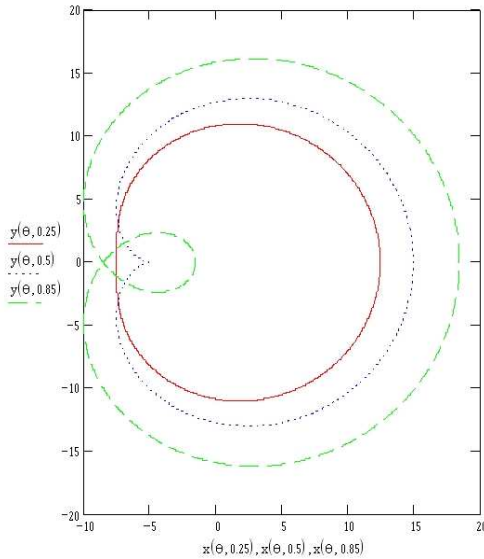


Figure I-1: Locus of one point on the coil calculated using MathCAD 13

Appendix II Derivation of the polar Limaçon equation

While it is easy to describe the x and y coordinates of planetary motion from geometric principles, it is interesting to be able to “name” the locus so that it can be related to other uses of the technology. This analysis shows that the original polar expression for the Limaçon (Equation II-1) [Rutter 2000] can be used to derive the coordinates of the planetary motion described in this thesis.

$$r(\theta) = a + b \cdot \cos(\theta) \qquad \text{Equation II-1}$$

Where: θ is the angle around which the Limaçon goes
 a is the diameter of both the centre and planetary gear
 b is the diameter of the bobbin on the planetary gear

This gives the following figure in Mathcad 13.

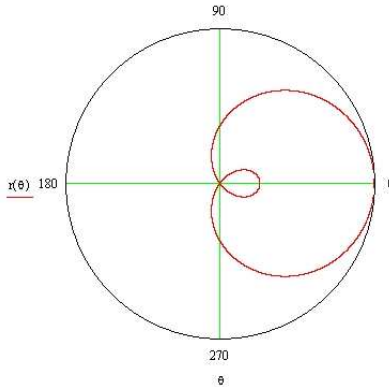


Figure II-1: Polar expression of the Limaçon equation

Note that the origin is not at the centre of the centre gear, but there is an offset on the x-axis of $\frac{1}{2} b$.

The R and r from Figure 1-4 are a and $\frac{1}{2} b$ respectively. Transforming a polar expression into an x and y parametric equation is done with the following two equations.

$$x = r \cdot \cos(\theta)$$

$$y = r \cdot \sin(\theta)$$

Substituting the polar expression for the Limaçon (Equation II-1) into these two equations gives the following derivations.

$$x = a \cdot \cos(\theta) + b \cdot \cos^2(\theta)$$

$$\cos(2\theta) = 2 \cdot \cos^2(\theta) - 1$$

$$x = a \cdot \cos(\theta) + \frac{b}{2} \cdot \cos(2\theta) + \frac{b}{2} = R \cdot \cos(\theta) + r \cdot \cos(2\theta) + r$$

$$= R \cdot \left(\cos(\theta) + \frac{r}{R} \cdot \cos(2\theta) \right) + r = R \cdot (\cos(\theta) + \beta \cdot \cos(2\theta)) + r$$

$$y = a \cdot \sin(\theta) + b \cdot \sin(\theta) \cdot \cos(\theta)$$

$$\sin(2\theta) = 2 \cdot \sin(\theta) \cdot \cos(\theta)$$

$$y = a \cdot \sin(\theta) + \frac{b}{2} \cdot \sin(2\theta) = R \cdot \sin(\theta) + r \cdot \sin(2\theta)$$

$$y = R \cdot \left(\sin(\theta) + \frac{r}{R} \cdot \sin(2\theta) \right) = R \cdot (\sin(\theta) + \beta \cdot \sin(2\theta))$$

To move the Limaçon along the x-axis so the centre of the solar gear is in the origin the expression for the x-axis needs to be subtracted by $(1/2 b)$. This results into the following two equations.

$$x(\theta) = R \cdot (\cos \theta + \beta \cdot \cos(2\theta)) \quad \text{Equation II-2}$$

$$y(\theta) = R \cdot (\sin \theta + \beta \cdot \sin(2\theta)) \quad \text{Equation II-3}$$

Where: θ is the angle around the centre axis ranging from 0 to 2π
 $x(\theta)$ is the x-axis coordinate at angle θ
 $y(\theta)$ is the y-axis coordinate at angle θ

The last two equations are the same as described by [Ito and Bowman 1978]

Appendix III Acceleration calculations

The x and y functions, derived in Appendix II, describe the displacement of one point on the coil. The second derivative of the displacement functions gives the acceleration functions of one point on the coil. Due to the rotation of the coil the liquid inside the coil will experience this acceleration. The displacement functions are derived to the time. This requires the angle from the displacement function to be changed into the rotational speed with the time.

The angle (θ) is the rotational speed of the centrifuge (ω) in radians per second multiplied by the time (t) in seconds.

$$\theta = \omega \cdot t$$

Using these definitions while deriving the x and y functions from Appendix II gives the following equations.

$$x(\theta) = R \cdot (\cos \theta + \beta \cdot \cos(2\theta))$$

$$x(t) = R \cdot \left(\cos(\omega \cdot t) + \frac{r}{R} \cdot \cos(2\omega \cdot t) \right)$$

$$x(t) = R \cdot \cos(\omega \cdot t) + r \cdot \cos(2\omega \cdot t)$$

$$AccnX(t) = \frac{d^2}{dt^2} x(t)$$

$$AccnX(t) = \frac{d^2}{dt^2} (R \cdot \cos(\omega \cdot t) + r \cdot \cos(2\omega \cdot t))$$

$$AccnX(t) = \frac{d}{dt} (-R\omega \sin(\omega \cdot t) - 2r\omega \sin(2\omega \cdot t))$$

$$AccnX(t) = -R\omega^2 \cos(\omega \cdot t) - 4r\omega^2 \cos(2\omega \cdot t)$$

$$AccnX(\theta) = -R\omega^2 (\cos(\theta) - 4\beta \cos(2\theta))$$

$$y(\theta) = R \cdot (\sin \theta + \beta \cdot \sin(2\theta))$$

$$y(t) = R \cdot \left(\sin(\omega \cdot t) + \frac{r}{R} \cdot \sin(2\omega \cdot t) \right)$$

$$y(t) = R \cdot \sin(\omega \cdot t) + r \cdot \sin(2\omega \cdot t)$$

$$AccnY(t) = \frac{d^2}{dt^2} x(t)$$

$$AccnY(t) = \frac{d^2}{dt^2} (R \cdot \sin(\omega \cdot t) + r \cdot \sin(2\omega \cdot t))$$

$$AccnY(t) = \frac{d}{dt} (-R\omega \cos(\omega \cdot t) - 2r\omega \cos(2\omega \cdot t))$$

$$AccnY(t) = -R\omega^2 \sin(\omega \cdot t) - 4r\omega^2 \sin(2\omega \cdot t)$$

$$AccnY(\theta) = -R\omega^2 (\sin(\theta) - 4\beta \sin(2\theta))$$

The final two equations ($AccnX(\theta)$ and $AccnY(\theta)$) were described in [Conway 1990] as the force working on the fluids inside the coil. However, as was pointed out by Wood [2002], these equations are the acceleration of the fluids inside the coil. The force is calculated as the mass times the acceleration and there is no mass term in the derived equations. The acceleration equations derived can be resolved in both the radial direction (Ar) and tangential direction (At) as is shown in Figure III-1.

The radial and tangential acceleration are calculated from the geometry of Figure III-1 as follows:

$$\sin(\phi) = \frac{AccnY(\theta)}{Accn(\theta)} \qquad \sin(\phi') = \frac{At}{Accn(\theta)}$$

$$\cos(\phi) = \frac{AccnX(\theta)}{Accn(\theta)} \qquad \cos(\phi') = \frac{Ar}{Accn(\theta)}$$

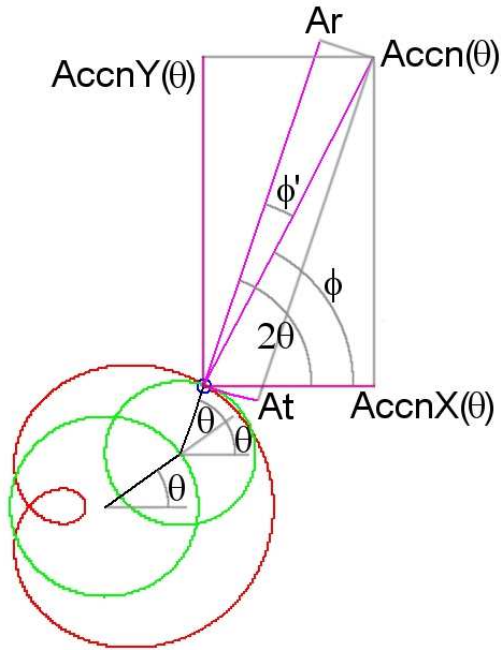


Figure III-1: Acceleration vectors

Going from unknown angles to known angles using the trigonometry rules for two angles give the following two sets of equations.

The equations for the acceleration in the radial direction are:

$$\frac{A_r}{Accn(\theta)} = \cos(\phi') = \cos(2\theta - \phi)$$

$$\cos(2\theta - \phi) = \cos(2\theta) \cdot \cos(\phi) + \sin(2\theta) \cdot \sin(\phi)$$

$$\frac{A_r}{Accn(\theta)} = \cos(2\theta) \cdot \frac{AccnX(\theta)}{Accn(\theta)} + \sin(2\theta) \cdot \frac{AccnY(\theta)}{Accn(\theta)}$$

$$A_r = \cos(2\theta) \cdot AccnX(\theta) + \sin(2\theta) \cdot AccnY(\theta)$$

The equations for the acceleration in the tangential direction are:

$$\frac{A_t}{Accn(\theta)} = \sin(\phi') = \sin(2\theta - \phi)$$

$$\sin(2\theta - \phi) = \sin(2\theta) \cdot \cos(\phi) - \cos(2\theta) \cdot \sin(\phi)$$

$$\frac{A_t}{Accn(\theta)} = \sin(2\theta) \cdot \frac{AccnX(\theta)}{Accn(\theta)} - \cos(2\theta) \cdot \frac{AccnY(\theta)}{Accn(\theta)}$$

$$A_t = \sin(2\theta) \cdot AccnX(\theta) - \cos(2\theta) \cdot AccnY(\theta)$$

This gives the vectors of the acceleration in the radial and tangential direction of the coil. The acceleration on the liquids in the coil is in the opposite direction by Newton's third law – action and reaction are equal and opposite. This gives the following two equations for the radial and tangential acceleration on the liquid inside the coil.

$$A_r = -\cos(2\theta) \cdot AccnX(\theta) - \sin(2\theta) \cdot AccnY(\theta) \quad \text{Equation III-1}$$

$$A_t = -\sin(2\theta) \cdot AccnX(\theta) + \cos(2\theta) \cdot AccnY(\theta) \quad \text{Equation III-2}$$

Appendix IV Ternary and Tetrahedron Calculations

The equations used for the calculation of the Ternary diagram (Figure 1-20) and the Tetrahedron (Figure 1-21) are given in this appendix.

First the equations of the Ternary diagram are discussed.

The corners of a triangle making up the Ternary diagram are shown in the table below and they are labelled A, B and C. These labels can be replaced with the appropriate components. The values of these corners are translated into X and Y coordinates for a triangle with equal sides with lengths of unity. When the bottom side of the triangle lies on the X-axis and the left bottom corner of the triangle is in the origin the X and Y coordinates of the triangle are calculated as follows.

$$X = B + 0.5 \cdot A \qquad \text{Equation IV-1}$$

$$Y = \sqrt{(1 - 0.5^2)} \cdot A = 0.866 \cdot A \qquad \text{Equation IV-2}$$

Calculating the X and Y coordinates from the Component coordinates gives the following table.

Table IV-1: Component and X & Y coordinates for the Ternary diagram

A	B	C	X	Y
1	0	0	0.5	0.866
0	1	0	1	0
0	0	1	0	0

The results from these calculations are shown in the ternary diagram outline shown in Figure IV-1.

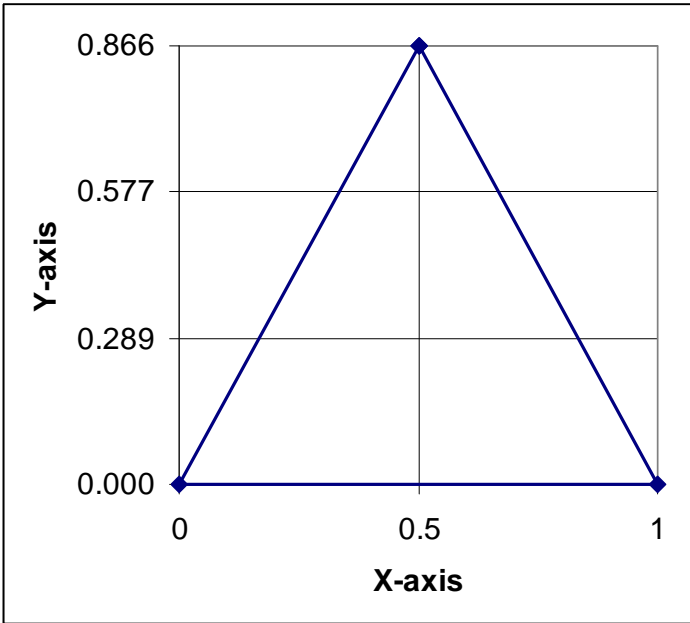


Figure IV-1: Ternary diagram outline

Using these two equations any value in the ternary diagram can be calculated as is shown in Figure 1-20.

In the same way the Tetrahedron is calculated. The bottom of the triangle is placed in the X-Y area with one side on the X-axis and one point in the origin. The equations to calculate the Tetrahedron X, Y and Z coordinates are as follows.

$$X = B + 0.5 \cdot A + 0.5 \cdot D \quad \text{Equation IV-3}$$

$$Y = \sqrt{(1-0.5^2)} \cdot A + \frac{1}{3} \cdot \sqrt{(1-0.5^2)} \cdot D$$

$$Y = 0.866 \cdot A + 0.289 \cdot D \quad \text{Equation IV-4}$$

$$Z = \sqrt{(1-0.5^2)} \cdot D = 0.866 \cdot D \quad \text{Equation IV-5}$$

The results from the equations are shown in the following table where four Tetrahedron component coordinates are translated into three Tetrahedron (X, Y and Z) coordinates.

Table IV-2: Tetrahedron Component and X, Y & Z coordinates

A	B	C	D	X	Y	Z
1	0	0	0	0.5	0.866	0
0	1	0	0	1	0	0
0	0	1	0	0	0	0
0	0	0	1	0.5	0.289	0.866

These results give the following Tetrahedron where the A is orange, the B is green, the C is blue and the D is red.

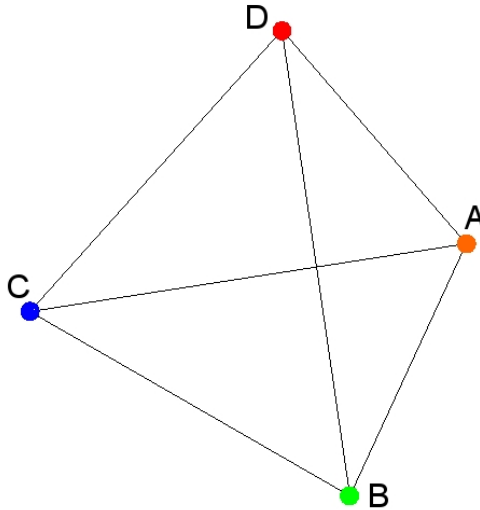


Figure IV-2: Tetrahedron with A, B, C and D

Appendix V Application Study Protocols

This appendix details five protocols discussed in Section 2.4. The first protocol is a part of the phase system selection method and the last four protocols are part of the CCCE method.

Solvent selection protocol:

- Approximately 2 mg of the mixture is manually put into each vial.
- The solvents are suspended into the vials in the appropriate amounts to make a total volume of 2 ml. (The amounts for the basic screen are calculated from Table 1-4 in Section 1.4.2.2 on page 46)
- The vials are capped and put into the HPLC tray
- The vials are shaken on an auto-mixer for about 15 minutes
- The vials are sonicated for approximately 30 minutes
- The vials are shaken on an auto-mixer for about 15 minutes
- The vials are checked visually to ensure appropriate solubility
- Both layers are analyzed on the HPLC using the fast HPLC method described in section 2.4.5.

Four protocols for the CCCE separation method:

Protocol 1: Priming of the pumps

- The direction of valve F is insignificant.
- Valves D and E are opened.
- The electronic valves 1 and 2 are switched so the liquid from the pumps goes into the waste.
- The pumps are started and allowed to flow for a few minutes ensuring all air and old phase is flushed out, after which they are stopped.
- Electronic valves 1 and 2 are switched back so that the liquid from the pump goes to the coil.

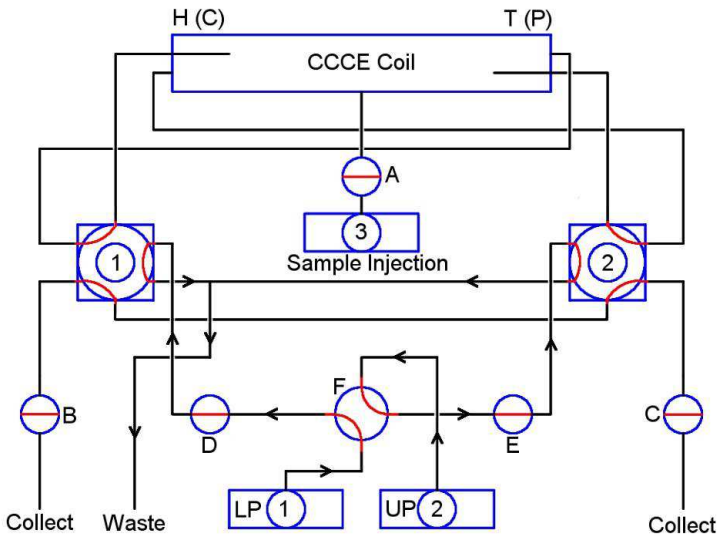


Figure V-1: Schematic diagram of the set-up with the valves and the arrows indicating the direction of the liquid flowing for the priming of the pumps

Protocol 2: Preparation of the coil

- Valve F is switched so the lower phase goes to Tail (periphery) via valve E and electronic valve 2.
- Valve C and E are opened (sequence is not important).
- Electronic valve 2 is checked (and if necessary switched) to make sure the liquid from the pump goes to the coil rather than to waste.
- The lower phase pump is started at a flow rate of 30 ml/min.
- After pumping approximately 1.5 coil volumes, the lower phase pump is stopped after 25 minutes.
- Valve C and E are closed.
- Valve F is switched back so the lower phase goes to the Head (centre) via valve D and electronic valve 1.

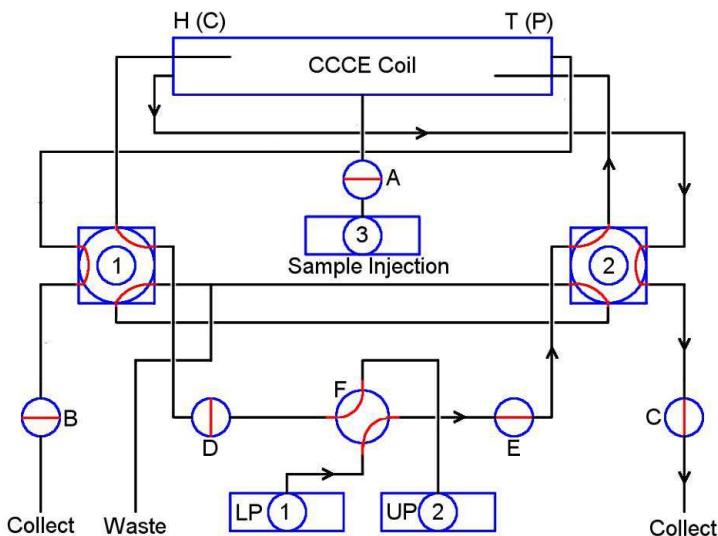


Figure V-2: Schematic diagram of the set-up with the valves and the arrows indicating the direction of the liquid flowing for the preparation of the coil for a CCCE run

Protocol 3: Performing a Dual Flow Extraction

- Start the centrifuge and gently bring it up to speed (1000 rpm).
- Ensure all pumps are primed with the correct phase or sample (Protocol 1).
- Ensure valve F is in the position where the lower phase goes to valve D
- Open on/off valves B, C, D and E
- Collect the liquid eluting from the lines with valve B and C in separate empty cylinders
- Start both pumps 1 and 2 simultaneously with a ramp of 30 seconds to the desired running flow rate
- Allow the system to equilibrate for 5 minutes
- Stop the pumps after 5 minutes

- Close on/off valves B, C, D and E
- Measure and record the eluted amounts of phases that were collected in the two cylinders (from the lines with valves B and C). This measurement is to determine the equilibrium conditions in the coil.
- Open on/off valves B, C, D and E
- Replace the two cylinders with two clean cylinders to collect phase for 5 minutes and to work out the eluting flow rates
- Start both pumps 1 and 2 simultaneously with a ramp of 30 seconds to the desired running flow rate
- Open valve A and record the amount of sample in the reservoir
- After flowing for 5 minutes into the cylinders both the collection and sample injection are started simultaneously
- Start sample injection pump 3 (which is set to pump the desired volume into the coil at the maximum flow rate of 5 ml/min)
- Start collecting fractions for both outlet streams of the required time each
- Ensure the sample pump stops when the desired volume is injected and when the sample pump has stopped close valve A
- Close valve A and record the amount of sample left in the reservoir
- Stop pumps 1 and 2 when the separation is finished
- Close on/off valves B, C, D and E
- Measure and record the phases collected in the two cylinders during the 5 minutes before the injection to determine the eluting flow rates of the phases
- Take 1 ml samples from each fraction into HPLC vials for analysis and number them accordingly.

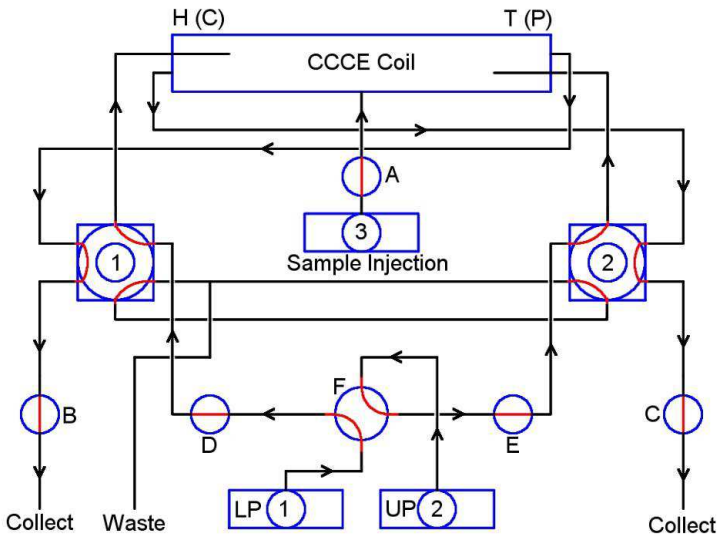


Figure V-3: Schematic diagram of the set-up with the valves and the arrows indicating the direction of the liquid flowing for the performing of a CCCE run

Protocol 4: Refilling the coil at the end of the run

This protocol describes the coil being filled with Lower Phase at the end of the separation.

- Leave the centrifuge running at 1000 rpm or restart the centrifuge and gently bring it up to speed to 1000 rpm
- Valve F is switched so the lower phase goes to electronic valve 2.
- Valve C and E are opened
- Electronic valve 2 is checked to make sure the liquid from the pump goes to the coil (if necessary switched)
- The lower phase pump is started at a flow rate of 30 ml/min
- The liquids from valve C are collected into a measuring cylinder for approximately 5 minutes
- After 5 minutes stop the lower phase pump
- The rotation of the centrifuge is stopped

- Valves C and E are closed
- Valve F is switched so the lower phase goes to electronic valve 1
- The amount of phases collected from the coil is measured and recorded to calculate the phase ratio during the separation in the coil

The position of the valves and the direction of the liquid flowing through the tubes for this protocol is the same as for protocol 2 and is shown in Figure V-2.

Appendix VI Publication of visualisation results



Available online at www.sciencedirect.com



Journal of Chromatography A, 1151 (2007) 99–102

JOURNAL OF
CHROMATOGRAPHY A

www.elsevier.com/locate/chroma

Observations of established dual flow in a spiral dual-flow counter-current chromatography coil

Remco van den Heuvel*, Ian Sutherland

Brunei Institute for Bioengineering, Brunei University, Uxbridge UB8 3PH, UK

Available online 1 February 2007

Abstract

This paper describes the observations made in dual-flow counter-current chromatography. For the first time, the behaviour of the phases inside a spiral dual-flow coil has been studied using stroboscopic visualisation. During the study it was observed that the phase distribution and the linear flow rate in the tubing were not uniform throughout the coil, but behaved differently at each end of the coil with a transition area in between. The location of the transition area is dependent on the flow rate of both the upper and the lower phase. Understanding and then explaining such counter-current flow will significantly help in the prediction of elution behaviour in true moving bed chromatography.
© 2007 Elsevier B.V. All rights reserved.

Keywords: Dual-flow; Counter-current chromatography; Spiral coil; Retention; Flow visualization; Experimental; True moving bed

1. Introduction

Counter-current chromatography (CCC) is a liquid–liquid separation technique where the mobile phase flows over the stationary phase which is retained within a spinning coil. In dual-flow CCC (DFCCC) both liquid phases are mobile. This is true moving bed or counter-current flow with the light and heavy liquid phases moving through the coil in opposite directions. This technique can be utilised for continuous liquid–liquid separations with the sample mixture of binary compounds being introduced in the middle of the coil between the two ends. These components distribute differently between the two moving phases, which results in the components of such a binary mixture eluting at opposite ends of the coil. DFCCC was first developed and described by Yoichiro Ito, the inventor of CCC [1] in 1985 for foam CCC where gas–liquid separations were performed. Liquid–liquid separations soon followed in the early 1990s in a series of papers by Lee et al. [2–4].

Ito et al. [5] proposed a theory to predict the retention time for components separated using DFCCC. This theory was tested using several synthetic dyes. It was logically assumed by Ito et al. that the phases distribute evenly throughout the coil. Our latest research, visualising such flows with stroboscopic light, shows that the phase distribution is far from uniform. This paper shows

how two immiscible phases behave in a spiral coil in dual-flow mode and would explain why the theory suggested by Ito et al. did not fit well with practice.

2. Experimental

2.1. The DFCCC centrifuge

The experiments were performed on a special design of a CCC centrifuge. Both the axis for the coil and the counter balance are extended out from the rotor plates. Perspex covers on the front of the centrifuge and on the coil allowed visualisation of the flow. Differentiation of the phases was achieved by specific dyes. The coil was visualised using stroboscopic light, triggered by the rotation of the rotor, allowing a still image of the coil at the top of the rotation.

The behaviour of the phases flowing through the spinning coil is studied at the top position. Digital images of the spinning coil at this position were taken using an Olympus SP-500 digital camera. The spiral dual-flow coil on the CCC centrifuge consists of 2.2 m PTFE tubing with a 5 mm internal diameter, wound in a spiral of 5.5 loops on an aluminium disk. The radius from the solar axis to the planetary axis is 101.6 mm (4 inch) and the β -value range of the coil is from 0.55 to 0.85 (being the ratio of the radial distance on the planetary disk, r to the distance between planetary axis and centre of rotation, R). There are four flow tubes connected to the coil, two at the centre of the disk

* Corresponding author. Tel.: +44 1895266925.
E-mail address: remco.van.den.heuvel@brunel.ac.uk (R. van den Heuvel).

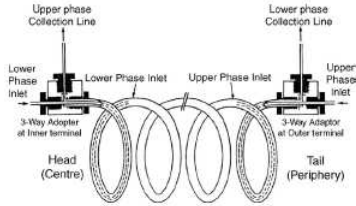


Fig. 1. Schematic diagram of the dual-flow coil with the inlets and outlets illustrated. Adapted from Ito 1985 [1].

($\beta=0.55$) and two at the periphery ($\beta=0.85$). At each end of the coil one tube is the outlet and one tube is the inlet. The inlets to the coil are inserted into the coil at least one half a turn to prevent backflow of the introduced phase as shown in Fig. 1. At the centre of the coil tube is inserted for one complete turn (35 cm) and at the periphery the inlet tube is inserted for half a turn (25 cm). The coil and centrifuge are schematically shown in Fig. 2.

2.2. Experimental set-up

The two pumps connected to the Cantilever CCC centrifuge were two-headed pumps giving a quasi-continuous flow, a Dynamax SD-1 pump with two 200 ml heads and a Knauer K-1800 pump with two 250 ml heads. Valves (on/off and four way/two channel) and connectors from Upchurch are used for connecting the pumps to the centrifuge and to direct the flow along the desired path. Fig. 3 shows how the pumps, centrifuge and valves are connected.

2.3. Phase systems used

The phase system used for the experiments is referred to as 4B [6]. This phase system consists of *n*-heptane, ethyl acetate, methanol and water with the ratios 1.4; 0.6; 1.0; 1.0. This phase

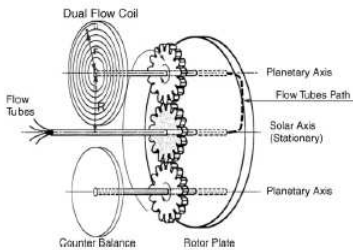


Fig. 2. Schematic diagram of the Cantilever centrifuge with the spiral dual-flow coil installed. Adapted from Ito 1985 [1].

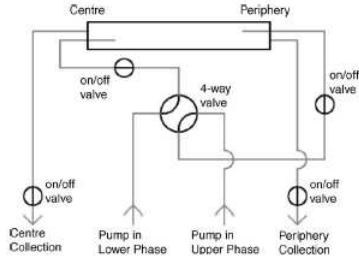


Fig. 3. Schematic set-up of the CCC centrifuge with the pumps and valves connected. The 4-way valve allows the inlets of the coil to be switched between the upper and lower phase.

system is one of a series of aqueous/organic phase systems which progress from largely hydrophobic to largely hydrophilic. 4B is an intermediate system in this series.

The two-phase systems were dyed using Sudan Blue for the upper organic layer and Procion Brilliant Yellow for the lower aqueous layer [7].

2.4. Operating procedure

The coil was rotated in clockwise direction at 1000 rpm for all experimental procedures. Clockwise rotation places the head of the coil at the centre and the tail at the periphery [6].

To prepare for the experiment the coil was filled, while stationary, with lower phase by pumping the phase in from tail to head. When the coil was almost full with lower phase, the coil was rotated in clockwise direction to push the remaining air out. To ensure all leads are full with lower phase the on/off valves where opened to allow the remaining air and lower phase to flow through. When no more air could be expelled the flow was stopped and the on/off valves were closed.

To start the experiment upper phase was pumped into the filled coil and the lower phase pump was started simultaneously. The blue upper phase was pumped from the peripheral tail to the central head and the yellow lower phase was pumped from the central head to the peripheral tail. The eluted phases from the coil were collected in two cylinders, one for the centre and one for the periphery. The stroboscopic light allowed the liquids inside the coil to be photographed and studied. When the liquids inside the coil were visibly equilibrated, the phase distribution was recorded with the digital camera, after which the experiment was stopped. The amount of upper and lower phase displaced from each end of the coil was measured.

To prepare the coil for the next experiment, the upper phase in the coil and system was replaced with lower phase. The upper phase was removed from the coil by pumping lower phase from tail to head through the spinning coil. The eluent was collected in a clean cylinder to determine the amount of upper phase in the coil and system. After this the next experiment was started.



Fig. 4. Picture of the coil spinning at 1000 rpm with 4B phase system and the phases at equilibrium at: (A) 50 ml/min for both the upper phase and the lower phase; (B) 150 ml/min for the upper phase and 50 ml/min lower phase flow rates; and (C) 85 ml/min for the upper phase flow rate and 10 ml/min for the lower phase flow rate. The asterisks mark the location of the coil terminals.

Each experiment, with the same flow rate combination, was repeated for different time durations to establish whether equilibrium was reached inside the coil. When the measured amount of mobile phase in the coil at the end of each experiment was the same, equilibrium was judged to be reached.

To investigate the relationship between flow rate and phase ratio inside the coil different flow rate combinations were used. The flow rates used for the experiments ranged from 0 ml/min to 200 ml/min for both phases.

3. Results

3.1. Visualisation

The images taken and flow situations observed showed that with different flow rates the fluids inside the coil behaved and distributed differently. The situations observed ranged from a coil mainly filled with yellow lower phase and the blue upper phase flowing past on the inner side of the tubing (Fig. 4A) to a coil which was mainly filled with upper phase and the lower phase flowed past along the outer side of the tubing (Fig. 4B).

When the lower phase flow rate is equal to or greater than the upper phase flow rate the coil is mainly filled with the lower phase.

When the upper phase flow rate is significantly higher than the lower phase flow rate the coil is mainly filled with upper phase.

For certain flow rate combinations the lower (heavy) phase occupies most of the outer loops of the coil while the upper (lighter) phase occupies most of the inner loops (Fig. 4C).

The position of the transition area is dependent on the flow rate combinations, phase system and temperature.

3.2. Phase ratio

For each experiment the amount of upper phase inside the coil and system was measured. This value was used to determine the percentage of lower phase inside the coil.

Fig. 5 shows the percentage of lower phase in the coil as a function of the upper phase flow rate for two different lower phase flow rates (10 and 50 ml/min). When the lower phase flow

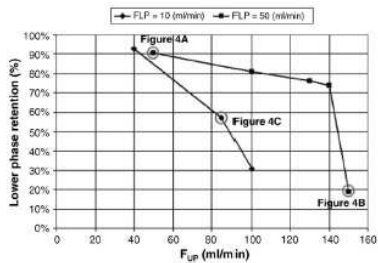


Fig. 5. Effect of flow rate on the percentage of lower phase inside the coil. The lines in the graph show the phase system 4B at lower phase flow rates of 10 ml/min and at 50 ml/min.

rate was 10 ml/min, increasing the upper phase flow rate from 40 to 85 to 100 ml/min decreased the percentage of lower phase in the coil. When the lower phase flow rate was 50 ml/min, increasing the upper phase flow rate from 50 through 100, 130, 140 to 150 ml/min also decreased the percentage of lower phase in the coil. Initially the decrease in the percentage of lower phase shows a linear relationship with the increasing upper phase flow rate. After the upper phase flow rate of 140 ml/min this shows a significant drop.

4. Discussion

During the experiments it was noted that with certain flow rate combinations the lower phase that initially occupied the coil was partly replaced by the upper phase flowing in. Due to the rotation the heavy lower phase naturally wants to go to the tail of the coil and the light upper phase naturally wants to go to the head [6]. The study of the behaviour of the phases flowing against each other through the coil shows that the phases do not distribute equally throughout the coil. The phase distribution can be compared with the modes of operation for normal single flow CCC. These modes are normal-phase mode and reversed-phase mode.

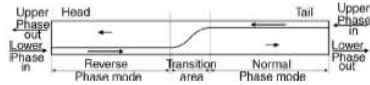


Fig. 6. Stretched out dual-flow coil with the observed phase distribution.

For normal-phase mode the organic (upper) phase is mobile and generally occupies a small volume inside the coil while the aqueous (lower) phase is stationary. For reversed phase the aqueous (lower) phase is mobile and generally occupies a small volume inside the coil. At the head of the dual-flow coil the phases are distributed as in reversed-phase mode and at the tail of the coil the phases distribute as in normal-phase mode. In between these two modes there is a transition area that appears at different locations in the coil for different flow rate combinations. This is shown schematically in Fig. 6.

The position of the transition area is dependent on the flow rates of both the phases, the physical properties of the phase system used and the rotational speed of the coil. When the flow rate of the lower phase is equal to the flow rate of the upper phase the transition area will be nearer the head of the coil. This means that the lower phase occupies a larger volume inside the coil than the upper phase. This is due to the denser and more viscous nature of the lower phase. To achieve equal volumes of upper and lower phase in the coil and a transition area in the centre of the coil the flow rate of the upper phase needs to be higher than the flow rate of the lower phase. In Fig. 4A the transition area is located at the centre outlet. The blue that can be seen at the periphery is the inlet tube filled with upper phase. Any other blue seen in Fig. 4A are the mixing waves occurring due to the rotation. Fig. 4B has the transition area located at the periphery outlet. The yellow at the centre of the coil is the inlet tube filled with lower phase. A small amount of yellow can be seen to the right of Fig. 4B due to the rotational forces.

Ito et al. [5] assume in the dual-flow theory that the phases distribute equally throughout the coil. However, the observations from this study suggest this is not the case. The distribution of the phases inside the coil appears to be more complex than initially thought and suggested. Phase distributions and linear flow rates vary radically in different areas of the coil. The distribution of the phases in the coil and the position of the transition area appear to

be related to the physical properties of the phases and their flow rates—the exact relationship will require a much more detailed study. Separations in dual-flow coils will be influenced by the location of the transition area and the distribution of the phases inside the coil.

5. Conclusion and future work

The results presented in this paper are initial results of an ongoing visualisation study of the behaviour of phase systems under dual-flow conditions. This study will be combined with computational fluid dynamics (CFD) modelling. The initial observations from the study appear to contradict the logical assumptions made by Ito et al. [5] in a publication where a theory of DFCCC was proposed. Phase systems flowing through a dual-flow coil appear not to distribute evenly along the length of the coil. The majority of the heavy phase collects at the tail and the majority of the light phase collects at the head of the coil. This complicates the proposed theory on DFCCC as it affects the assumptions on which the theory is based. More research will be carried out to investigate the phase behaviour in DFCCC and to develop a rigorous theory to predict separations.

Acknowledgements

We thank the EPSRC for the doctoral training post for the first author and Pfizer Ltd., particularly Robert Crook and Ben Mathews, for financial support. We also thank Carola Koenig for the useful discussion.

References

- [1] Y. Ito, J. Liq. Chromatogr. 8 (1985) 2131.
- [2] Y.W. Lee, C.E. Cook, Y. Ito, J. Liq. Chromatogr. 11 (1988) 37.
- [3] Y.W. Lee, J. Chromatogr. 538 (1991) 37.
- [4] Y.W. Lee, in: Y. Ito, W.D. Conway (Eds.), High-Speed Countercurrent Chromatography (Chemical Analysis Series), 132, Wiley, New York, 1996, p. 93.
- [5] Y. Ito, T. Goto, S. Yamada, H. Matsumoto, H. Oka, N. Takahashi, H. Nakazawa, H. Nagase, Y. Ito, J. Chromatogr. A 1108 (2006) 20.
- [6] I.A. Sutherland, J. Muytjens, M. Prins, P.L. Wood, J. Liq. Chromatogr. Related Technol. 23 (2000) 2259.
- [7] P.L. Wood, The Hydrodynamics of CCC in J-type Centrifuges, Brunel University, London, 2002.

Appendix VII

Data from retention study 4.3

#	F_{UP}/F_{LP} (ml/min)	% UP	V_{UP} (ml)	Equilibrium at flow			End of the experiment		
				# loops	Length section (cm)	Volume section (ml)	# loops	Length section (cm)	Volume section (ml)
1	10/10	0%	22.0	2 3/4	99.6	19.6	2 5/8	94.5	18.6
2	10/10	0%	20.0	2 3/16	77.0	15.1	2 3/8	84.4	16.6
17	10/10	0%	23.0	2 3/4	99.6	19.6	2 3/4	99.6	19.6
3	50/10	0%	43.0	4 15/16	199.0	39.1	4 13/16	192.8	37.9
18	50/10	0%	39.0	4 9/16	180.7	35.5	4 3/8	171.8	33.7
4	10/50	0%	6.0	1/8	3.9	0.8	3/8	11.9	2.3
19	10/50	0%	6.0	1/8	3.9	0.8	3/8	11.9	2.3
5	50/50	0%	12.0	1/8	3.9	0.8	15/16	30.8	6.0
6	50/50	0%	10.0	3/8	11.9	2.3	15/16	30.8	6.0
20	50/50	0%	9.0	5/8	20.2	4.0	15/16	30.8	6.0
7	10/10	50%	20.0	2 5/16	81.9	16.1	2 1/4	79.4	15.6
28	10/10	50%	18.0	2 1/16	72.1	14.2	2 1/16	72.1	14.2
8	50/10	50%	46.0	5 1/2	227.4	44.7	5 1/8	208.3	40.9

29	50/10	50%	47.0	5 1/2	227.4	44.7	5 1/8	208.3	40.9
9	10/50	50%	5.0	1/8	3.9	0.8	3/8	11.9	2.3
30	10/50	50%	5.5	1/8	3.9	0.8	3/8	11.9	2.3
10	50/50	50%	9.5	3/4	24.4	4.8	1	33.0	6.5
31	50/50	50%	9.0	3/4	24.4	4.8	1 1/16	35.2	6.9
11	10/10	100%	19.0	2 1/16	72.1	14.2	2 1/16	72.1	14.2
21	10/10	100%	23.0	2 3/4	99.6	19.6	2 3/4	99.6	19.6
12	50/10	100%	47.0	5 1/2	227.4	44.7	5 1/8	208.3	40.9
22	50/10	100%	46.0	5 1/2	227.4	44.7	5 1/16	205.2	40.3
26	50/10	100%	37.0	4 3/8	171.8	33.7	4 3/16	162.9	32.0
13	10/50	100%	5.5	1/8	3.9	0.8	3/8	11.9	2.3
23	10/50	100%	7.0	1/8	3.9	0.8	3/8	11.9	2.3
14	50/50	100%	9.5	5/8	20.2	4.0	1	33.0	6.5
27	50/50	100%	10.0	5/8	20.2	4.0	1	33.0	6.5
16	40/20	50%	31.0	3 11/16	140.0	27.5	3 5/8	137.3	26.9
24	40/20	50%	28.0	3 3/8	126.2	24.8	3 1/4	120.8	23.7
15	30/30	50%	9.0	3/8	11.9	2.3	3/4	24.4	4.8
25	30/30	50%	8.0	3/8	11.9	2.3	3/4	24.4	4.8

Appendix VIII Experimental design calculations

This appendix addresses the calculations with the experimental design analysis in section 4.4.3 on page 122. The calculation methods described are extracted from [Box et al. 1978].

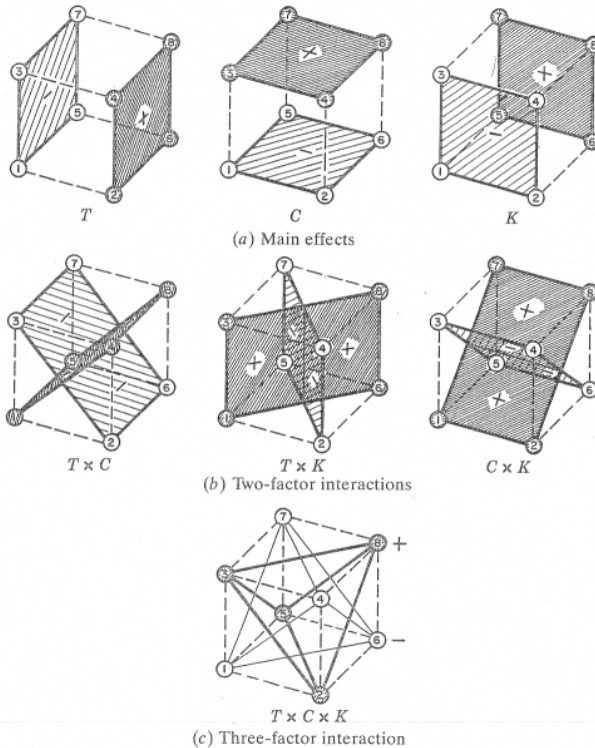


Figure VIII-1: Geometric representation of contrasts corresponding to main effects and interactions [Box et al. 1978]

Example calculations corresponding to the variables in Figure VIII-1 for the main effect and the two and three-factor interactions are as follows.

Experimental design calculations

$$\text{Effect } T = \text{Average}(+) - \text{Average}(-) \quad \text{Equation VIII-1}$$

$$\text{Interaction } TxC = \text{Average}(+) - \text{Average}(-) \quad \text{Equation VIII-2}$$

$$\text{Interaction } TxCxK = \text{Average}(+) - \text{Average}(-) \quad \text{Equation VIII-3}$$

The following table shows the raw data of the upper phase volume in the system at the end of the experiment with the experiment number ([#]). In the table the maximum difference between the repeats (d) and the square value of this difference is calculated.

Table VIII-1: 2³ factorial design with average and estimations of the variances

F _{UP} / F _{LP} (ml/min)	% UP (%)	V _{UP} ^(#) (ml)	V _{UP} ^(#) (ml)	V _{UP} ^(#) (ml)	Mean V _{UP} (ml)	d	d ²
10/10	0	22 ⁽¹⁾	20 ⁽²⁾	23 ⁽¹⁷⁾	21.7	3.00	9.00
50/10	0	43 ⁽³⁾	39 ⁽¹⁸⁾		41.0	4.00	16.0
10/50	0	6 ⁽⁴⁾	6 ⁽¹⁹⁾		6.00	0.00	0.00
50/50	0	12 ⁽⁵⁾	10	9 ⁽²⁰⁾	10.3	3.00	9.00
10/10	100	19 ⁽¹¹⁾	23 ⁽²¹⁾		21.0	4.00	16.0
50/10	100	47 ⁽¹²⁾	46 ⁽²²⁾	37 ⁽²⁶⁾	43.3	10.0	100
10/50	100	5.5 ⁽¹³⁾	7 ⁽²³⁾		6.25	1.50	2.25
50/50	100	9.5 ⁽¹⁴⁾	10 ⁽²⁷⁾		9.75	0.50	0.25

$$\begin{aligned} \text{Total} &= 152.5 \\ s^2 &= 9.53 \\ V(\text{effect}) &= 2.01 \\ \text{Standard Error} &= 1.42 \end{aligned}$$

The equations to calculate the s^2 (which is the estimated variance (σ^2)), the $V(\text{effect})$ and the standard error in the table are as follows.

$$s^2 = \frac{\sum d^2}{2 \cdot g} = \frac{\sum d^2}{2 \cdot 8} \quad \text{Equation VIII-4}$$

$$V(effect) = \frac{4}{N} \sigma^2 = \frac{4}{19} s^2 \quad \text{Equation VIII-5}$$

$$\text{Standard Error} = \sqrt{V(effect)} \quad \text{Equation VIII-6}$$

Where g is the number of different experimental conditions for this 2³ factorial experimental design (8).

Appendix IX Application Chromatograms

study: "Batch"

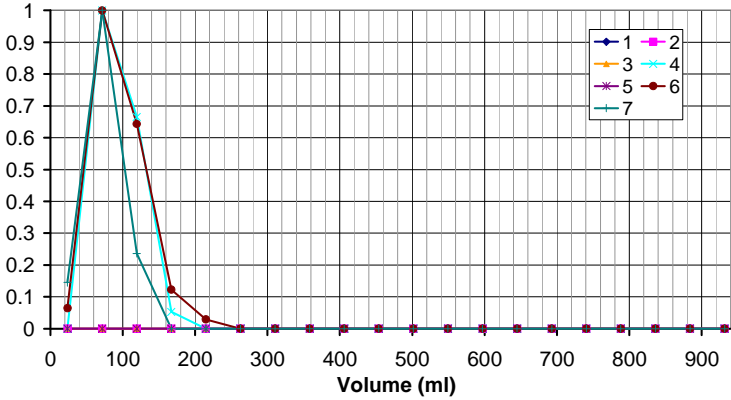


Figure IX-1: Batch separation B-1 on Pfizer-C. Upper phase eluting from the centre outlet. Flow rate for the upper and lower phase is 20 ml/min.

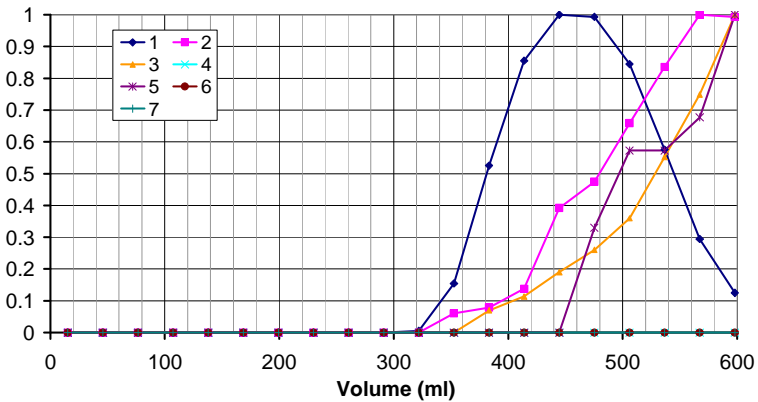


Figure IX-2: Batch separation B-1 on Pfizer-C. Lower phase eluting from the peripheral outlet. Flow rate for the upper and lower phase is 20 ml/min.

Application study: "Batch" Chromatograms

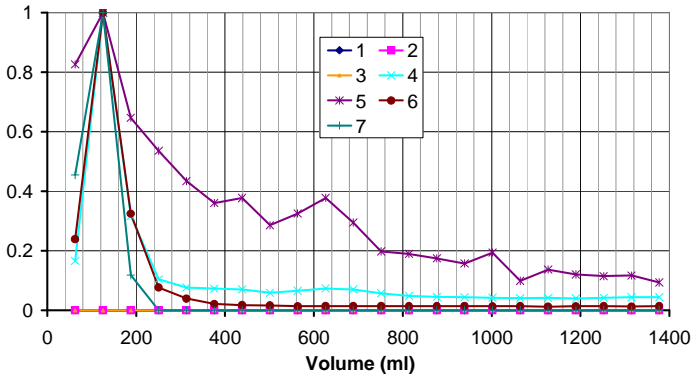


Figure IX-3: Batch separation B-2 on Pfizer-C. Upper phase eluting from the centre outlet. Flow rates for the upper and lower phase are 30 and 20 ml/min respectively.

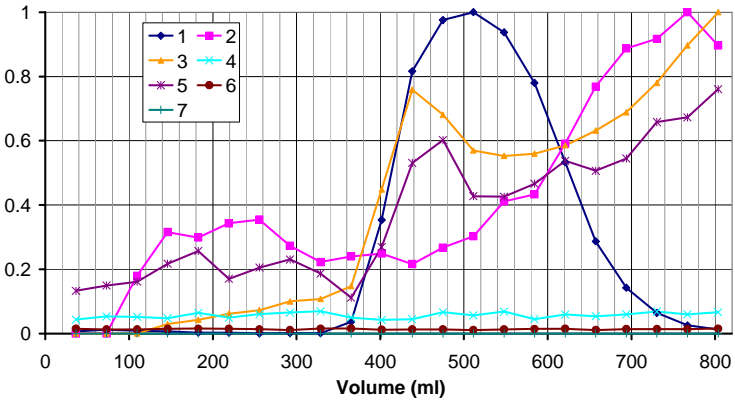


Figure IX-4: Batch separation B-2 on Pfizer-C. Lower phase eluting from the peripheral outlet. Flow rates for the upper and lower phase are 30 and 20 ml/min respectively.

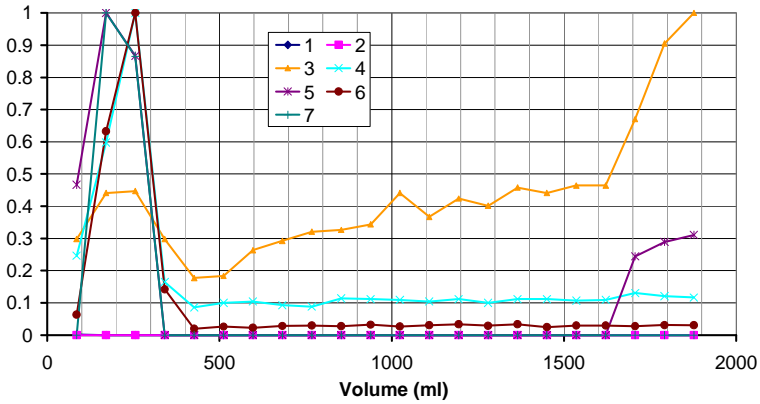


Figure IX-5: Batch separation B-3 on Pfizer-C. Upper phase eluting from the centre outlet. Flow rates for the upper and lower phase are 50 and 20 ml/min respectively.

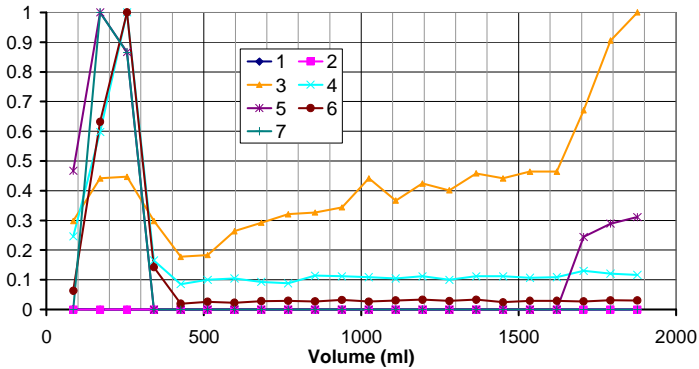


Figure IX-6: Batch separation B-3 on Pfizer-C. Lower phase eluting from the peripheral outlet. Flow rates for the upper and lower phase are 50 and 20 ml/min respectively.

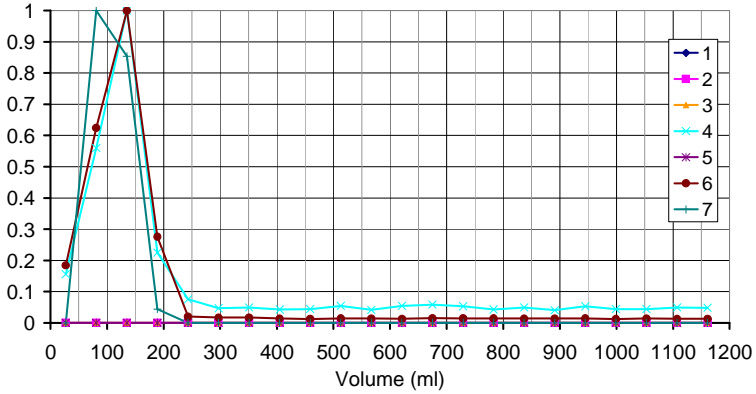


Figure IX-7: Batch separation B-4 on Pfizer-C. Upper phase eluting from the centre outlet. Flow rate for the upper and lower phase is 30 ml/min.

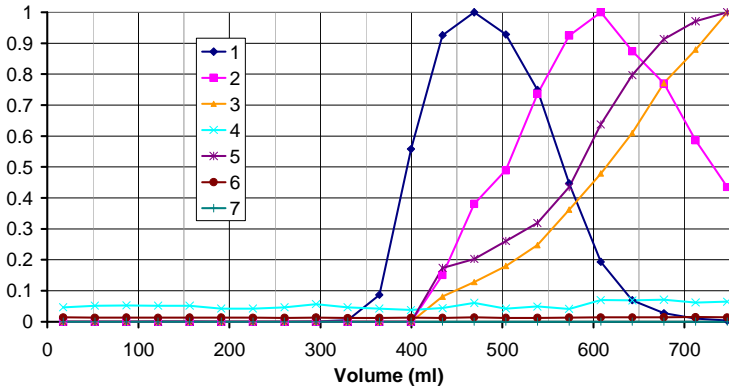


Figure IX-8: Batch separation B-4 on Pfizer-C. Lower phase eluting from the peripheral outlet. Flow rate for the upper and lower phase is 30 ml/min.

Appendix X Application study: "Continuous" Chromatograms

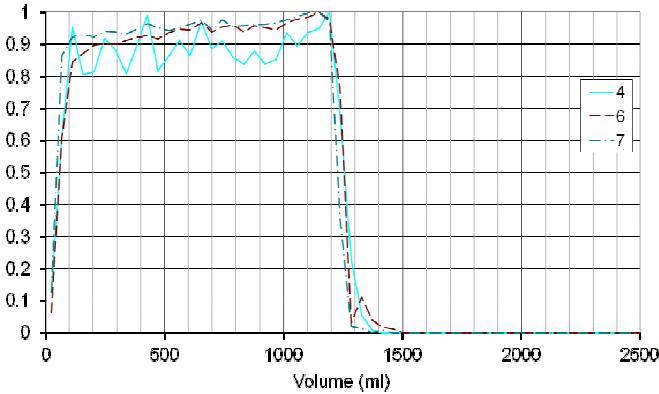


Figure X-1: Continuous separation C-1 on Pfizer-C. Upper phase eluting from the centre outlet. Flow rate for the upper and lower phase is 30 ml/min. Sample concentration loaded is 29 mg/ml.

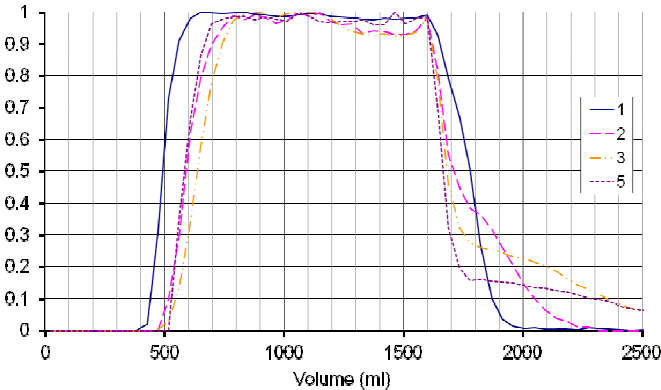


Figure X-2: Continuous separation C-1 on Pfizer-C. Lower phase eluting from the peripheral outlet. Flow rate for the upper and lower phase is 30 ml/min. Sample concentration loaded is 29 mg/ml.

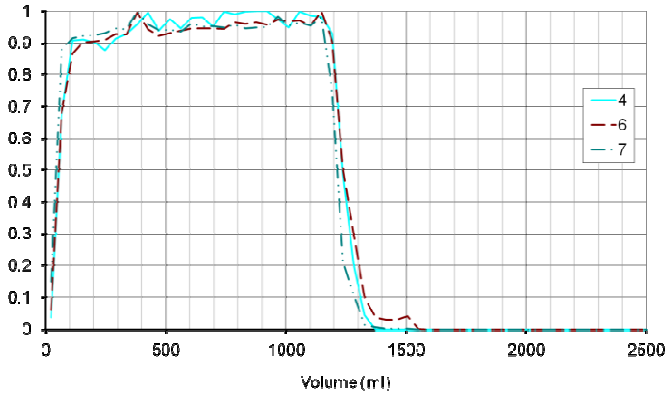


Figure X-3: Continuous separation C-2 on Pfizer-C. Upper phase eluting from the centre outlet. Flow rate for the upper and lower phase is 30 ml/min. Sample concentration loaded is 53 mg/ml.

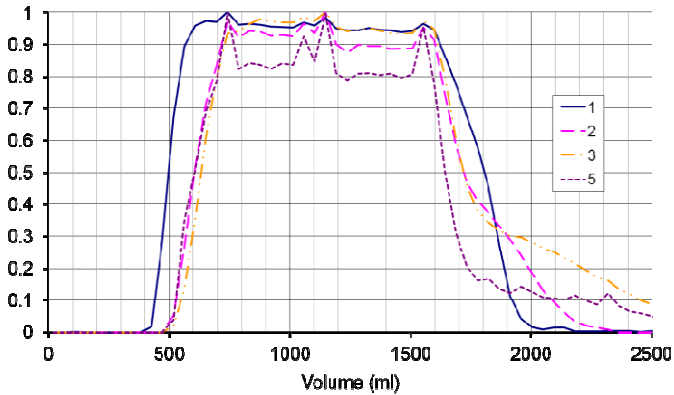


Figure X-4: Continuous separation C-2 on Pfizer-C. Lower phase eluting from the peripheral outlet. Flow rate for the upper and lower phase is 30 ml/min. Sample concentration loaded is 53 mg/ml.

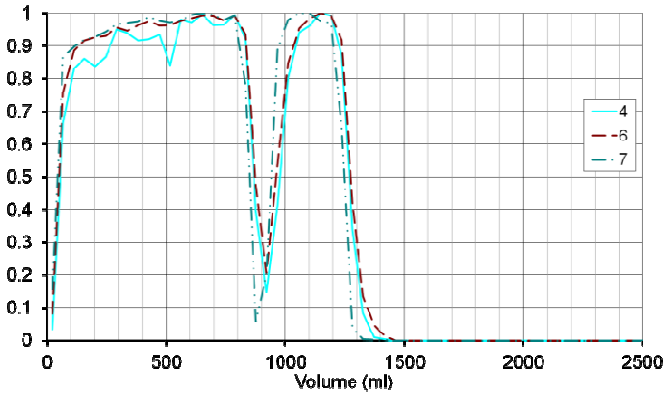


Figure X-5: Continuous separation C-3 on Pfizer-C. Upper phase eluting from the centre outlet. Flow rate for the upper and lower phase is 30 ml/min. Sample concentration loaded is 118 mg/ml.

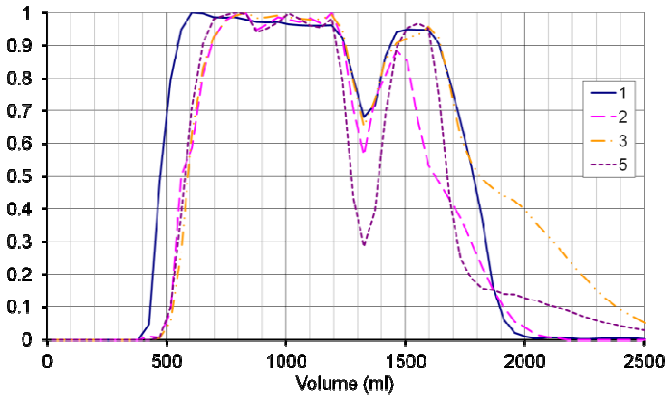


Figure X-6: Continuous separation C-3 on Pfizer-C. Lower phase eluting from the peripheral outlet. Flow rate for the upper and lower phase is 30 ml/min. Sample concentration loaded is 118 mg/ml.

Appendix XI Application study: "Continuous" Pfizer-D separation

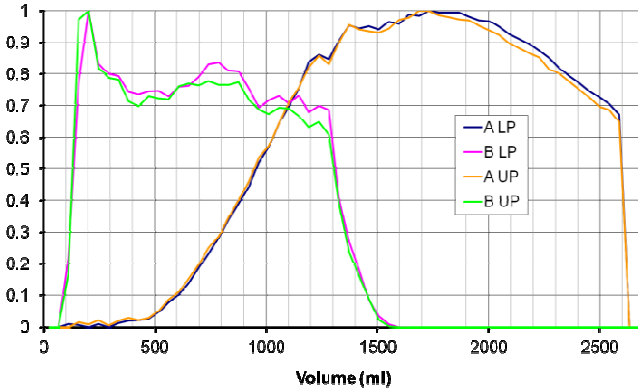


Figure XI-1: Continuous separation C-4 on Pfizer-D. Upper and Lower phase eluting from the centre outlet. Flow rate for the upper and lower phase both are 30 ml/min.

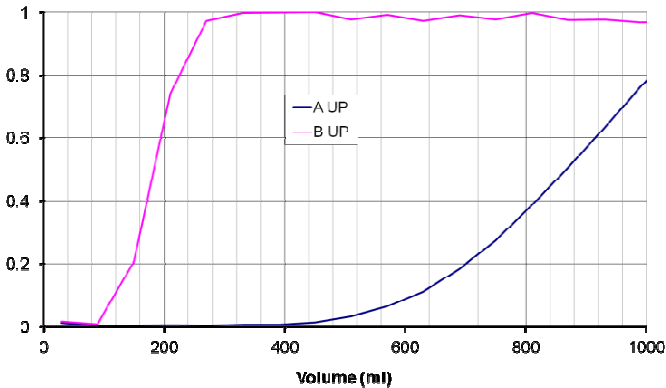


Figure XI-2: Continuous separation C-5 on Pfizer-D. Upper phase eluting from the centre outlet. Flow rate for the upper and lower phase are 35 and 15 ml/min respectively.

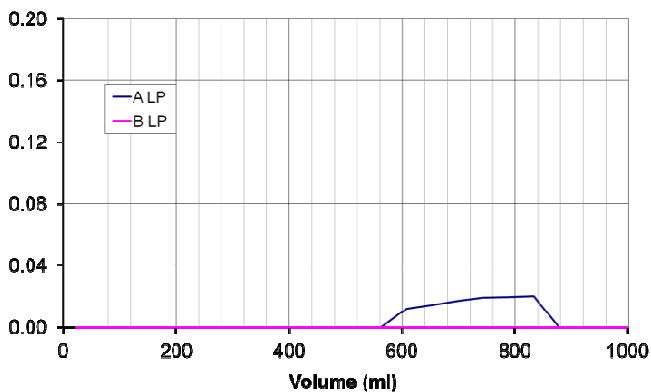


Figure XI-3: Continuous separation C-5 on Pfizer-D. Lower phase eluting from the peripheral outlet. Flow rate for the upper and lower phase are 35 and 15 ml/min respectively.

Appendix XII References

Abraham, M.H.; *100 years of chromatography – or is it 171?*; Journal of Chromatography A, Volume 1061, Page 113-114, **2004**

Barker, P.E. and Ganetsos, G.; in Ganetsos, G. and Barker, P.E. (Editors); *Preparative and Production scale Chromatography*; Chromatographic science series, Volume 61, Page 173-186, Marcel Dekker, New York, **1992**.

Berthod, A., Ed. *Countercurrent Chromatography, The Support-Free Liquid Stationary Phase*; Comprehensive Analytical Chemistry XXXVIII; Elsevier, Amsterdam, **2002**.

Berthod, A.; Ruiz-Angel, M.J. and Carda-Broch, S.; *Elution-Extrusion Countercurrent Chromatography. Use of the Liquid Nature of the Stationary Phase to Extend the Hydrophobicity Window*; Analytical Chemistry, Volume 75, Page 5886-5894, **2003**.

Berthod, A.; *Band broadening inside the chromatographic column: The interest of a liquid stationary phase*; Journal of Chromatography A, Volume 1126, Page 347-356, **2006**.

Berthod, A. and Hassoun, M.; *Using the liquid nature of the stationary phase in countercurrent chromatography IV. The cocurrent CCC method*; Journal of Chromatography A, Volume 1116, Page 143-148, **2006**.

Bhatangar, M. and Ito, Y.; *Foam Counter-current Chromatography on various test samples and the effects of additives on foam affinity*; Journal of Liquid Chromatography, Volume 11 (1), Page 21-36, **1988**.

Box, G.E.P.; Hunter, W.G. and Hunter, J.S.; *Statistics For Experimenters, An Introduction to Design, Data Analysis and Model Building*; Wiley series in probability and mathematical statistics, John Wiley & Sons, New York, **1978**.

Camacho-Frias, E. and Foucault, A.; *Solvent Systems in Centrifugal Partition Chromatography*; Analysis, Volume 24, Page 159-167, **1996**.

Charton, F. and Nicoud, RM.; *Complete design of a simulated moving bed*; Journal of Chromatography A, Volume 702, Page 97-112, **1995**.

Conway, W.D.; *Counter-current Chromatography: Apparatus, Theory and Applications*; Vch Publishers Inc., New York, ISBN 0-89573-331-5, **1990**

Craig, L.C.; *Identification of small amounts of organic compounds by distribution studies: II. Separation by counter-current distribution*; Journal of Biological Chemistry, Volume 155, Page 519-553, **1944**.

Craig, L.C. and Craig, D.; *Laboratory Extraction and Countercurrent Distribution*; in Weissberger, A. (editor), Separation and Purification; Technique of Organic Chemistry, Volume III, Interscience Publishers Ltd. London, Page 149 - 332, **1956**.

de Moivre, Abraham; *The Doctrine of Change: a Method of Calculating the Probability of Events in Play*; Third Edition, Millar, London, **1756**.

Du, Q.; Wu, C.; Qian, G.; Wu, P. and Ito, Y.; *Relationship between the flow-rate of the mobile phase and retention of the stationary phase in Counter-current Chromatography*; Journal of Chromatography A, Volume 835, Page 231-235, **1999**.

Dubant, S.; Internal communication at Pfizer Ltd., **2007**.

Field, G.; *Chromatography; or, a Treatise on Colours and Pigments of their Powers in Painting*; Charles Tilt, London, **1835**.

Garrard, I.J.; *A Systematic Approach to the Development of a Countercurrent Chromatography Protocol with Examples from Polar, Intermediate and Nonpolar Compounds*; PhD thesis at Brunel University, **2005A**.

Garrard, I.J.; *Simple Approach to the Development of a CCC Solvent Selection Protocol Suitable for Automation*; Journal of Liquid Chromatography & Related Technologies, Volume 28, Page 1923-1935, **2005B**.

Giddings, J.C.; Ed. *Dynamics of Chromatography, Part 1, Principles and Theory*; Chromatographic Science, Marcel Dekker, New York, **1965**.

Ito, Y.; *New Horizontal Flow-Through Coil Planet Centrifuge for Counter-Current Chromatography. I. Principle of Design and Analysis of Acceleration;* Journal of Chromatography, Volume 188, Page 33 – 42, **1980A**.

Ito, Y.; *New Horizontal Flow-Through Coil Planet Centrifuge for Counter-Current Chromatography. II. The Apparatus and its Partition Capabilities;* Journal of Chromatography, Volume 188, Page 43 – 60, **1980B**.

Ito, Y.; *Counter-current Chromatography;* Journal of Biochemical and Biophysical Methods, Volume 5, Page 105-129, **1981**.

Ito, Y.; *Experimental observations of the hydrodynamic behaviour of solvent systems in high-speed counter-current chromatography: II. Phase distribution diagrams for helical and spiral columns;* Journal of Chromatography A, Volume 301, Pages 387-403, **1984**.

Ito, Y.; *Foam counter-current chromatography based on dual counter-current system;* Journal of Liquid Chromatography, Volume 8 (12), Pages 2131-2152, **1985**.

Ito, Y.; *High-Speed Countercurrent Chromatography;* CRC Critical Reviews in Analytical Chemistry, Volume 17 (1), Page 65-142, **1986**.

Ito, Y.; *Golden rules and pitfalls in selecting optimum conditions for high-speed counter-current chromatography;* Journal of Chromatography A, Volume 1065 (2), Pages 145-168, **2005**.

Ito, Y. and Bowman, R. L.; *Foam Counter-current Chromatography: New Foam Separation Technique with Flow-Through Coil Planet Centrifuge;* Separation Science, Volume 11(3), Page 201-206, **1976**.

Ito, Y. and Bowman, R. L.; *Preparative Counter-current Chromatography with a Slowly Rotating Helical Tube;* Analytical Biochemistry, Volume 78, Page 506-512, **1977A**.

Ito, Y. and Bowman, R. L.; *Horizontal Flow-Through Coil Planet Centrifuge without Rotating Seals;* Analytical Biochemistry, Volume 82, Page 63-68, **1977B**.

Ito, Y. and Bowman, R. L.; *Preparative Counter-current Chromatography With Horizontal Flow-Through Coil Planet*

Centrifuge; Journal of Chromatography, Volume 147, Page 221-231, **1978**.

Ito, Y.; Weinstein, M. A.; Aoki, I.; Harada, R.; Kimura, E. and Nunogaki, K.; *The Coil Planet Centrifuge*; Nature, Volume 212, Number 5066, Page 985-987, **1966**.

Ito, Yuko; Goto, T.; Yamada, S.; Matsumoto, H.; Oka, H.; Takahashi, N.; Nakawawa, H.; Magase, H. and Ito, Y.; *Application of dual counter-current chromatography for rapid sample preparation of N-methylcarbamate pesticides in vegetable oil and citrus fruit*, Journal of Chromatography A, Volume 1108, Page 20-25, **2006**.

Kostanian, A.E.; *Modelling counter-current chromatography: a chemical engineering perspective*; Journal of Chromatography A, Volume 973, Page 39-46, **2002**.

Kostanian, A.E.; Berthod, A.; Ignatova, S.N.; Maryutina, T.A.; Spivakov, B.Ya. and Sutherland, I.A.; *Countercurrent chromatographic separation: a hydrodynamic approach developed for extraction columns*; Journal of Chromatography A, Volume 1040, Page 63-72, **2004**.

Kostanian, A.E. and Voshkin, A.A.; *Analysis of new counter-current chromatography operating modes*; Journal of Chromatography A, Volume 1151 (1-2), Pages 126-130, **2007**.

Lee, Y.W.; Cook, C.E. and Ito, Y.; *Dual Counter-current Chromatography*; Journal of Liquid Chromatography, Volume 11(1), Page 37-53, **1988**.

Lee, Y.W.; *Dual counter-current chromatography —its applications in natural products research*; Journal of Chromatography A, Volume 538, Issue 1, Pages 37-44, **1991**.

Lee, Y.W.; in Ito, Y. and Conway W.D. (editors), *High-Speed Countercurrent Chromatography*; Chemical Analysis, Volume 132, Wiley Interscience, **1996** (ISBN: 0471637491).

Mandava, N.B. and Ruth, J.M.; in Mandava, N.B. and Ito, Y. (editors), *Counter-current Chromatography Theory and Practice*; Chromatographic Science Series, Volume 44, Marcel Dekker Inc., New York, **1988** (ISBN: 0824778154)

References

Martin, A.J.P. and Syngé, R.L.M.; *A new form of chromatogram employing two liquid phases*; *Biochemical Journal*, Volume 35, Page 1358-1368, **1941**.

Nernst, W.; *Verteilung eines Stoffes zwischen zwei Lösungsmitteln and zwischen Lösungsmitteln und Dampfraum*; *Z.f.physik. Chem.*, Volume 8, **1891**.

Nichols, P.L.; *Useful Relations for Countercurrent Distribution Computations*; *Analytical Chemistry*, Volume 22, Page 915-918, **1950**.

Oka, F.; Oka, H. and Ito, Y.; *Systematic Search for Suitable Two-Phase Solvent Systems for High Speed Counter-Current Chromatography*; *Journal of Chromatography*, Volume 538, Page 99-108, **1991**.

Phillips, C.S.G.; *Second Symposium on Gas Chromatography*, Amsterdam, May 22, **1958**.

Post, O. and Craig, L.C.; *A New Type of Stepwise Countercurrent Distribution Train*; *Analytical Chemistry*, Volume 35, Page 641-647, **1963**.

Renault, J.H.; Nuzillard, J.M.; Intes, O. and Maciuk, A., in Berthod, A. (editor), *Countercurrent Chromatography, The Support-Free Liquid Stationary Phase*; *Comprehensive Analytical Chemistry XXXVIII*; Elsevier, Amsterdam, **2002**.

Rutter, J.W., in Chapman and Hall (editors), *Geometry of Curves*, CRC Press, Boca Raton, FL, **2000**

Sutherland, I.A.; Heywood-Waddington, D. and Peters, T.J.; *Toroidal Coil Countercurrent Chromatography: A Fast Simple Alternative to Countercurrent Distribution Using Aqueous Two Phase Partition: Principles, Theory, and Apparatus*; *Journal of Liquid Chromatography & Related Technologies*, Volume 7, Page 363-376, **1984**.

Sutherland, I.A.; Heywood-Waddington, D. and Ito, Y.; *Countercurrent Chromatography. Applications to the separation of biopolymers, organelles and cells using either aqueous-organic or*

aqueous-aqueous phase systems; Journal of Chromatography, Volume 384, Page 197-207, **1987**.

Sutherland, I.A.; Muytjens, J.; Prins, M. and Wood, P.L.; *A new hypothesis on phase distribution in counter-current chromatography*; Journal of Liquid Chromatography & Related Technologies, Volume 23, Issue 15, Page 2259, 18p, **2000**.

Sutherland, I.A.; Du, Q. and Wood, P.L.; *The Relationship between Retention, Linear Flow, and Density Difference in Countercurrent Chromatography*; Journal of Liquid Chromatography and Related Technologies, Volume 24(11&12), Page 1669-1683, **2001**.

Sutherland, I.A.; De Folter, J. and Wood, P.L.; *Modelling CCC Using an Eluting Countercurrent Distribution Model*; Journal of Liquid Chromatography & Related Technologies, Volume 26(9&10), Page 1449-1474, **2003**.

Sutherland, I.A.; *Recent progress on the industrial scale-up of counter-current chromatography*; Journal of Chromatography A, Volume 1151, Page 6-13, **2007**.

Tswett, M.; *On a new category of absorption phenomena and their application to biochemical analysis*; Proc. Warsaw Soc. Nat. Sci., Biol. Sect., Volume 14 (6), **1903**.

Tswett, M.; *Physikalisch-chemische Studien über das Chlorophyll. Die Adsorptionen (Physical-Chemical study of chlorophyll. The Absorption)*; Ber. Deutsch. bot. Gesell., Volume 24, Page 316–323, **1906A**.

Tswett, M.; *Adsorptionsanalyse und chromatographische Methode. Anwendung auf die Chemie des Chlorophylls (Absorption analysis and chromatographic method. Applications on the chemistry of chlorophyll)*; Ber. Deutsch. bot. Gesell., Volume 24, Page 384-393, **1906B**.

van den Heuvel, R. and Sutherland, I.A.; *Observations of established dual flow in a spiral dual-flow counter-current chromatography coil*; Journal of Chromatography A, Volume 1151, Page 99-102, **2007**.

References

Williamson, B. and Chraig, L.C.; *Identification of small amount of organic compounds by distribution studies*; Journal of Biological Chemistry, Volume 168, Page 687-697, **1947**

Wood, P.L.; *The Hydrodynamics of CCC in J-type Centrifuges*; Brunel University, London, **2002**.